POLITECNICO DI TORINO

Master's degree in Civil Engineering

Master's Degree Thesis

Research on 3-D Vibration and Seismic Isolation Structure of Over-track Buildings

Supervisors: Gianfranco Piana, Ding Jiemin

Candidate: Zheng Jiaqing, S274337

September 2021

Acknowledgements

On the occasion of graduation, there are too many things to say and too many people to thank.

Thanks to my two supervisors Professor Gianfranco Piana and Ding Jiemin. Both of you gave me many suggestions on my dissertation, and helped me determine the topic, research contents and research methods. You have played a significant guiding role in my thesis.

Thanks to Professor Pietro Cornetti. You gave me many small tips on the daily life and academic career which helped me go through all the difficulties in Turin. And thanks for your patience in answering all the double degree questions.

Thanks to my seniors Wu Honglei and Chen Changjia. You gave me many technical supports of finite element analysis and structural concepts. It’s due to your kindly help that I can successfully complete the numerical simulation part and explain the results clearly.

Thanks to my colleagues Yi Epan, Cui Junheng, Liu Zhixuan, Yan Xuelin, Chen Hao, Chen Shengxin, Jiao Yunshuo, Mao Qiuyi, Deng Zhixin, Liu Xiafang and Xiao Kangli. All of you accompanied me for the three years of study in Politecnico and Tongji University. We discussed together, studied together, did the course project together. Thanks for your companionship, we went through the difficult period of Covid-19 smoothly.

In the end, thanks to the experts and professors who reviewed this thesis and attended the defense of the thesis.

Zheng Jiaqing

April 2021

ABSTRACT

In response to the vertical vibration isolation and horizontal seismic isolation requirements of the over-track buildings, a three-dimensional vibration and seismic isolation layer is introduced between the superstructure and the underground structure, which can not only isolate the environmental vibration and secondary noise generated during the daily operation of the subway, but also can effectively reduce the horizontal seismic response and improve the aseismic performance of the structure. According to the arrangements of viscous dampers in the isolation layer, this thesis selects three structural systems: pure three-dimensional vibration and seismic isolation structure (that is, the isolation layer has no viscous dampers), three-dimensional vibration and seismic isolation + vertical viscous dampers structure and three-dimensional vibration and seismic isolation + horizontal viscous dampers structure, to carry out systematic analysis and research starting from the vertical vibration isolation performance and horizontal seismic isolation performance.

First of all, starting from the significance of the property development of the over-track buildings, this thesis enhances the engineering application value to study the three-dimensional vibration and seismic isolation structure, and summarizes the composition and classification of the three-dimensional vibration and seismic isolation structure. Then the research status of three-dimensional vibration and seismic isolation devices, three-dimensional vibration and seismic isolation structures and rocking effects are presented, and the main research contents and innovation points of this thesis are clarified.

Secondly, this thesis introduces the vertical vibration reduction mechanism and horizontal seismic reduction mechanism of three-dimensional vibration and seismic isolation technology, as well as the restoring force models and FEM software simulation methods of commonly used vibration isolation devices, seismic isolation devices and damping devices, and proposes the definition of the rocking angle, then studies several major factors affecting the rocking angle, summarizes the vibration evaluation standards of the indoor floor, which laid the foundation for the analysis and research later.

Thirdly, the vertical vibration isolation performance of the three-dimensional vibration and seismic isolation structure is studied. Through the finite element numerical simulation, the influence of the vertical stiffness of the isolation layer on the indoor vibration response of the pure three-dimensional vibration and seismic isolation structure, and the influence of the vertical damping coefficient and damping index of vertical dampers on the indoor vibration response of the three-dimensional vibration and seismic isolation + vertical viscous dampers structure are studied. In view of the two different structural forms, the reasonable range of parameter values are given starting from the engineering design point of view.

Fourthly, the horizontal seismic isolation performance of the three-dimensional vibration and seismic isolation structure is studied. Through the finite element numerical simulation, the influence of the vertical stiffness of the isolation layer on the horizontal seismic response of the pure three-dimensional vibration and seismic isolation structure, the influence of the vertical damping coefficient and damping index of vertical dampers on the horizontal seismic response of the three-dimensional vibration and seismic isolation + vertical viscous dampers structure, and the influence of the horizontal damping coefficient and damping index of the horizontal dampers on the horizontal seismic response of the three-dimensional vibration and seismic isolation + horizontal viscous dampers structure are studied. In view of the three different structural forms, the reasonable range of parameter values are given starting from the engineering design point of view. At the end of this chapter, the horizontal seismic reduction performance of different structural systems is compared to provide a reference for engineering design.

Finally, based on the previous research results, the three-dimensional vibration and seismic isolation technology is applied to an actual engineering project, verifying the feasibility and effectiveness of the three-dimensional vibration and seismic isolation technology.

Key Words: Over-track buildings, three-dimensional vibration and seismic isolation structure, viscous dampers, vertical vibration isolation, horizontal seismic isolation, parameter analysis

SOMMARIO

In risposta ai requisiti di isolamento dalle vibrazioni verticali e di isolamento sismico orizzontale degli edifici soprastanti le linee metropolitane, viene introdotto un sistema di isolamento tridimensionale delle vibrazioni tra la sovrastruttura e la struttura sotterranea. Tale sistema non solo può isolare la sovrastruttura dalle vibrazioni ambientali e dal rumore secondario generato durante il funzionamento quotidiano della metropolitana, ma può anche ridurre efficacemente la risposta sismica orizzontale e migliorare le prestazioni antisismiche della stessa. Per effettuare un'analisi comparativa sistematica e indagare sulle prestazioni di isolamento dalle vibrazioni verticali e orizzontali (sismiche), la tesi individua tre sistemi strutturali di isolamento a seconda della disposizione degli smorzatori viscosi nello strato di isolamento: (1) sistema puro di isolamento tridimensionale dalle vibrazioni verticali e sismiche (cioè, lo strato di isolamento non ha smorzatori viscosi); (2) sistema tridimensionale di isolamento dalle vibrazioni verticali e sismiche + smorzatori viscosi verticali; (3) sistema tridimensionale di isolamento dalle vibrazioni verticali e sismiche + smorzatori viscosi orizzontali.

Prima di tutto, partendo dall'importanza della corretta definizione delle proprietà degli edifici soprastanti le metropolitane, si esalta la rilevanza ingeneristica dello studio dei sistemi tridimensionali di isolamento delle vibrazioni verticali e sismiche, e si riassume la composizione e la classificazione di tali sistemi isolanti. Viene quindi presentato lo stato della ricerca sui dispositivi di isolamento tridimensionale delle vibrazioni e sui loro effetti sulle strutture, e vengono chiariti i principali contenuti della ricerca e i punti di innovazione del presente lavoro di tesi.

In secondo luogo, si introducono i meccanismi di riduzione delle vibrazioni verticali e sismiche orizzontali propri delle tecnologia di isolamento tridirezionali, così come i modelli di forza di richiamo e i metodi di simulazione tramite programmi ad elementi finiti (FEM) dei dispositivi di isolamento delle vibrazioni comunemente usati, dei dispositivi di isolamento sismico e dei dispositivi di smorzamento. Si fornisce, inoltre, la definizione dell'angolo di rollio(rocking), quindi si analizzano i fattori principali che influenzano l'angolo di rollio, si riassumono i metodi di valutazione delle vibrazioni del pavimento interno, che gettano le basi per l'analisi e la ricerca successive.

In terzo luogo, viene studiata la prestazione di isolamento verticale del sistema tridimensionale di isolamento delle vibrazioni verticali e sismiche della sovrastruttura. Attraverso la simulazione numerica agli elementi finiti, si studiano l'influenza della rigidità verticale dello strato di isolamento sulla risposta alle vibrazioni interne per il sistema puro di isolamento tridimensionale, l'influenza del coefficiente di smorzamento verticale e dell'indice di smorzamento degli ammortizzatori verticali sulla risposta alle vibrazioni interne della struttura per il sistema tridimensionale di isolamento + ammortizzatori viscosi verticali. Alla luce delle due diverse tipologie strutturali, partendo dal punto di vista della progettazione ingegneristica, viene fornita una gamma ragionevole di valori dei parametri.

In quarto luogo, viene studiata la prestazione di isolamento sismico orizzontale del sistema tridimensionale di isolamento delle vibrazioni verticali e sismiche della sovrastruttura. Attraverso la simulazione numerica agli elementi finiti, si studiano l'influenza della rigidità verticale dello strato di isolamento sulla risposta sismica orizzontale per il sistema puro di isolamento tridimensionale, l'influenza del coefficiente di smorzamento verticale e dell'indice di smorzamento degli ammortizzatori verticali sulla risposta sismica orizzontale per il sistema tridimensionale di isolamento + ammortizzatori viscosi verticali, e l'influenza del coefficiente di smorzamento orizzontale e dell'indice di smorzamento degli ammortizzatori orizzontali sulla risposta sismica orizzontale per il sistema tridimensionale di isolamento + ammortizzatori viscosi orizzontali. Alla luce delle tre diverse tipologie strutturali, partendo dal punto di vista della progettazione ingegneristica, viene fornito un ragionevole intervallo di valori dei parametri. Alla fine del capitolo, le prestazioni di riduzione sismica orizzontale dei diversi sistemi strutturali vengono confrontate per fornire un riferimento per la progettazione ingegneristica.

Successivamente, sulla base dei risultati della ricerca precedente, la tecnologia di isolamento tridimensionale delle vibrazioni verticali e sismiche viene applicata a un progetto di ingegneria reale, verificandone la fattibilità e l'efficacia.

Infine, l’ultimo capitolo riporta le conclusioni e alcune raccomandazioni.

Parole chiave: Edifici soprastanti linee metropolitane, struttura tridimensionale di isolamento delle vibrazioni verticali e sismiche, smorzatori viscosi, isolamento verticale delle vibrazioni, isolamento sismico orizzontale, analisi parametrica

Contents

Chapter 1 Introduction

1.1 Introduction

As a new public transportation tool in the city, the subway has greatly promoted the daily travel efficiency and has made a huge contribution to the economic development of the city. In recent years, many cities in China have begun to build rail transit, and the rail network has become increasingly dense, effectively solving ground traffic congestion, automobile exhaust pollution and many other problems, and improving the level of safety and travel efficiency for citizens.

The subway can bring many conveniences to citizens' lives. However, as the rural population migrates to the cities in large numbers, the urban population density is increasing, the urban buildings are increasingly concentrated, and the utilization rate of urban space is increasing. Based on the above background, many real estate developers are beginning to develop property above the running track, metro depots and subway stations. The building functions include commerce, residential, office, school, hospital, etc. This type of building is called "over-track building".

With the acceleration of the urbanization process in the world, the property development of over-track buildings is of great significance:

(1) Using urban space efficiently, avoiding waste of land resources, and enriching the urban layout.

(2) Integrating the public transportation space with the space for commercial, residential, office, etc., to provide convenience for citizens' lives.

(3) Increasing the income of subway companies and encouraging more cities to invest in subway construction.

1.2 Vibration and seismic isolation method for over-track buildings

1.2.1 Vibration and seismic isolation demand

The vibration and seismic isolation demand of over-track buildings is mainly reflected in the daily vertical subway vibration isolation and horizontal seismic isolation.

On the one hand, because the surrounding environmental vibration and secondary noise pollution are easily caused during the subway operation, people living in the over-track buildings often face some certain degree of health problems [1-3]. At the same time, severe environmental vibration will also have an adverse effect on the structure [4-7] and the precise instruments and equipment inside [8-10]. The environmental vibration isolation of the over-track buildings is imminent.

On the other hand, buildings built above the metro depots and subway stations often set the underground part as the subway operation area, and there is often a large span, while the above ground part is set as residential, commercial areas, generally with a small span, as shown in Figure 1.1. Therefore, it is difficult for the vertical load-bearing members of the upper structure to extend to the earth, which will often lead to uneven lateral stiffness of the overall structure and insufficient seismic performance [11]. The over-track buildings located in high-intensity zone shall adopt seismic isolation technology to reduce the seismic response.

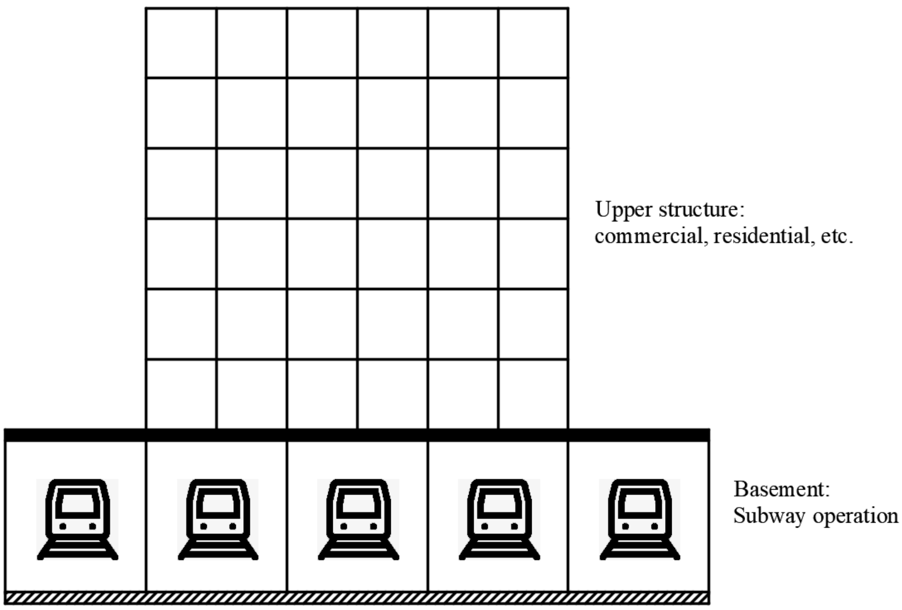

Figure 1.1 Common property development patterns of over-track buildings

1.2.2 Vertical vibration isolation method

The most effective way to isolate vertical subway vibration is to introduce a vibration isolation layer at the base or the bottom of the upper structure. The vertical natural period of the isolated system will be prolonged due to the low vertical stiffness of spring bearings in the vibration isolation layer [12, 13]. Currently the commonly used vertical vibration isolation bearings include steel springs, disc springs and laminated thick rubber bearings. Through frequency domain analysis of the environmental vibration caused by subway operation, it can be seen that the dominant frequency band of subway vibration is 40~220Hz. While the vertical natural frequency of the spring vibration isolation system is between 1~3.5Hz, which obviously deviates from the dominant frequency band of subway vibration wave, indicating that the isolated system can effectively isolate the environmental vibration caused by subway operation.

1.2.3 Horizontal seismic isolation method

There are mainly three structural systems to isolate horizontal earthquakes: energy dissipation structure, horizontal seismic isolation structure, and 3-D vibration and seismic isolation structure, as shown in Figure 1.2.

Both the energy dissipation structure (Figure 1.2a) and the horizontal seismic isolation structure (Figure 1.2b) are equipped with energy dissipation devices in the main structure to dissipate or isolate the seismic energy inputted into the structure, thereby improving the aseismic performance of the structure. These two types of structures have a high safety guarantee performance, when repairing after the earthquake, only the damaged energy-consuming members should be replaced [14, 15]. At present, it has gradually been widely used in real engineering design.

Currently, the design of seismic mitigation and isolation of structures generally only considers the horizontal seismic action, and does not consider or calculate the vertical seismic action equivalently according to the representative value of the vertical gravity load. However, in recent years, from the seismic acceleration waves and seismic damage data recorded in the Tangshan Earthquake, Wenchuan Earthquake, Hanshin Earthquake and other major earthquakes[16, 17], in high-intensity areas, especially in areas close to geological faults, the vertical seismic action component is quite strong, and may even exceed the horizontal component, which becomes the main reason for the collapse and damage of the structure. At the same time, many buildings with high safety levels, such as nuclear power facilities, high-speed reactors, large precise laboratories, etc., must be ensured that there is almost no damage of internal facilities under the action of horizontal and vertical earthquakes. The higher requirements for non-structural damage control have been put forward for these important buildings. Based on these demands, researchers proposed a three-dimensional seismic isolation structure (Figure 1.2c), that is, by setting up a three-dimensional seismic isolation layer with very small horizontal and vertical stiffness, the horizontal and vertical natural periods of the structure can be prolonged to achieve the features of isolating both the horizontal and vertical seismic actions at the same time.

In addition, the three-dimensional seismic isolation structure has a perfect performance of isolating the vertical subway vibration. Due to the reduction of the vertical stiffness of the isolation layer, the natural frequency of the structure deviates further from the dominant frequency of subway vibration, thereby reducing the vibration response in the building. In the end, the three-dimensional seismic isolation structure becomes the “3-D vibration and seismic isolation structure”.

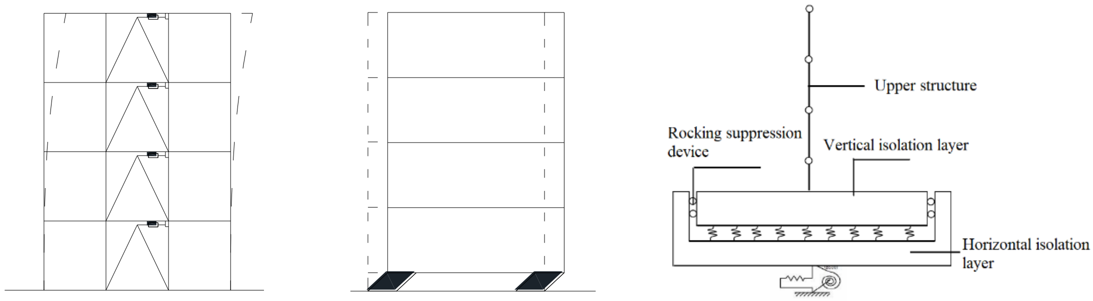

(a) Energy dissipation structure (b) Horizontal seismic isolation structure (c) 3-D vibration and seismic isolation structure

Figure 1.2 Aseismic structural system

1.3 3-D vibration and seismic isolation structure

1.3.1 Composition of the 3-D vibration and seismic isolation structure

The layout of the 3-D vibration and seismic isolation structure system applied to the over-track buildings is shown in Figure 1.3. The underground story belongs to the subway operation area, the upper stories are used for residential, commercial, etc. A three-dimensional vibration and seismic isolation layer is set between the underground story and the upper stories.

The 3-D vibration and seismic isolation layer is composed of the horizontal seismic isolation devices (used to reduce the horizontal stiffness of the 3-D isolation layer) and the vertical vibration isolation devices (used to reduce the vertical stiffness of the 3-D isolation layer). The research on horizontal seismic isolation devices is very mature, including natural rubber bearings, lead rubber bearings, high damping rubber bearings, and skateboard bearings. The vertical vibration isolation devices include steel spring bearings, disc spring bearings, laminated thick rubber bearings and air spring bearings.

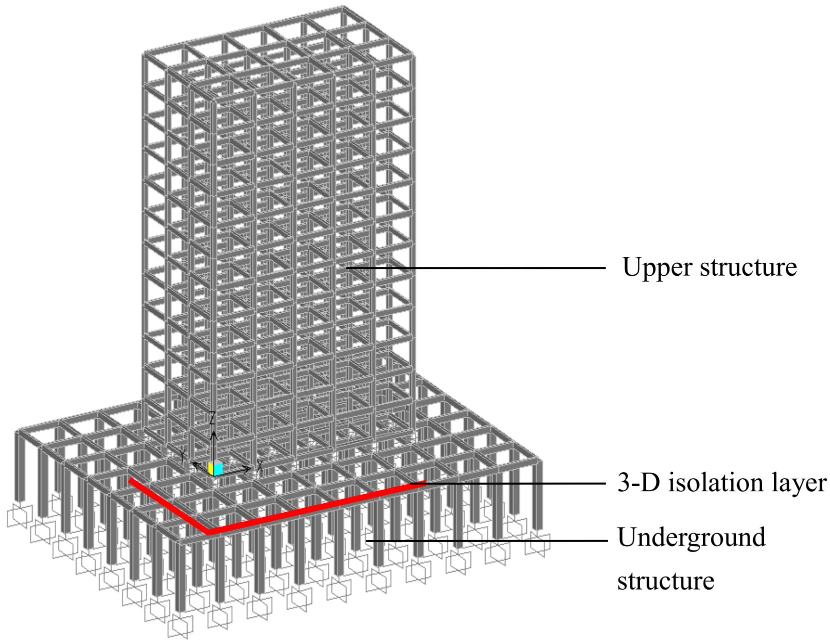

Figure 1.3 Layout of the 3-D vibration and seismic isolation structure

The tandem 3-D vibration and seismic isolation device connects the horizontal seismic isolation device and the vertical vibration isolation device in series through the connecting plate, thus has both horizontal seismic isolation and vertical vibration isolation capacity, as shown in Figure 1.4. This bearing connects the horizontal rubber bearing and the vertical disc spring in series, and uses a vertical sliding guide to limit the horizontal deformation of the disc spring, so that the horizontal seismic isolation and vertical vibration isolation performance are decoupled. At the same time, the vertical viscous dampers can be selectively introduced in parallel with the disc spring to further suppress the rocking effect of the upper structure and enhance the seismic energy dissipation capacity of the structure [18].

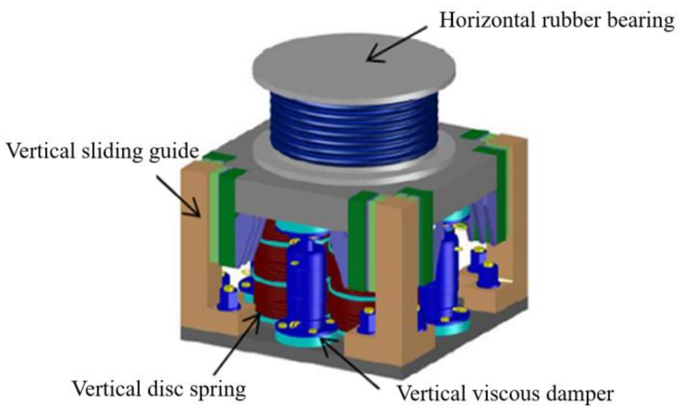

Figure 1.4 Schematic diagram of the tandem 3-D vibration and seismic isolation bearing

Based on the 3-D vibration and seismic isolation bearing shown in Figure 1.4, this thesis studies the pure 3-D vibration and seismic isolation structure, the 3-D vibration and seismic isolation + vertical viscous dampers in the isolation layer structure, and the 3-D vibration and seismic isolation + horizontal viscous dampers in the isolation layer structure, tries to figure out the response of the upper structure under the action of the subway vibration acceleration wave and the seismic acceleration wave.

1.3.2 Research status of 3-D vibration and seismic isolation technology

In recent years, the research on 3-D vibration and seismic isolation technology has mainly focused on the development of new 3-D vibration and seismic isolation bearings, the shaking table tests, and numerical simulation of the 3-D vibration and seismic isolation structures. In Japan and the United States, the 3-D vibration and seismic isolation technology has been applied in many nuclear power plants, reactors, high-speed furnaces and other high-safety buildings with special seismic isolation demands, which can effectively reduce the horizontal and vertical seismic response of the structure and ensure the structural and non-structural facilities inside the buildings intact under severe earthquakes. In addition, buildings with special vibration isolation demands such as chip factories and precise laboratories also use this technology to isolate surrounding environmental vibration and ensure the high-precision operation of the internal equipment, and reduce the seismic response in the meanwhile.

1.3.2.1 3-D vibration and seismic isolation bearings

Based on the traditional rubber isolation bearings, researchers have created a laminated thick rubber bearing by increasing the thickness of the rubber layer of the traditional bearing, which has both horizontal and vertical isolation performance. Through static, dynamic and fatigue tests, Yabana et al.[19] explored the influence of the first shape factor, second shape factor, and vertical ultimate compressive stress of the laminated thick rubber bearing on the mechanical properties, and found that the laminated thick rubber bearing has the same isolation performance as the 3-D vibration and seismic isolation bearing. Kanazawa et al.[20] applied the laminated thick rubber bearing to the structural model of a fast nuclear reactor. Through the shaking table tests, it was found that the 3-D vibration and seismic isolation structure can both effectively reduce the horizontal and vertical seismic response.

Uriu et al.[21] proposed a new type of 3-D vibration and seismic isolation device shown in Figure 1.5. The system consists of a laminated rubber bearing at the bottom and a vertical air spring at the top. The vertical ground vibration and vertical earthquake are isolated by air springs, and the horizontal earthquake is isolated by rubber bearings. At the same time, vertical viscous dampers are arranged in other positions of the 3-D isolation layer to control structural rocking. Suhara et al.[22] proposed a 3-D air spring isolation bearing with a vertical guide rail shown in Figure 1.6. A steel or concrete cylinder is embedded in the air cavity and can slide up and down along the rubber guide rail to form an air spring. The upper part of the cylinder is connected with a rubber bearing, and the right side of the system is equipped with an inflation device and a leveling device. In addition, many foreign scholars have proposed a variety of improved hydraulic or air spring 3-D isolation devices. For example, Kageyama et al.[23] proposed an air spring isolation device reinforced by polyester fiber fabric and pre-stressed cables, Kashiwazaki et al.[24] proposed a hydraulic 3-D vibration and seismic isolation bearing.

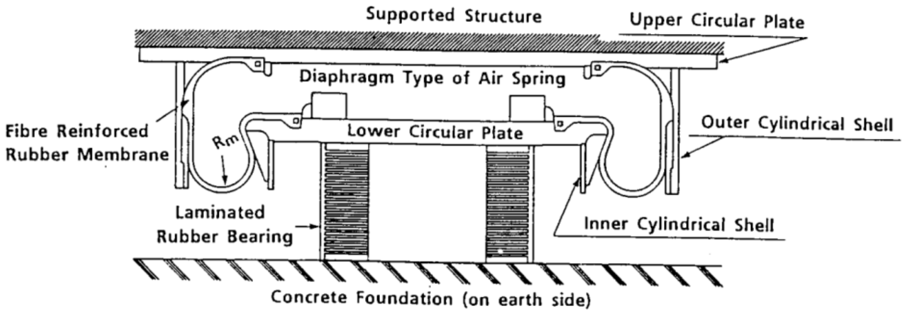

Figure 1.5 Air spring 3-D vibration and seismic isolation device

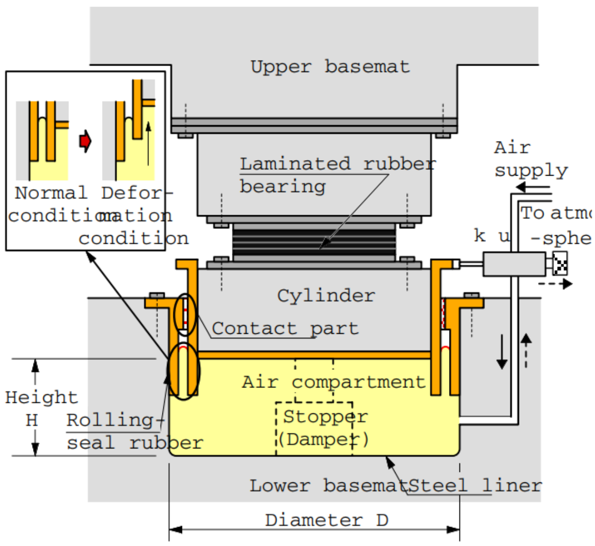

Figure 1.6 Air spring 3-D vibration and seismic isolation device with a vertical guide rail

In China, Xiong Shishu et al.[25] proposed a new type of 3-D vibration and seismic isolation bearing. It is composed of a lead rubber bearing and a disc spring in series, and damping material is arranged in parallel with the vertical spring to control the rocking effect of the structure effectively. The damping material can reduce both the horizontal and vertical seismic response. Wei Lushun et al.[26] proposed a 3-D isolation device in which horizontal isolation bearings, disc springs and connecting plates are arranged in series. Wang Wei et al.[27] proposed a new type of 3D-MIB bearing in which the lead rubber bearing, disc spring and vertical guide rail are connected. Guo Yangzhao et al.[28] studied the working principle and design theory of an LRB-DSB 3-D isolation bearing.

1.3.2.2 Engineering applications of the 3-D isolation structure

Table 1.1 Engineering applications of some 3-D isolation structures

Type	Project	Horizontal seismic mitigation and isolation device	Vertical seismic and vibration isolation device
High safety level buildings	A sodium-cooled fast reactor in Japan[29]	Rubber bearing and viscous damper	Disc spring and viscous damper
	A nuclear reactor in Japan[30-32]	Laminated rubber bearing and viscous damper	Disc spring and viscous damper
	A fast nuclear reactor plant in Japan	Air spring	Spiral steel spring with negative rigidity rod
	A chip manufacturing factory in Japan[33]	Rubber bearing and viscous damper	Spiral steel spring and viscous damper
Over-track buildings	An over-track residential building in Japan[34]	Lead laminated thick rubber bearing	
	A residential building in Los Angeles, USA[35]	Viscous damper	Spiral steel spring
	Shanghai Opera House[36]	Viscous damper	Spiral steel spring
	Beijing Bawangfen subway station[37]	Laminated rubber bearing and natural rubber bearing	Multilayer rubber bearing
	Beijing East Dianmen subway station[38]	Steel spring vibration and seismic isolation device	

The development and experimental research of 3-D isolation devices have been relatively mature, but due to the high cost of 3-D isolation bearings, the difficulty of construction, and the lack of corresponding design codes, there is few application opportunities of 3-D isolation structure. However, when it comes to the high safety level structures and the over-track buildings that require vertical subway vibration isolation, the 3-D isolation structure has advantages which other structural systems cannot replace. Table 1.1 lists the engineering applications of some 3-D isolation structures.

1.3.2.3 Rocking effect of the 3-D isolation structure

Although the 3-D isolation structure has good vertical vibration and horizontal seismic isolation performance, as the vertical stiffness of the isolation layer decreases, or the height / aspect ratio of the structure increases, the rigid rocking effect of the upper structure will appear under the action of horizontal earthquakes.

Tomita et al.[39] used a 2-D simplified model to study the influence of the eccentricity between the center of gravity and rigidity in the isolation layer on the structural rocking effect, and found that as long as the vertical eccentricity is less than 5%, there is no need to introduce additional rocking suppression devices in the isolation layer. Zhou et al.[40] applied the 3-D isolation bearings with different vertical stiffness to a nuclear power plant model and found that when the vertical natural frequency of the structure is lower than 1 Hz, the structure will have a serious overall rocking effect. Mori et al.[41] applied a 3-D vibration and seismic isolation device with vertical viscous dampers in the isolation layer to a civil building, and conducted free vibration tests on a 3-D isolation structure without vertical damping and a 3-D isolation structure with vertical damping. It is found that the rocking effect of the 3-D isolation structure with vertical damping is effectively controlled.

1.4 Research contents and innovations

The main research content of this thesis includes the following aspects:

(1) Chapter 2 introduces the vibration mitigation and seismic mitigation mechanism of the 3-D vibration and seismic isolation structure, summarizes the constitutive models and finite element software simulation methods of commonly used seismic and vibration isolation devices, and proposes the key problem of 3-D isolation structures — rocking effect, and finally summarizes the indoor vibration evaluation standards.

(2) Chapter 3 studies the vertical vibration isolation performance of the 3-D vibration and seismic isolation structure, analyzes the influence of the vertical

stiffness of the isolation layer on the indoor vibration response of the pure 3-D vibration and seismic isolation structure, and the influence of the vertical damping coefficient and damping index of vertical dampers on the indoor vibration response of the 3-D vibration and seismic isolation + vertical viscous dampers structure.

(3) Chapter 4 studies the horizontal seismic isolation performance of the 3-D vibration and seismic isolation structure, analyzes the influence of the vertical stiffness of the isolation layer on the horizontal seismic response of the pure 3-D vibration and seismic isolation structure, the influence of the vertical damping coefficient and damping index of vertical dampers on the horizontal seismic response of the 3-D vibration and seismic isolation + vertical viscous dampers structure, and the influence of the horizontal damping coefficient and damping index of horizontal dampers on the horizontal seismic response of the 3-D vibration and seismic isolation + horizontal viscous dampers structure.

(4) Chapter 5 applies the 3-D vibration and seismic isolation structural system to the Shanghai Jinqiao over-track building, and compares it with the traditional rigid structural system to verify the feasibility and effectiveness of the 3-D vibration and seismic isolation technology.

This thesis mainly has the following innovations:

(1) Conduct a systematic parameter study on the rocking effect of 3-D isolation buildings, put forward the concepts of rocking angle and unfavorable inter-story drift angle, and verify several main factors influencing the rocking effect of the upper structures.

(2) Considering the vertical vibration isolation and horizontal seismic isolation requirements of the over-track buildings, it is recommended that the control of the inter-story drift angle of the 3-D isolation structure should refer to the unfavorable inter-story drift angle, rather than the traditional real inter-story drift angle.

(3) From the perspective of engineering design, carry out a comprehensive and systematic parameter study of the pure 3-D vibration and seismic isolation structure, the 3-D vibration and seismic isolation + vertical viscous dampers structure, and the 3-D vibration and seismic isolation + horizontal viscous dampers structure. The recommended value of parameters for engineering design is given, which provides references for the 3-D vibration and seismic isolation structural design.

Chapter 2 Working mechanism and analytical method

2.1 Vibration and seismic mitigation mechanism

2.1.1 Vibration mitigation mechanism

Since the vertical stiffness of the 3-D isolation layer is much lower than that of the upper structure, the whole system can be equivalent to a single degree of freedom vibration system in the vertical direction, as shown in Figure 2.1. Where, *k* is the total vertical stiffness of the isolation layer, *c* is the vertical damping of the isolation layer, *m* is the total weight of the upper structure, u_b is the base displacement input of the subway vibration, and *u(t)* is the displacement response of the upper structure.

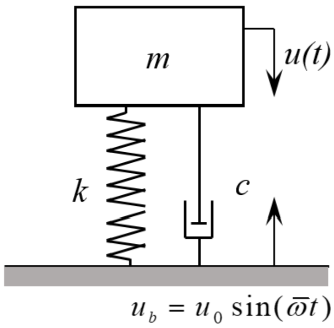

Figure 2.1 Schematic diagram of a single-degree-of-freedom vibration isolation system

The differential equation for vertical structural vibration is:

$$m\ddot{u} + c(\dot{u} - \dot{u_b}) + k(u - u_b) = 0 \tag{2.1}$$

Assuming that the base displacement excitation is a sine function $u_b = u_0 \sin(\varpi t)$, the frequency ratio μ is defined as the ratio of the base excitation frequency f_e to the natural vibration frequency f_0 of the system:

$$\mu = f_e/f_0 \tag{2.2}$$

Where, the base excitation frequency is $f_e = \overline{\omega}/2\pi$, the natural vibration frequency is $f_0 = \sqrt{k/m}/2\pi$.

Then the steady-state vibration amplitude u_m can be obtained:

$$u_m = u_0 \sqrt{\frac{1 + 4D^2\mu^2}{(1-\mu^2)^2 + 4D^2\mu^2}} \tag{2.3}$$

The transmission ratio V_f is defined as:

$$V_f = \frac{u_m}{u_0} = \sqrt{\frac{1 + 4D^2\mu^2}{(1-\mu^2)^2 + 4D^2\mu^2}} \tag{2.4}$$

Where, the damping ratio of the system is $D = c/2\sqrt{km}$.

The vibration isolation efficiency is defined as η:

$$\eta = 1 - V_f \tag{2.5}$$

Based on equation 2.4, the transmission ratio curve of a single-degree-of-freedom vibration isolation system can be drawn as shown in Figure 2.2. It can be seen from the figure that when the frequency ratio is less than $\sqrt{2}$, the transmission ratio is always larger than 1, indicating that the base vibration is amplified; when the frequency ratio of the system is close to 1, the transmission ratio is far greater than 1 due to resonation, and the vibration response of the upper structure is violent; when the frequency ratio is greater than $\sqrt{2}$, the transmission ratio is less than 1, and the system begins to have the capacity of vibration isolation.

The vibration isolation efficiency of a SDOF system is mainly affected by the frequency ratio and the system damping ratio. When the frequency ratio is greater than $\sqrt{2}$, as the frequency ratio increases, the transmission ratio decreases and the vibration isolation efficiency increases. When the frequency ratio is greater than $\sqrt{2}$, as the system damping ratio increases, the transmission ratio increases and the vibration isolation efficiency decreases.

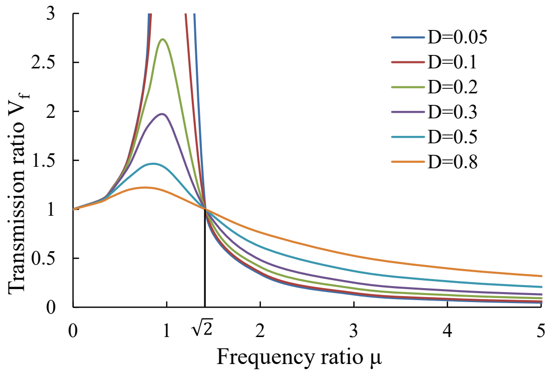

Figure 2.2 The transmission ratio curve of a single-degree-of-freedom vibration isolation system

Table 2.1 shows the vibration isolation efficiency of a system without vertical damping in the isolation layer under different frequency ratios. It can be seen that the greater the frequency ratio, the larger the vibration isolation efficiency.

The vertical natural frequency of high-rise 3-D isolation structures is usually between 0.8 and 2.0 Hz, while the main frequency of vibration caused by subway is generally between 40 and 200 Hz, the frequency ratio is much greater than $\sqrt{2}$, so the 3-D vibration and seismic isolation structure can effectively isolate the vertical subway vibration.

Table 2.1 Vibration isolation efficiency of a single-degree-of-freedom vibration isolation system

Frequency ratio μ	$\sqrt{2}$	2	3	4	5
Vibration isolation efficiency η (%)	0	66.7	87.5	93.3	95.8

2.1.2 Seismic mitigation mechanism

The seismic mitigation mechanism of the 3-D isolation structure is mainly reflected in two aspects: natural period prolonging effect and additional damping effect. Since the horizontal stiffness of the isolation layer is generally much smaller than the lateral stiffness of the upper structure, the horizontal natural period of the 3-D isolation structure is extended, and reaches far away from the site characteristic period, which can effectively reduce the horizontal seismic response of the upper structure. At the same time, the seismic isolation devices and the damping devices dissipate energy through repeated movements under the action of earthquakes, which can provide an additional damping ratio to the overall system, and thereby reduce the seismic response of the structure.

From the design response spectrum in the codes, one can intuitively see the influence of natural period prolonging effect and additional damping effect on the 3-D isolation structure, as shown in Figure 2.3. With the prolonging of the natural period and the increase of the damping ratio, the seismic effect coefficient keeps decreasing, and the seismic response of the structure decreases.

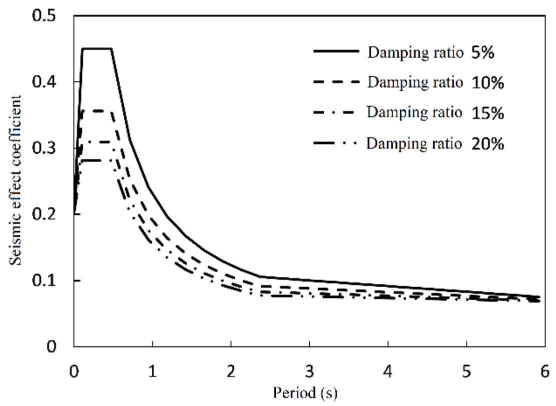

Figure 2.3 Design response spectra under different damping ratios

2.2 Constitutive model and simulation method of isolation and damping devices

2.2.1 Constitutive model and simulation method of isolation devices

The horizontal seismic isolation devices usually used in 3-D isolation bearings mainly include: natural rubber bearings, lead rubber bearings. And the vertical vibration isolation devices usually use disc spring.

2.2.1.1 Rubber bearings

The force-displacement models of natural rubber bearings and lead rubber bearings are shown in Figure 2.4 and Figure 2.5 respectively. The area enclosed by the hysteresis curve of the lead rubber bearing is quite large in Figure 2.5(a), indicating that the lead rubber bearing has a perfect capacity of dissipating seismic energy.

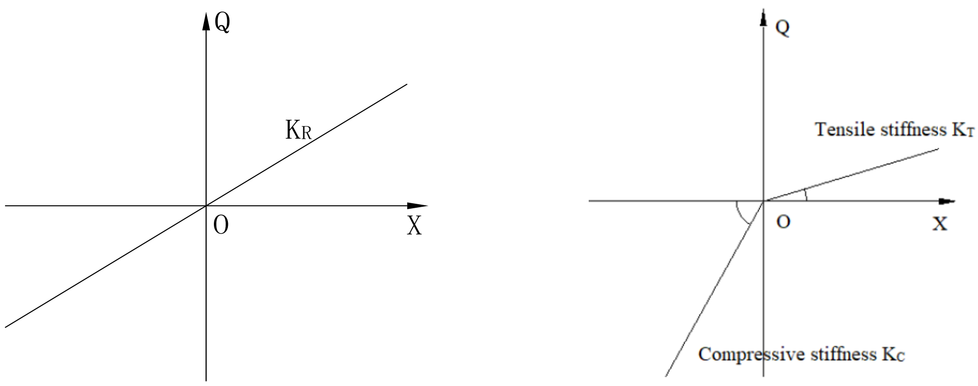

(a) Constitutive model for shear force (b) Constitutive model for axil force

Figure 2.4 The force-displacement models of natural rubber bearings

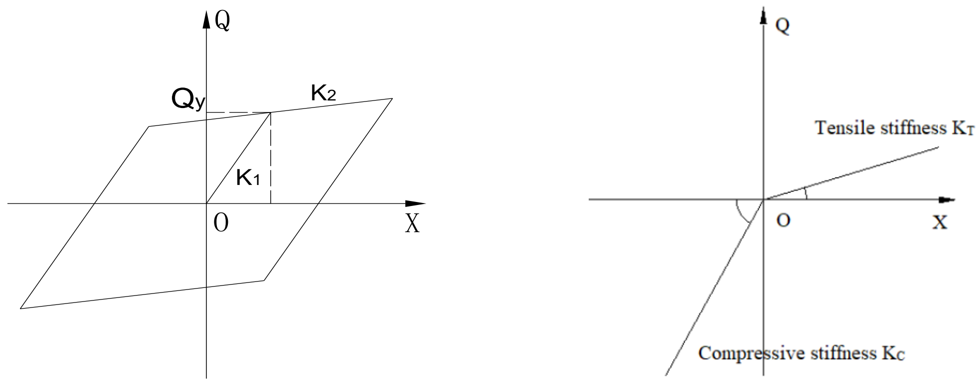

(a) Constitutive model for shear force (b) Constitutive model for axil force

Figure 2.5 The force-displacement models of lead rubber bearings

In the structural finite element analysis software SAP2000, the horizontal shear restoring force model of natural rubber bearings and lead rubber bearings can be simulated by the "Rubber Isolator" element, and the vertical axial restoring force model can be simulated by the combination of "Rubber Isolator + Gap" elements.

2.2.1.2 Disc spring

The geometry of a single disc spring is shown in Figure 2.6. In practical applications, several disc springs are often stacked in pairs to form a disc spring group, as shown in Figure 2.7. The vertical axial restoring force model of the disc spring group is shown in Figure 2.8.

In the structural finite element analysis software SAP2000, the vertical axial restoring force model of the disc spring group can be simulated by the "Linear" element.

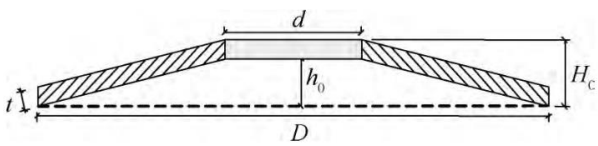

Figure 2.6 Geometry of a single disc spring

Figure 2.7 A disc spring group

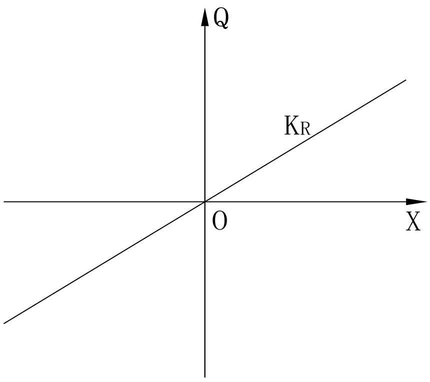

Figure 2.8 The vertical axial force-displacement model of a disc spring group

2.2.2 Constitutive model and simulation method of damping devices

The damping device usually used in 3-D isolation layer is mainly viscous damper. The most used axial restoring force model of viscous dampers is Maxwell model, as shown in Figure 2.9. This model includes two elements in series: ideal spring and ideal sticky pot. The ideal spring is used to simulate elastic deformation, while the ideal sticky pot is used to simulate viscous deformation. The relationship between axial force and axial displacement is shown in equation 2.6:

$$f = kd_k = cv^{\alpha} \qquad (2.6)$$

Where, k is the stiffness of the spring element, c is the damping coefficient of the damping element, α is the damping index of the damping element, d_k is the deformation of spring element, and v is the deformation speed of the sticky pot element.

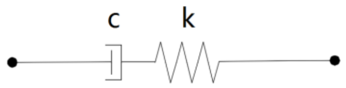

Figure 2.9 Composition of the Maxwell model used for viscous dampers

In the structural finite element analysis software SAP2000, the viscous dampers can be simulated by the "Damper" element.

2.3 Rocking effect of 3-D vibration and seismic isolation structure

2.3.1 Introduction of rocking effect

The rocking effect of a 3-D isolation structure is caused by the deviation between the application point of the seismic load and the restoring force of the isolation layer. This deviation will produce overturning moment applied on the isolation layer. Because the vertical stiffness of the isolation layer is low, the entire upper structure will rotate rigidly under the action of the overturning moment. Therefore, if the length of the deviation increases, or the vertical stiffness of the isolation layer decreases, the rocking effect of the upper structure will increase.

In the traditional horizontal seismic isolation structure, the vertical stiffness of the isolation layer is much higher than the horizontal stiffness, and the aspect ratio of the building is small, so the rocking effect will hardly occur. However, in the 3-D isolation structure, the vertical stiffness of the isolation layer is much lower than that of the horizontal seismic isolation structure. The overall rocking effect of the upper structure will significantly aggravate the horizontal displacement response of floors, which must be paid great attention to in real engineering design.

Take one high-rise over-track building as an example, the finite element analysis model is shown in Figure 2.10. The analytical model adopts reinforced concrete frame structure system. The basement platform has a height of 11m used for the operation of subway; the upper structure has 12 stories and the standard story height is 5m used for daily living. The total height of the structure is 60m. The standard story of the upper structure has 5 spans in the X direction, 3 spans in the Y-direction, and each span is 8m. The thickness of the floor slab in the standard story is 120mm, and 200mm in the basement. The upper standard story has a dead load of 5kN/m^2 and a live load of 3 kN/m^2. The seismic fortification intensity is 8 degrees (0.3g), the design earthquake group is Group 3, the site category is Class II, and the site characteristic period is 0.45s.

The analytical model adopts three structural systems respectively to carry out seismic time history analysis: 3-D vibration and seismic isolation system (3DISO), horizontal seismic isolation system (HISO) (with the same layout and parameters of rubber bearings), 3-D vibration and seismic isolation + vertical viscous dampers in the isolation layer system (3DISOVD). The rotation angles of each floor are shown in Figure 2.11. It can be seen that, compared with HISO structure, 3DISO and 3DISOVD structures have an almost equal increase in the rotation angle of each floor, which is due to the rigid rocking of the upper structure.

Based on Figure 2.11, one can define the average value of the increase in the story rotation angles of the 3-D isolation structure relative to the horizontal seismic isolation structure as the rocking angle. It can be seen that the vertical dampers in the 3-D isolation layer can significantly reduce the rocking effect of the upper structure.

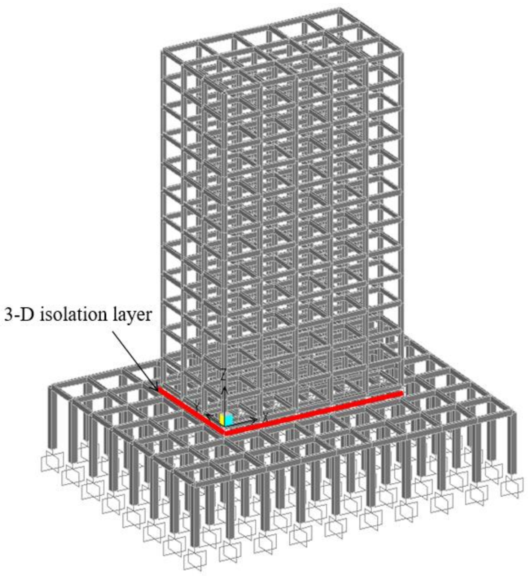

Figure 2.10 Structural model in SAP2000

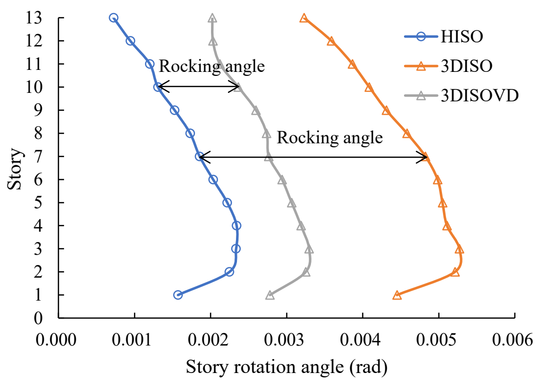

Figure 2.11 Story rotation angle of three systems

The rocking effect of a 3-D isolation structure will increase the inter-story drift angle and the lateral displacement of top floor in the upper structure under the action of horizontal earthquakes. At the same time, it also puts forward higher requirements for the structure's wind-vibration comfort level. The composition of inter-story drift angle of the 3-D isolation structure is shown in equation 2.7:

$$\theta_{real} = \theta_{rigid} + \theta_{danger} \tag{2.7}$$

Where, θ_{real} is the real inter-story drift angle of the structure, θ_{rigid} is the rigid rocking angle, θ_{danger} is the unfavorable inter-story drift angle which will cause inter-story shear in the structure.

2.3.2 Prediction of the rocking angle

The derivation diagram of the rocking angle is shown in Figure 2.12. Assuming that the upper structure rotates rigidly under the action of horizontal earthquakes, the rotation angle is θ. The seismic action is simplified as the equivalent seismic load F_{ek} acting in the middle of the building, which will cause the horizontal restoring force F_{iso} in the isolation layer. The deviation between the application points of these two forces produces a base overturning moment M_{ek}, which will cause the resisting moment M_{iso} and the axial restoring force $f_{ed,i}$ of the 3-D isolation bearings in the isolation layer.

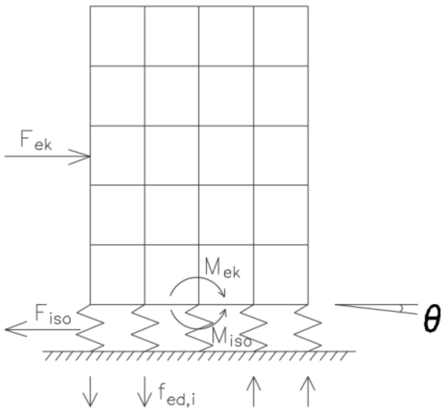

Figure 2.12 Derivation diagram of the rocking angle

$$M_{ek} = F_{ek} \cdot 0.5H = BHm\alpha_{max} \cdot 0.5H \tag{2.8}$$

$$M_{iso} = \sum k_i(\theta L_i)L_i \tag{2.9}$$

According to $M_{ek} = M_{iso}$, one can obtain:

$$\theta = \frac{BH^2}{\sum k_i {L_i}^2} \cdot 0.5m\alpha_{max} \tag{2.10}$$

Where, B is the width of the building, H is the height of the building, m is the representative value of vertical gravity load in a unit volume of the building, α_{max}

is the seismic effect coefficient, k_i is the vertical stiffness of the i-th 3-D isolation bearing, L_i is the distance between the position of the i-th isolation bearing and the rigid centroid of the isolation layer.

It can be seen from Equation 2.10 that the rocking angle is related to the vertical stiffness of the isolation bearings, the total height of the building, the aspect ratio of the building, and the layout of the 3-D isolation layer.

2.3.3 Influencing factors of rocking angle

Adopt the same analytical model in section 2.3.1, and take the fortification seismic response of the upper structure as an example to verify several main factors influencing the rocking angle.

2.3.3.1 Vertical stiffness of the 3-D isolation layer

It can be seen from Equation 2.10 that the rocking angle is approximately inversely proportional to the vertical stiffness of the isolation layer. In this section, 6 comparison cases are analyzed. The plane layout of the 3-D isolation layer is the same for 6 cases, as shown in Figure 2.13. The vertical stiffness of the isolation layer and the vertical natural frequency of the structure are shown in Table 2.2. In all 6 cases, the layout of the upper structure and the total horizontal stiffness of the isolation layer keep unchanged.

Table 2.2 Parameters of different cases

Case	Vertical stiffness of the isolation layer (kN/mm)	Vertical natural frequency of the structure (Hz)
1	417	0.84
2	626	1.02
3	1043	1.30
4	2085	1.78
5	3128	2.11
6	4171	2.37
HISO	102416	4.96

The story rotation angle and rocking angle of the comparison cases are shown in Figure 2.14 and Figure 2.15. The ratio of the rocking angle to the maximum inter-story drift angle is shown in Figure 2.16. It can be seen that as the vertical total stiffness of the isolation layer decreases, the vertical natural frequency of the structure decreases, the rocking angle increases, and is approximately inversely proportional to the vertical stiffness of the isolation layer. At the same time, the ratio of the rocking angle to the maximum inter-story drift angle also increases.

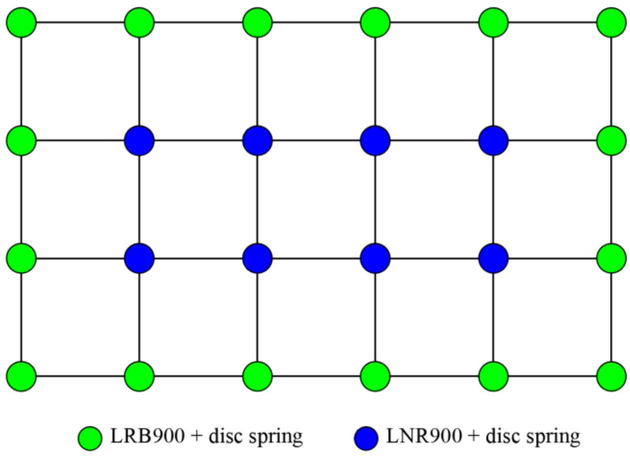

Figure 2.13 The plane layout of 3-D vibration and seismic isolation bearings

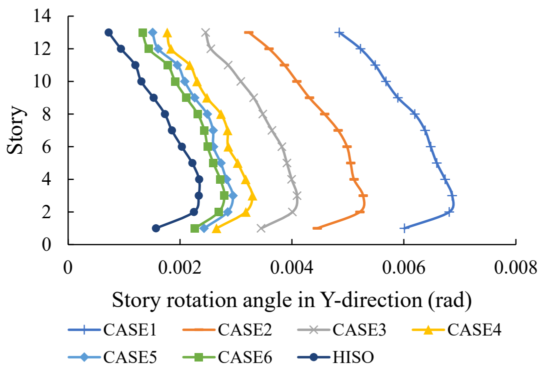

Figure 2.14 Story rotation angle of 6 cases

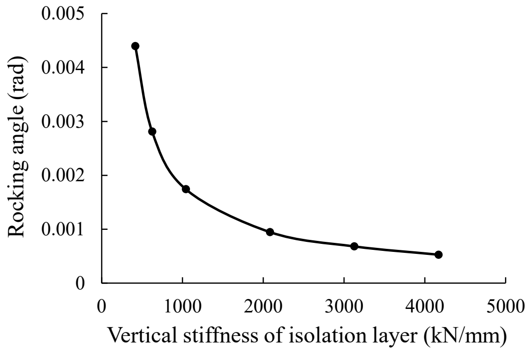

Figure 2.15 Rocking angle of 6 cases

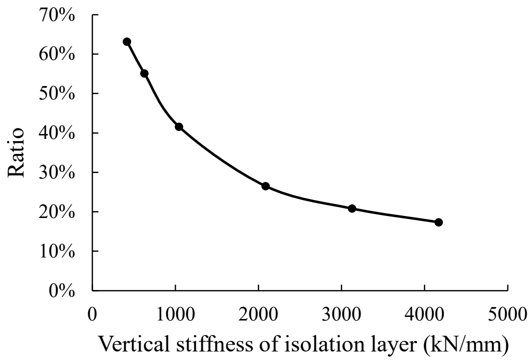

Figure 2.16 Ratio of the rocking angle to the maximum inter-story drift angle of 6 cases

2.3.3.2 Aspect ratio

In this section, 5 comparison cases are analyzed. Keeping the vertical stiffness of each 3-D isolation bearing and the total height of the building H = 60m unchanged, the layout of the isolation layer of different cases is shown in Figure 2.17, and the aspect ratio of the building in X-direction is shown in Table 2.3, the relative error of the vertical natural frequency between 5 cases is within 8%.

Table 2.3 Parameters of different cases

Case	Aspect ratio in X-direction	Vertical natural frequency of the structure (Hz)
1	1.25	1.01
2	1.5	1.02
3	1.875	1.03
4	2.5	1.06
5	3.75	1.10

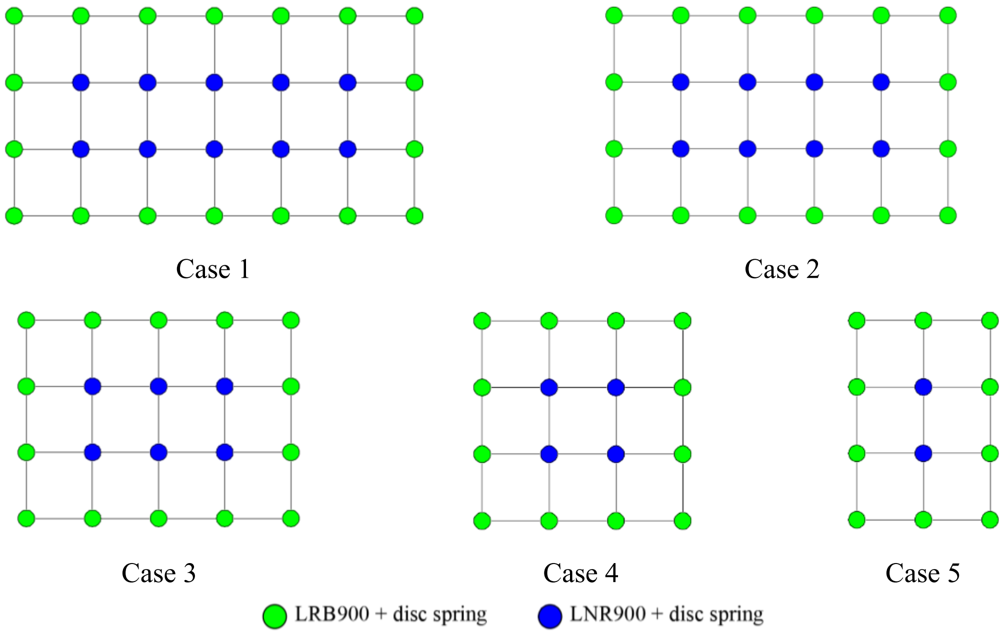

Figure 2.17 The plane layout of 3-D vibration and seismic isolation bearings in 5 cases

The story rotation angle and rocking angle of the comparison cases are shown in Figure 2.18 and Figure 2.19. The ratio of the rocking angle to the maximum inter-story drift angle is shown in Figure 2.20. It can be seen that the rocking angle of the upper structure increases linearly with the aspect ratio, which is consistent with the theoretical derivation in Section 2.3.2, and the ratio of the rocking angle to the maximum inter-story drift angle also increases with the structural aspect ratio.

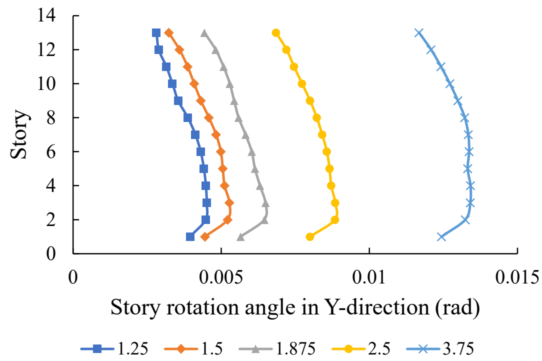

Figure 2.18 Story rotation angle of 5 cases

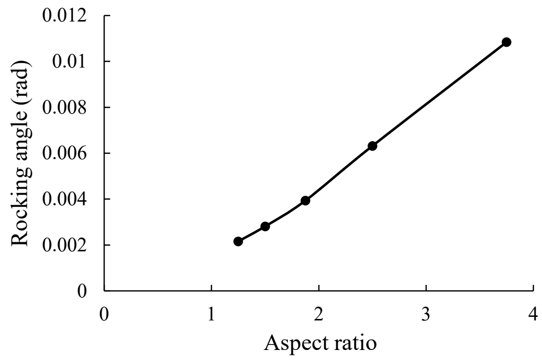

Figure 2.19 Rocking angle of 5 cases

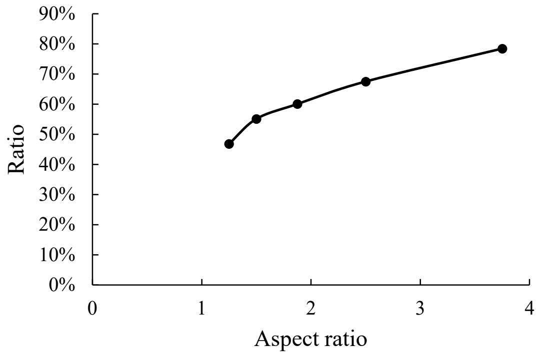

Figure 2.20 Ratio of the rocking angle to the maximum inter-story drift angle of 5 cases

2.4 Vibration evaluation standards

2.4.1 Vertical peak acceleration

Under the excitation of the subway vibration wave, the comparison between the vertical peak acceleration in the 3-D isolation structure and the unisolated structure can be very clear and useful, and the calculation method is very simple. The ratio of the vertical peak acceleration in the 3-D isolation structure to that in the unisolated structure can be used as the initial reference data for vibration isolation design. Generally speaking, if the ratio is below 10%, the vibration isolation structure has a good performance in isolating environmental vibration.

2.4.2 Z vibration level

According to the design code "Standard of vibration in urban area environment" GB10070-88[42], the vibration acceleration level:

$$L_a = 20lg(a/a_0) \tag{2.11}$$

Where, a is the effective vibration acceleration, a_0 is the calibrated vibration acceleration, generally using $a_0 = 10^{-6}$ m/s^2.

After adjusting the vibration acceleration level L_a according to the Z weighting factor, one obtaines the Z vibration level VL_z (Unit: dB):

$$VL_z = 20\lg(a'_{rms}/a_0) \tag{2.12}$$

$$a'_{rms} = \sqrt{\sum a_{frms,i}^2 \cdot 10^{0.1C_{f,i}}} \tag{2.13}$$

Where, a'_{rms} is the effective vibration acceleration in the frequency range of 1~80Hz, $a_{frms,i}$ is the effective vibration acceleration at the i-th 1/3 octave (shown in equation 2.14), $C_{f,i}$ is the Z weighting factor at the i-th 1/3 octave.

$$a_{frms,i} = \sqrt{\sum a_i{}^2} \tag{2.14}$$

According to GB10070-88, the limitations of environmental vibration are shown in Table 2.4:

Table 2.4 The limit of urban environmental vibration standard in China (VL_z: dB)

Zone	Daytime	Nighttime
Special residential	65	65
Residential, education	70	67
Mix center, business center	75	72
Industrial	75	72
Both sides of traffic arterial road	75	72
Both sides of the main railway	80	80

2.4.3 Prediction of secondary noise

According to the design code "Standard for limit and measuring method of building vibration and secondary noise caused by urban rail transit" JGJ/T170-2009[43], when predicting the secondary radiation noise of the structure, the equivalent A-weighted sound pressure level L_{Aeq} (unit: dB) in the frequency range of 16~200Hz is used as the evaluation quantity. The calculation formula of the equivalent A-weighted sound pressure level is as follows:

$$L_{Aeq} = 10\lg(\sum 10^{0.1(L_{p,i}(f_i)-C_{f,i})}/12) \tag{2.15}$$

$$L_{p,i}(f_i) = VL_i - 20\lg(f_i) + 37 \tag{2.16}$$

Where, $L_{p,i}(f_i)$ is the unweighted sound pressure level at the i-th 1/3 octave, $C_{f,i}$ is the calibrated factor at the i-th 1/3 octave, VL_i is vibration acceleration level at the i-th 1/3 octave, f_i is the centroid frequency of the i-th 1/3 octave.

According to JGJ/T170-2009, the indoor secondary radiation noise limits are shown in Table 2.5:

Table 2.5 The limit of urban environment secondary radiation noise in China (L_{Aeq}: dB)

Zone	Daytime	Nighttime
Special residential	38	35
Residential, education	38	35
Mix center, business center	41	38
Industrial	45	42
Both sides of traffic arterial road	45	42

Chapter 3 Parameter study of vertical vibration isolation performance

3.1 Introduction

The dominant frequency band of ground vibration caused by the subway is 40~200Hz. Because the vertical stiffness of isolation layer in 3-D vibration and seismic isolation structure is reduced, the vertical natural frequency of the structure is generally between 0.8~2Hz. According to the vibration transferring ratio curve of SDOF system, it can be seen that the frequency ratio is far greater than $\sqrt{2}$, so the 3-D vibration and seismic isolation structure has a prominent performance of isolating the daily vibration caused by the subway.

As the vertical stiffness of isolation layer decreases, the vertical natural frequency of structure decreases, so that the frequency ratio increases, and the vibration isolation performance increases. If the vertical viscous dampers are introduced into the isolation layer, as the damping coefficient increases or the damping index decreases, the damping ratio of the whole system increases and then the vibration isolation performance decreases.

3.2 Vibration isolation performance of the pure 3-D vibration and seismic isolation structure

3.2.1 Analytical model

Take the typical structural layout of the over-track buildings as an example, the analytical model adopts reinforced concrete frame structure system. The basement platform has a height of 11m used for the operation of subway; the upper structure has 12 stories and the standard story height is 5m used for daily living. The total height of the structure is 60m. The standard story of the upper structure has 5 spans in the X direction, 3 spans in the Y-direction, and each span is 8m. The thickness of the floor slab in the standard story is 120mm, and 200mm in the basement. The upper standard story has a dead load of 5kN/m^2 and a live load of 3kN/m^2. The overall structural model is shown in Figure 3.1, and the dimensions of cross sections are shown in Table 3.1.

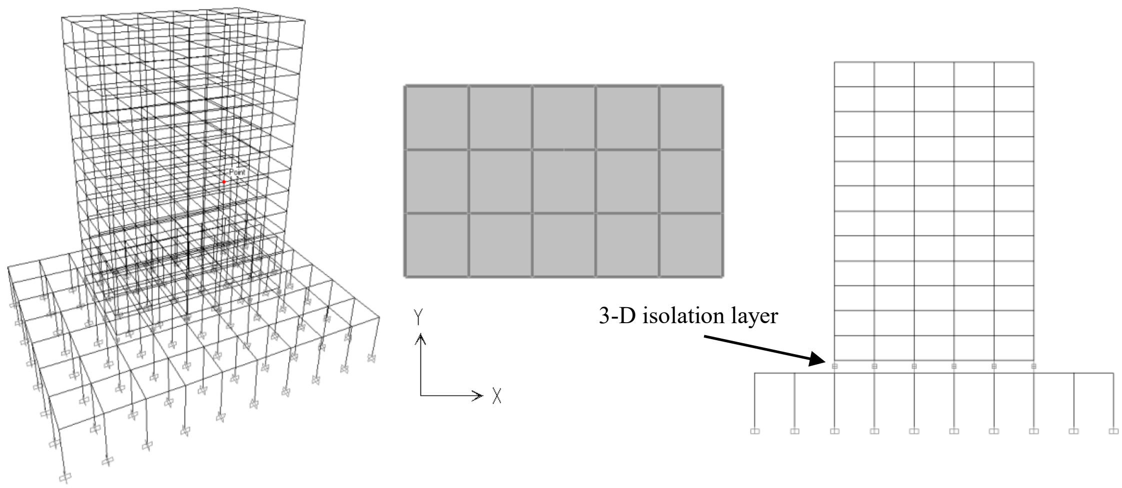

(a) The overall structural model (b) Floor plan (c) Elevation

Figure 3.1 The structural model of analytical model

Table 3.1 The dimension of cross sections in analytical model

Story	Frame column		Frame beam		Floor slab	
	Dimensions (mm)	Concrete class	Dimensions (mm)	Concrete class	Thickness (mm)	Concrete class
Basement	1300×1300	C50	500×1000	C30	200	C30
1~12	800×800	C50	400×900	C30	120	C30

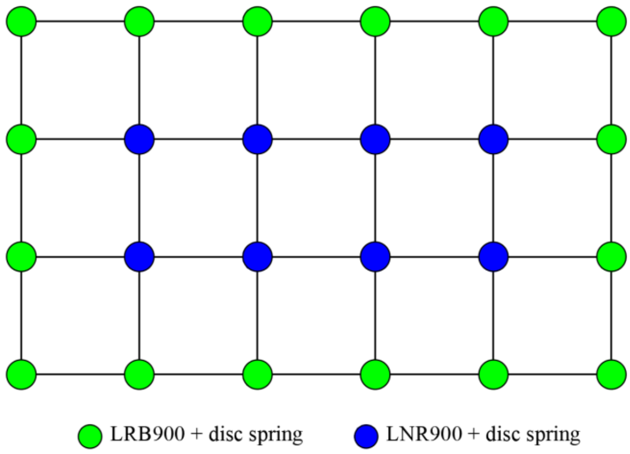

Figure 3.2 The plane layout of 3-D vibration and seismic isolation bearings

A total of 24 3-D vibration and seismic isolation bearings are arranged in the isolation layer, of which 16 are lead rubber bearings + disc springs in series, 8 are natural rubber bearings + disc springs in series. The plane layout of 3-D isolation bearings is shown in Figure 3.2, and the performance parameters of the rubber bearings are shown in Table 3.2. Figure 3.3 shows the long-term surface pressure distribution of the rubber bearings under the action of the representative value of the gravity load. It can be seen that the maximum long-term surface pressure of the rubber bearings is 9.8 MPa, which is less than 15 MPa and meets the daily use requirements of the rubber bearing.

Table 3.2 The performance parameters of the rubber bearings

Rubber bearing	Vertical stiffness (kN/mm)	100% Equivalent horizontal stiffness (kN/mm)	Stiffness before yielding (kN/mm)	Yielding force (kN)	Stiffness ratio after yielding
LRB900	4438	2.565	18.441	203	0.077
LNR900	3926	1.387	-	-	-

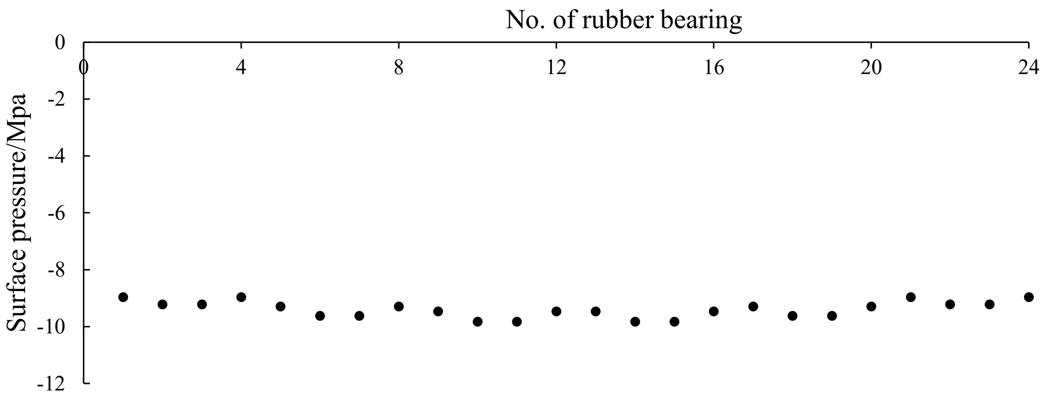

Figure 3.3 The long-term surface pressure distribution of the rubber bearings

Two subway vibration waves are used for time history analysis to obtain the vibration response of the upper structure. The first one was measured near the South Shanxi Road Metro Station of Line 1 in Shanghai, and the second one was measured near the Wuzhong Road Metro Station of Line 15 in Shanghai. The acceleration diagram and spectrum diagram of the two subway vibration waves (hereinafter referred to as DTB1 and DTB2) are shown in Figure 3.4 and Figure 3.5.

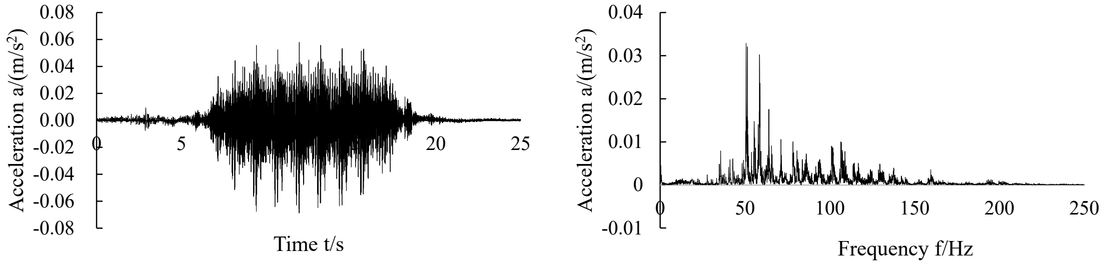

(a) Acceleration diagram (b) Spectrum diagram

Figure 3.4 South Shanxi Road Metro Station subway vibration wave (DTB1)

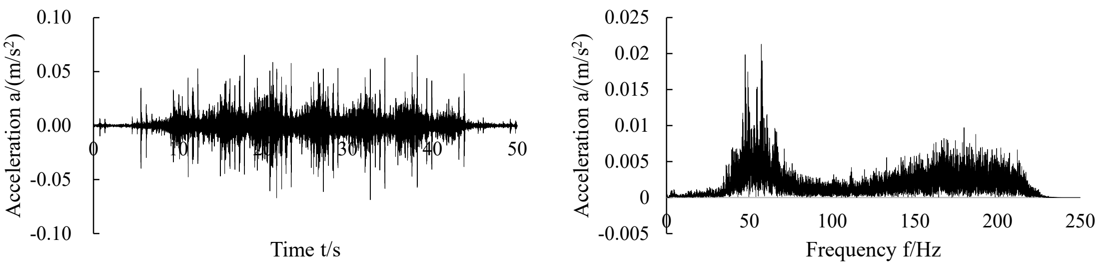

(a) Acceleration diagram (b) Spectrum diagram

Figure 3.5 Wuzhong Road Metro Station subway vibration wave (DTB2)

It can be seen from Figure 3.4(b) and Figure 3.5(b) that the dominant frequency band of DTB1 is 30~140Hz, the maximum point appears near 50Hz with a value close to 0.032m/s^2. And the dominant frequency band of DTB2 is 30~75Hz, 140~220Hz, the maximum point appears near 50Hz with a value close to 0.023m/s^2.

3.2.2 Study of vertical stiffness of 3-D isolation layer

3.2.2.1 Case design

Keep the parameters and layout of the horizontal rubber isolation bearings in the isolation layer unchanged, the total horizontal stiffness of the isolation layer K_h = 52.14kN/mm. Then change the vertical stiffness of each disc spring, and explore how the total vertical stiffness of isolation layer K_v influence the vertical vibration isolation performance of the structure. In the analytical model, the stiffness of each disc spring is the same. The parameter design of each case is shown in Table 3.3.

Table 3.3 Parameter design of 3-D isolation layer in different cases

Case	Stiffness ratio K_v/K_h	Total vertical stiffness (kN/mm)	Vertical deformation (mm)	Vertical natural frequency (Hz)
1	8	417	322	0.84（4）
2	12	626	214	1.02（5）
3	20	1043	129	1.30（6）
4	40	2085	64	1.78（7）
5	60	3128	43	2.11（9）
6	80	4171	32	2.37（10）
HISO	1964	102416	1	4.96（18）

Attention: The numbers in parentheses of the last column are the modal order of the vertical translational variation mode; “HISO” means horizontal isolation structure.

A total of 13×3 = 39 joints in the upper structure are selected as the indoor vibration evaluation points, as shown in Figure 3.6. Among them, the m-series evaluation points are located at the corner of the building, the l-series evaluation points are located at the beam-column joints inside the building, and the k-series evaluation points are located at the mid-span of the beam inside the building.

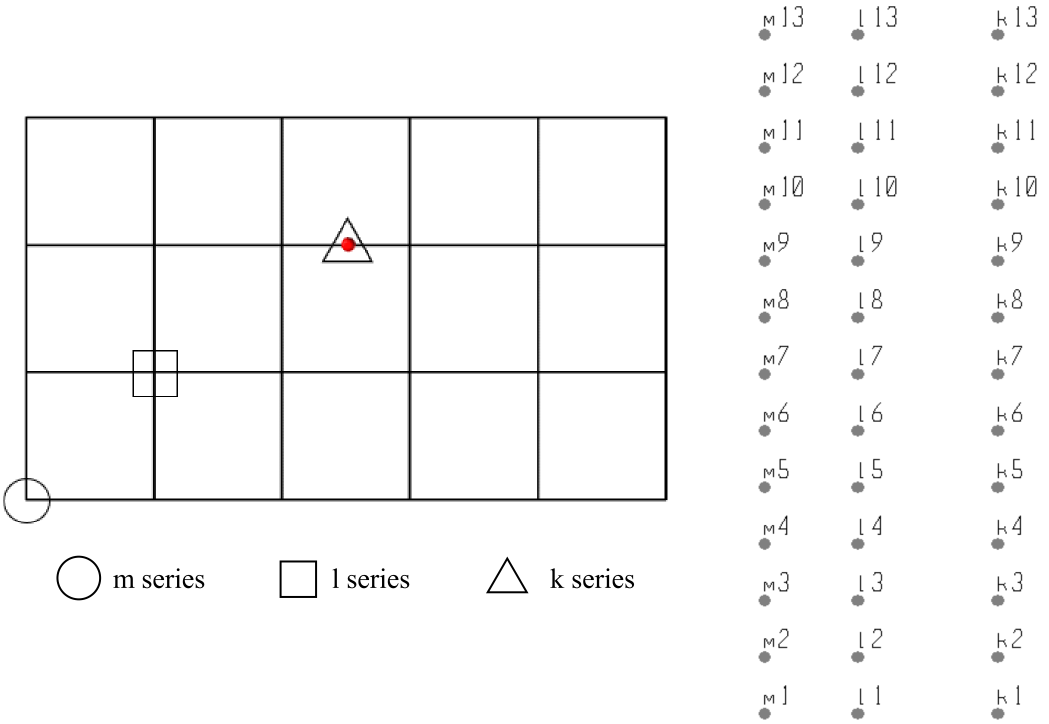

(a) Location in the plan (b) Location in the elevation

Figure 3.6 The positon of indoor vibration evaluation points

3.2.2.2 Comparison of calculation results

(1) Vertical peak acceleration

Under the excitation of the subway vibration wave, time history analysis was performed. The ratio of vertical peak acceleration (3-D vibration and seismic isolation structure / original rigid structure) of the m, l, and k joints in the upper structure is shown in Figure 3.7. It can be seen that the peak vertical acceleration in 3-D isolation structure is significantly reduced. And as the vertical stiffness of the isolation layer decreases, the vertical natural frequency of the structure decreases, the frequency ratio increases, the transmission ratio decreases, the vibration isolation efficiency increases, so that the vertical peak acceleration ratio decreases, and the reduction rate remains basically constant.

The vibration isolation efficiency under the action of DTB2 is greater than DTB1, because the dominant frequency band of DTB1 is 30~140Hz, while the dominant frequency band of DTB2 is 30~75 and 140~220Hz, the frequency ratio of DTB2 is greater than DTB1, and the transmission ratio of DTB2 is less than DTB1. What’s more, the maximum acceleration of DTB2 in the spectrum diagram is smaller than DTB1, so the vertical vibration isolation efficiency of the structure under the action of DTB2 is greater than that of DTB1, and the vertical peak acceleration ratio under the action of DTB2 is smaller than DTB1.

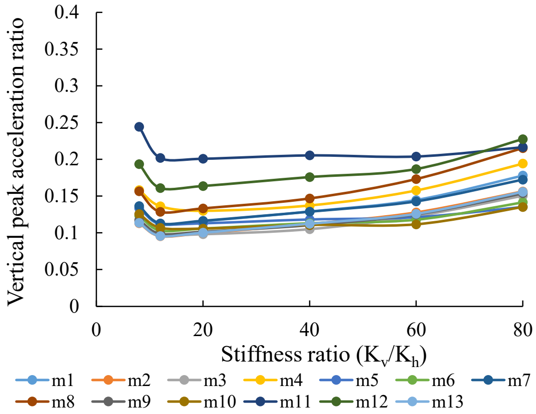

（a）DTB1-m series

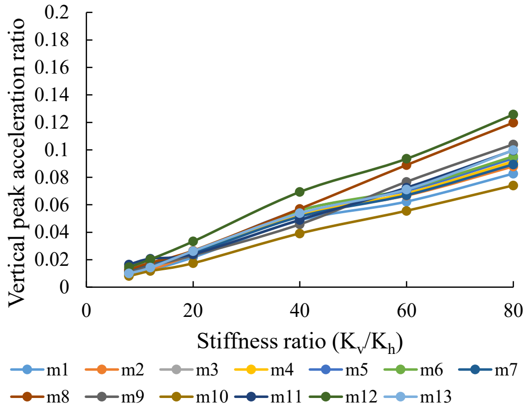

（b）DTB2-m series

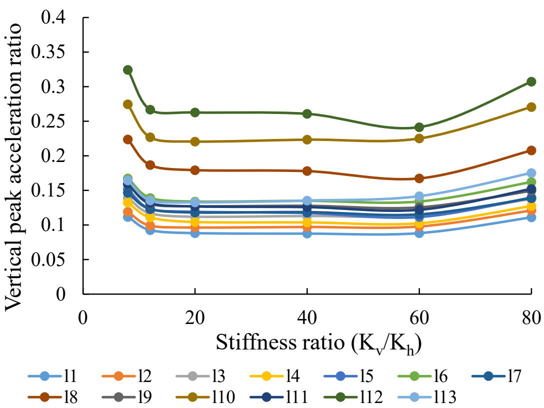

（c）DTB1-l series

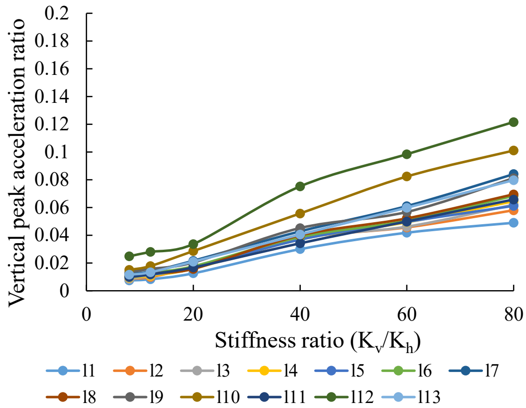

（d）DTB2-l series

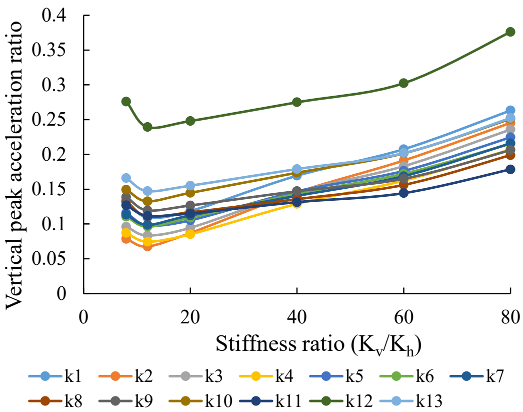

（e）DTB1-k series

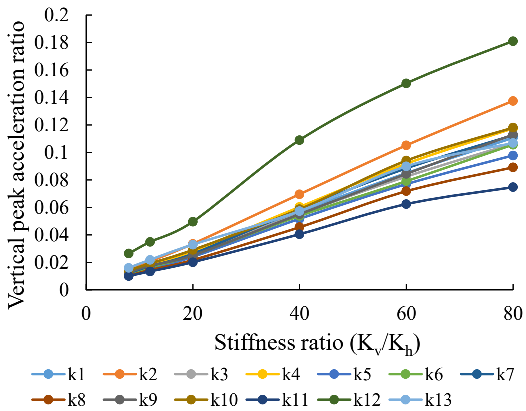

（f）DTB2-k series

Figure 3.7 The ratio of vertical peak acceleration (3-D vibration and seismic isolation structure / original rigid structure)

Due to the local vertical movement in the middle of the beam, the vertical deformation in the mid-beam is greater than the edge of the beam, so the vertical peak acceleration ratio of the m and l evaluation points located at the beam-column joints is slightly smaller than the k evaluation points located at the mid-beam.

(2) Z vibration level

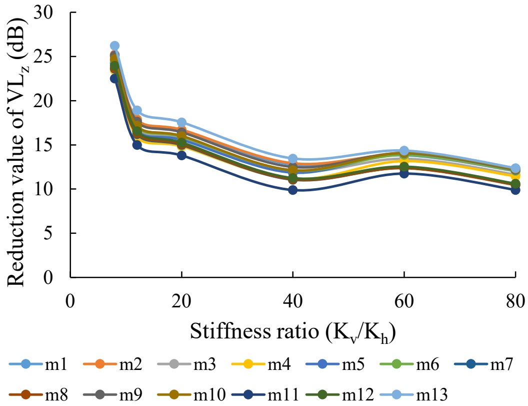

（a）DTB1-m series

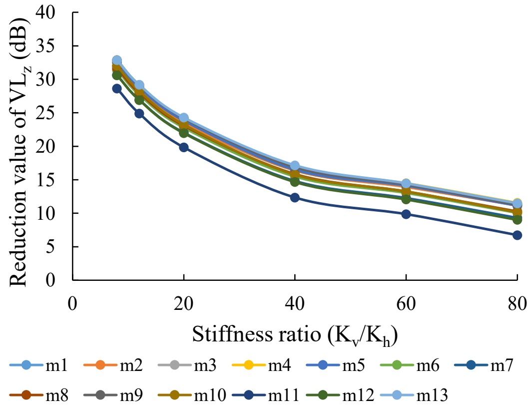

（b）DTB2-m series

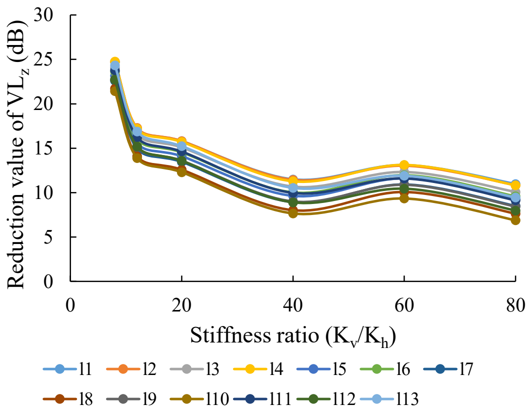

（c）DTB1-l series

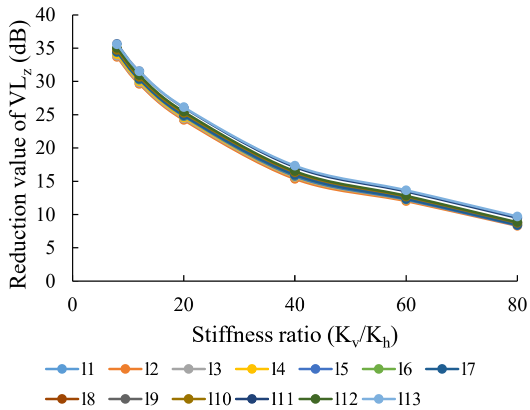

（d）DTB2-l series

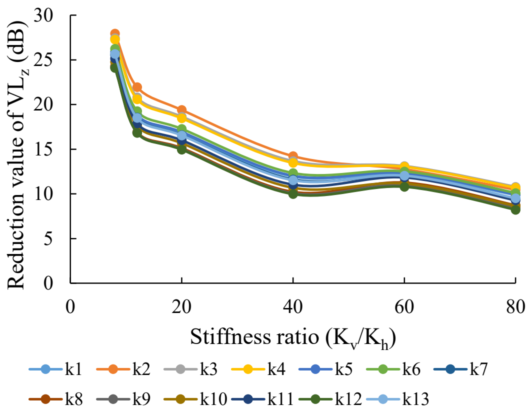

（e）DTB1-k series

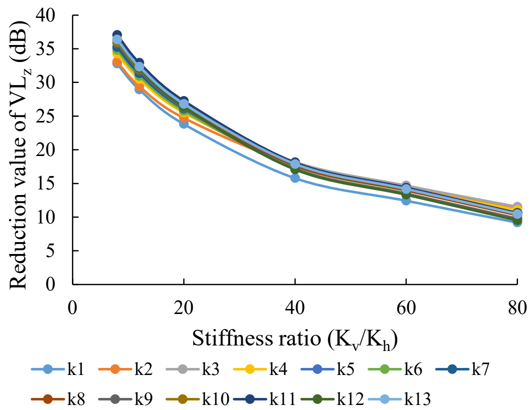

（f）DTB2-k series

Figure 3.8 The reduction value of Z vibration level VL_z (3-D vibration and seismic isolation structure minus original rigid structure)

The Z vibration level reduction value of m, l, and k-series in the upper structure (3-D vibration and seismic isolation structure minus original rigid structure) is shown in Figure 3.8. It can be seen that the Z vibration level in 3-D isolation structure is significantly reduced. And as the vertical stiffness of the isolation layer decreases, the reduction value of Z vibration level increases, and the increasing speed becomes faster and faster.

The vibration isolation efficiency of the structure under the action of DTB2 is greater than that of DTB1. The reason is that the Z vibration level evaluates the comprehensive vibration response in the frequency range of 1~80Hz, the frequency ratio under the action of two subway vibration waves is close, but the maximum acceleration of DTB2 is smaller than DTB1 in the spectral diagram, the vertical vibration isolation efficiency under the action of DTB2 is greater than that of DTB1, finally the Z vibration level reduction value under the action of DTB2 is greater than that of DTB1.

(3) Secondary noise prediction

The equivalent A-weighted sound pressure level reduction value of m, l, and k-series in the upper structure (3-D vibration and seismic isolation structure minus original rigid structure) is shown in Figure 3.9.

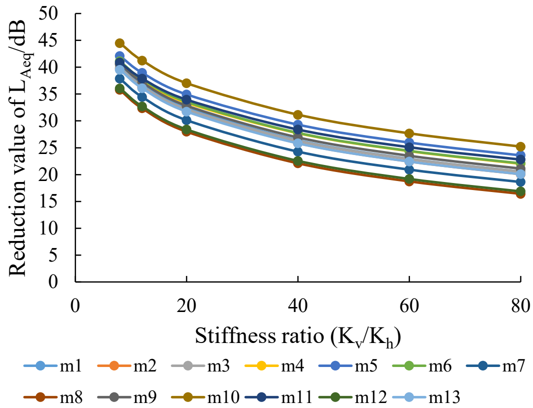

（a）DTB1-m series

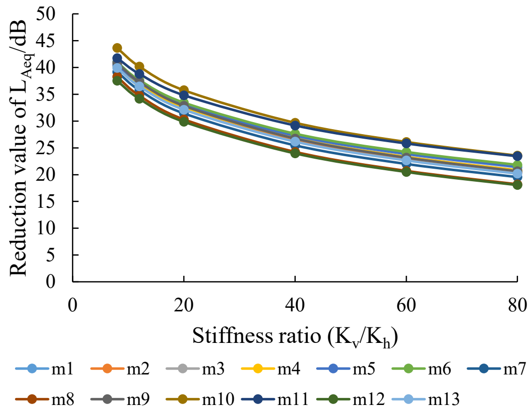

（b）DTB2-m series

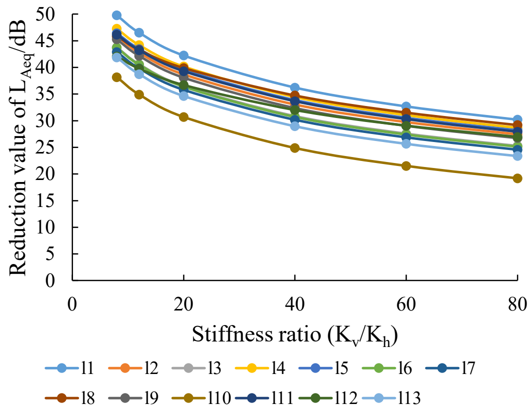

（c）DTB1-l series

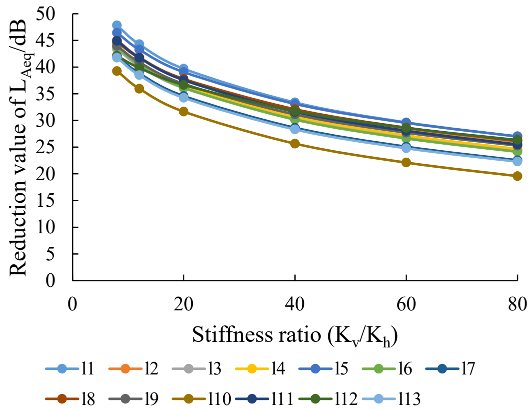

（d）DTB2-l series

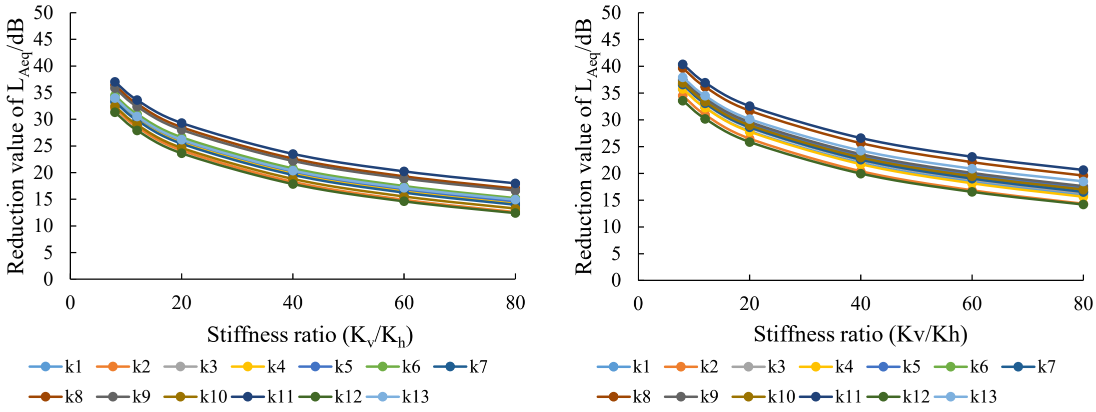

（e）DTB1-k series （f）DTB2-k series

Figure 3.9 The reduction value of equivalent A-weighted sound pressure level L_{Aeq} (3-D vibration and seismic isolation structure minus original rigid structure)

It can be seen that the equivalent A-weighted sound pressure level of 3-D isolation structure is significantly reduced. And as the vertical stiffness of the isolation layer decreases, the reduction value increases, and the increasing speed becomes faster and faster. What's more, the reduction values under the action of the two subway vibration waves are very close.

3.2.3 Conclusion of the section

(1) As the vertical stiffness of the isolation layer decreases, the vertical natural frequency of the structure decreases, the frequency ratio increases, the transmission ratio decreases, the vibration isolation efficiency increases, so that the vertical peak acceleration ratio of 3-D isolation structure and original rigid structure decreases, and the reduction rate remains basically constant.

(2) As the vertical stiffness of the isolation layer decreases, the reduction value of the Z vibration level (3-D vibration and seismic isolation structure minus original rigid structure) increases, and the increasing speed becomes faster and faster.

(3) As the vertical stiffness of the isolation layer decreases, the reduction value of the equivalent A-weighted sound pressure level (3-D vibration and seismic isolation structure minus original rigid structure) increases, and the increasing speed becomes faster and faster.

(4) As the vertical stiffness of the isolation layer decreases, the overall vertical vibration isolation efficiency increases, and the increasing speed becomes faster and faster.

(5) As for the high-rise over-track buildings, the vertical stiffness of the

isolation layer should be designed so that the vertical natural frequency of the structure is smaller than 1.3 Hz.

3.3 Vibration isolation performance of the 3-D vibration and seismic isolation + vertical viscous dampers structure

3.3.1 Analytical model

In order to study the vibration response of the upper structure after the vertical viscous dampers are introduced into the isolation layer, based on the analytical model in section 3.2.1, the total vertical stiffness of the isolation layer is fixed to be $K_v = 12K_h =$ 626 kN/mm with the stiffness of a single disc spring to be $K_v/24 = 26.07$ kN/mm. Then four vertical viscous dampers are added to the four corners of the isolation layer. The layout of the isolation layer is shown in Figure 3.10.

3.3.2 Study of damping coefficient of vertical dampers

3.3.2.1 Case design

Keeping the parameters and layout of the 3-D vibration and seismic isolation bearings in the isolation layer unchanged, the damping index of the viscous dampers is fixed at α = 0.5, and the damping coefficient C is respectively 500, 1000, 2000, 3000, 4000, 5000 $kN/(m/s)^{\alpha}$ for different cases.

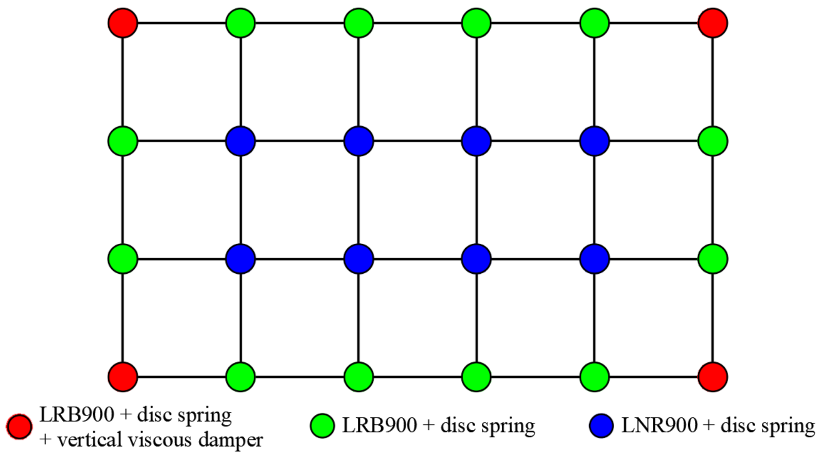

Figure 3.10 The plane layout of 3-D vibration and seismic isolation layer

3.3.2.2 Comparison of calculation results

(1) Vertical peak acceleration

Under the excitation of the subway vibration wave, time history analysis was performed. The ratio of vertical peak acceleration (3-D vibration and seismic isolation structure / original rigid structure) of the m, l, and k joints in the upper structure is shown in Figure 3.11. The damping coefficient C = 0 means that there are not any vertical viscous dampers in the isolation layer (that is, the pure 3-D vibration and seismic isolation structure).

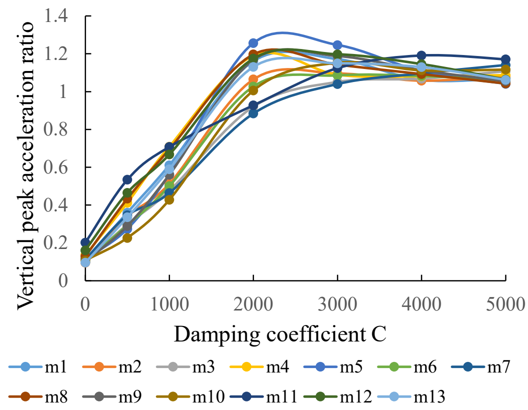

（a）DTB1-m series

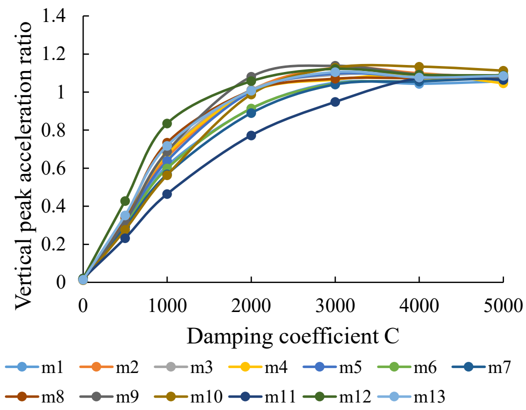

（b）DTB2-m series

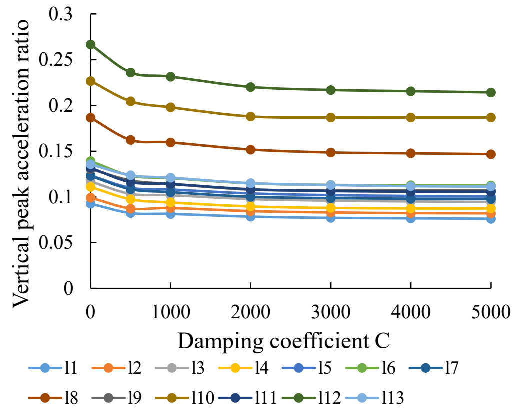

（c）DTB1-l series

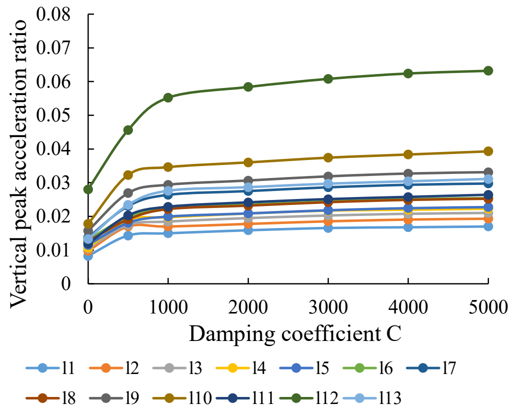

（d）DTB2-l series

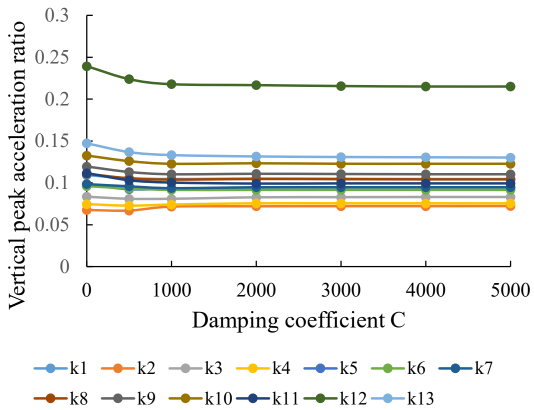

（e）DTB1-k series

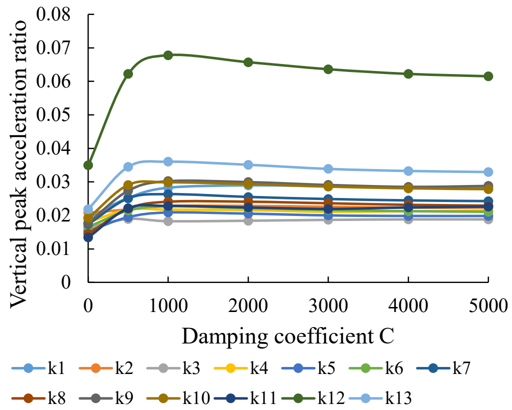

（f）DTB2-k series

Figure 3.11 The ratio of vertical peak acceleration (3-D vibration and seismic isolation structure / original rigid structure)

It can be seen that as the vertical damping coefficient C increases, the vertical peak acceleration ratio of the m-series joints above the vertical viscous dampers first increases sharply, and after $C \geq 2000$, the ratio is even greater than 1, and basically remains unchanged, which means that at this range, the indoor joints above the vertical viscous dampers of the 3-D isolation structure even has a vibration amplification phenomenon relative to the unisolated structure; the vertical peak acceleration ratio of the l and k-series joints far from the corners remains basically unchanged or slightly increases, and the increasing value is significantly smaller than the m-series joints, indicating that the vertical viscous dampers in the isolation layer has a significantly greater negative impact on the vertical vibration response above it than other parts.

Under the action of two subway vibration waves, for the same damping coefficient C, the vertical peak acceleration ratio of the m-series joints above the viscous dampers is basically the same, while the vertical peak acceleration ratio of the l and k-series joints far from the corners is obviously DTB1 > DTB2.

(2) Z vibration level

The Z vibration level of m, l, and k-series in the upper structure is shown in Figure 3.12. It can be seen that as the vertical damping coefficient C increases, the Z vibration levels of the three evaluation series joints all increase sharply first, after $C \geq 2000$, the value remains basically unchanged. At the range of $C \geq 2000$, the Z vibration level of the m-series joints above the vertical viscous dampers is about 19dB higher than that of the pure 3-D isolation structure under the action of DTB1, and 28dB higher under the action of DTB2; the Z vibration level of the l, k-series joints far from the corners is about 4dB higher than that of the pure 3-D isolation structure under the action of DTB1, and 14dB higher under the action of DTB2, indicating that the vertical viscous dampers in the isolation layer has a significantly greater negative impact on the vertical vibration response above it than other parts in the building. It can also be obtained that the negative impact of vertical viscous dampers is greater under the action of DTB2 compared to DTB1.

According to the design code "Standard of vibration in urban area environment" GB10070-88, the upper structure belongs to residential area, and its daytime environmental vibration limit is 70dB (see Table 2.4). It is obvious that under the action of two subway vibration waves, even if small viscous damping is introduced at the four corners of the isolation layer, such as the damping coefficient

C = 500, the indoor vibration response of the upper structure will exceed the minimum requirements of the code.

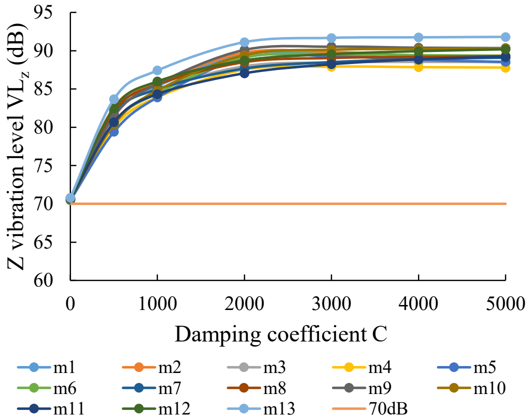

（a） DTB1-m series

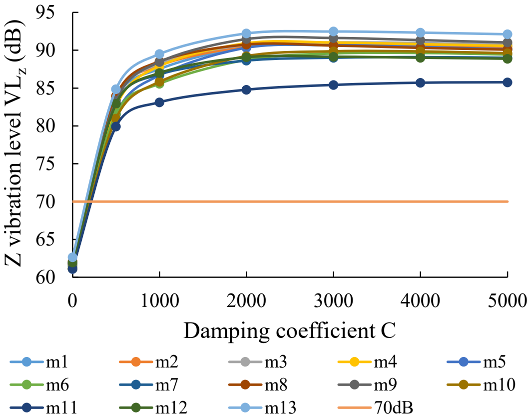

（b） DTB2-m series

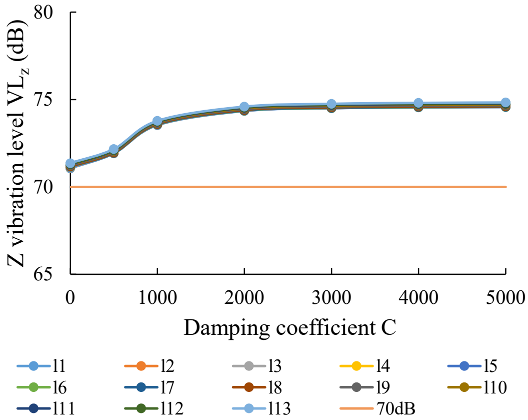

（c） DTB1-l series

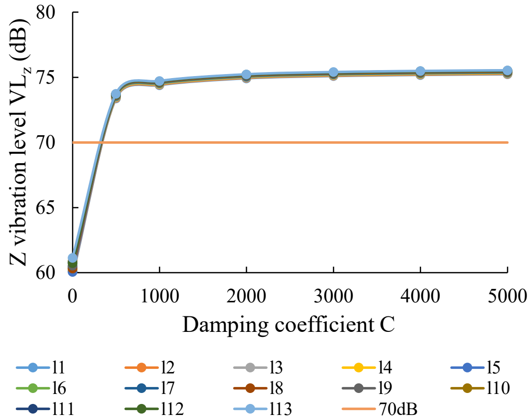

（d） DTB2-l series

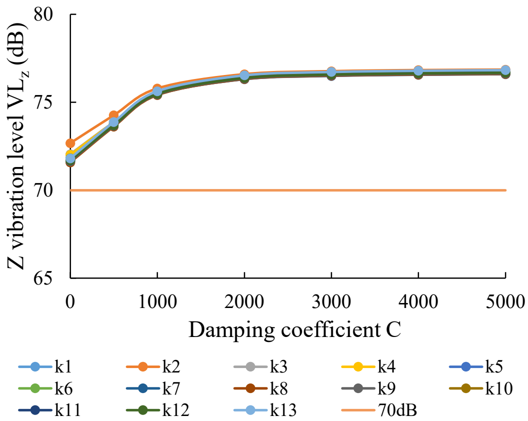

（e） DTB1-k series

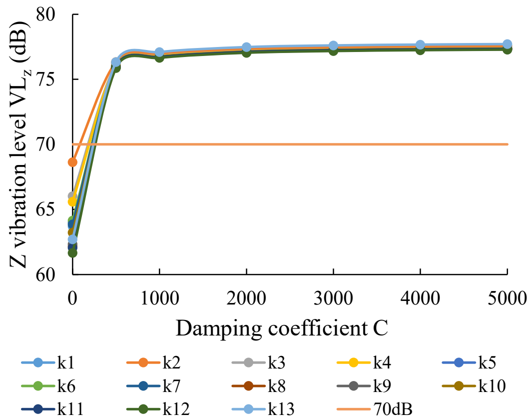

（f） DTB2-k series

Figure 3.12 The Z vibration level VL_z of 3-D vibration and seismic isolation structure

(3) Secondary noise prediction

The equivalent A-weighted sound pressure level of the m, l, and k-series joints in the indoor upper structure is shown in Figure 3.13. It can be seen that as the vertical damping coefficient C increases, the equivalent A-weighted sound pressure level of the m-series joints above the viscous dampers first increases sharply, after $C \geq 2000$ it remains basically unchanged and is about 37dB higher than that of the pure 3-D isolation structure both under the action of DTB1 and DTB2. However, the equivalent A-weighted sound pressure level of the l and k-series joints far from the corners basically does not change with the vertical damping coefficient.

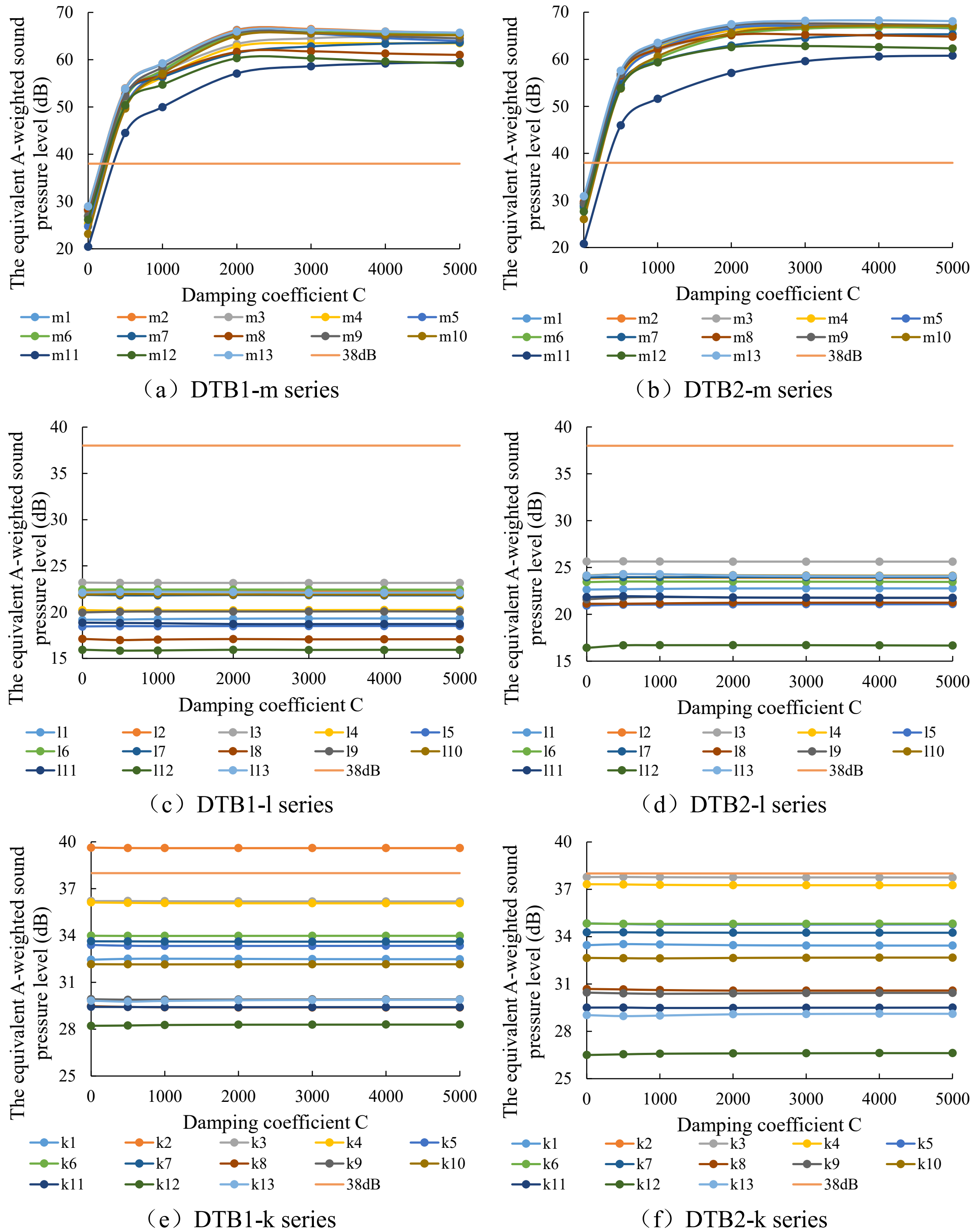

Figure 3.13 The equivalent A-weighted sound pressure level L_{Aeq} of 3-D vibration and seismic isolation structure

According to the design code "Standard for limit and measuring method of building vibration and secondary noise caused by urban rail transit" JGJ/T170-2009, the limit of environmental secondary radiation noise for residential areas is 38dB during the daytime (see Table 2.5). It is obvious that under the action of two subway vibration waves, even if small viscous damping is introduced at the four corners of the isolation layer, such as the damping coefficient C = 500, the vibration response of the m-series joints at the four corners of the building will exceed the minimum requirements of the code.

3.3.2.3 Explanation of the results

Table 3.4 and Figure 3.14 show the vertical additional dynamic stiffness ratio of the isolation layer with different vertical damping coefficient under the action of two subway vibration waves. The additional dynamic stiffness ratio η is defined as shown in equation 3.1:

$$\eta = \frac{K_{damper}}{K_v} \tag{3.1}$$

Where, K_{damper} is the additional dynamic stiffness of the viscous damper, whose calculation method is shown in formula 3.2, and K_v is the total vertical stiffness of the isolation layer.

$$K_{damper} = \sum \frac{F_{dmax,i}}{u_{dmax,i}} \tag{3.2}$$

Where, $F_{dmax,i}$ is the maximum damping force of the i-th viscous damper, $u_{dmax,i}$ is the maximum axial deformation of the i-th viscous damper.

In case of the same vertical damping coefficient, the vertical additional dynamic stiffness ratio under the action of DTB2 is greater than DTB1, so the increase in vibration response relative to the pure 3-D isolation structure of DTB2 is greater than that of DTB1. When the damping coefficient C is less than or equal to 2000, as the damping coefficient C increases, the vertical additional dynamic stiffness ratio keeps increasing, then the vertical total stiffness of the isolation layer keeps increasing. According to the conclusions in Section 3.2, the indoor vertical vibration response of the upper structure keeps increasing. When the damping coefficient $C \geq 2000$, the vertical additional dynamic stiffness ratio reaches more than 3. At this stage, the increase in the total vertical stiffness of the isolation layer has a stable adverse effect on the indoor vibration response. Therefore, the vertical peak acceleration and Z vibration level basically no longer change with the damping coefficient after $C \geq 2000$. In addition, because the m-series joints are located above the viscous dampers, the local vertical stiffness of corners at the isolation layer is much greater than other parts, so the vertical vibration response of the m-series joints is greater than that of the l and k-series joints.

Table 3.4 The vertical additional dynamic stiffness ratio of isolation layer under different damping coefficients

Input		No damper	500	1000	2000	3000	4000	5000
DTB1	Additional dynamic stiffness (kN/mm)	0	397	879	1852	3050	4865	6949
	Additional dynamic stiffness ratio	0	0.64	1.41	2.98	4.90	7.82	11.18
DTB2	Additional dynamic stiffness (kN/mm)	0	1091	2692	5881	9868	15106	18703
	Additional dynamic stiffness ratio	0	1.75	4.33	9.46	15.87	24.29	30.08

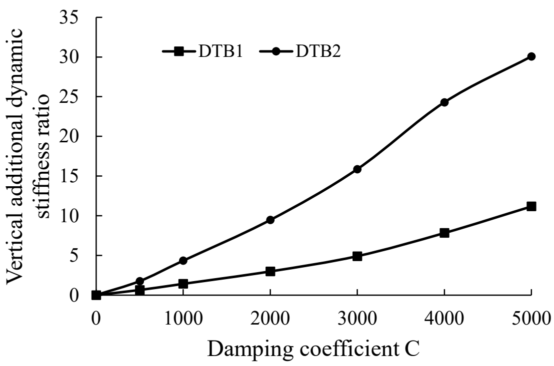

Figure 3.14 The vertical additional dynamic stiffness ratio

3.3.3 Study of damping index of vertical dampers

3.3.3.1 Case design

Keeping the parameters and layout of the 3-D vibration and seismic isolation bearings in the isolation layer unchanged, the damping coefficient of the viscous dampers is fixed at $C = 2000kN/(m/s)^{\alpha}$, and the damping index α is respectively 0.1、0.3、0.5、0.7、0.9 for different cases.

3.3.3.2 Comparison of calculation results

(1) Vertical peak acceleration

Under the excitation of the subway vibration wave, time history analysis was performed. The ratio of vertical peak acceleration (3-D vibration and seismic isolation structure / original rigid structure) of the m, l, and k joints in the upper structure is shown in Figure 3.15.

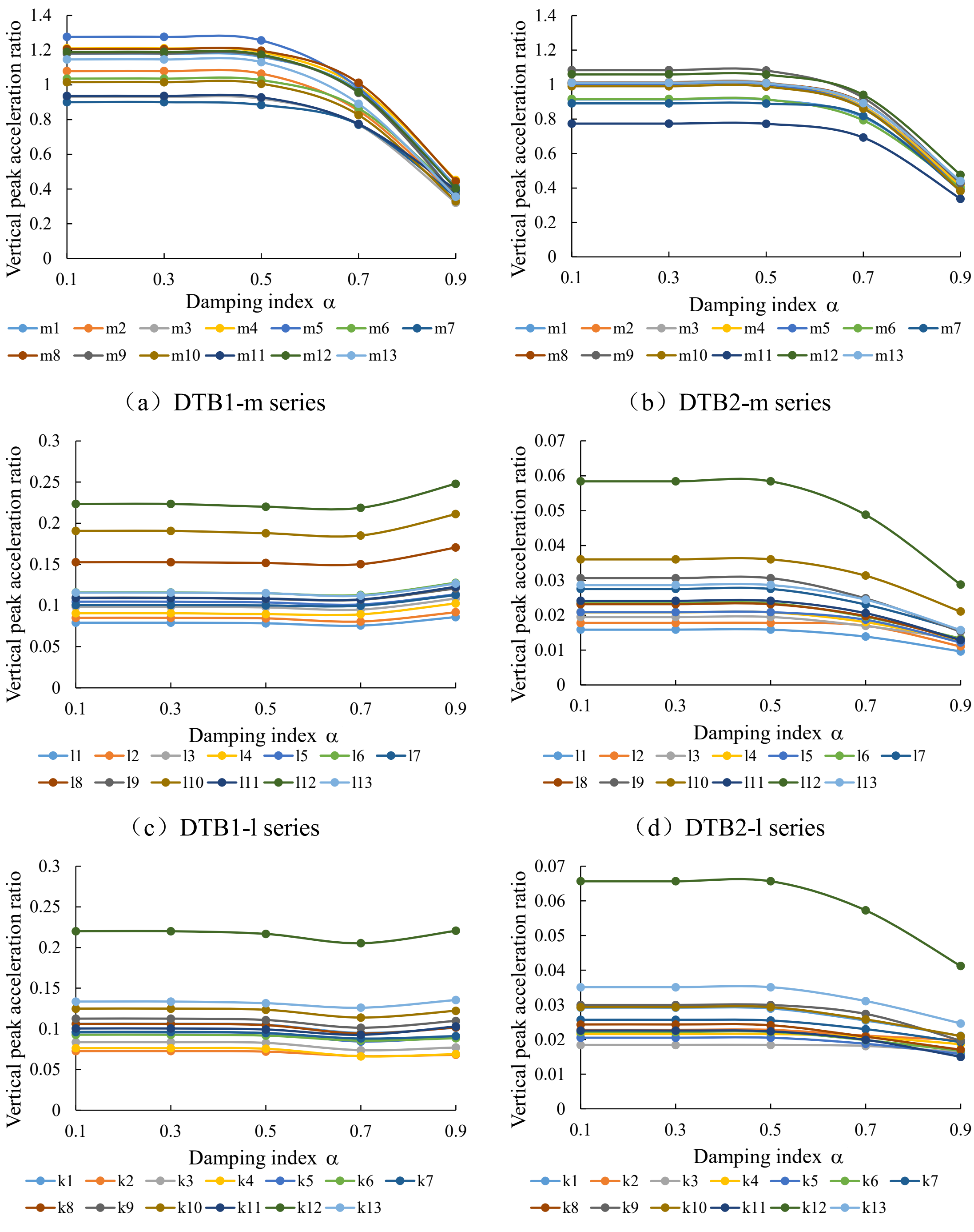

（e）DTB1-k series　　（f）DTB2-k series

Figure 3.15 The ratio of vertical peak acceleration (3-D vibration and seismic isolation structure / original rigid structure)

It can be seen that as the vertical damping index α decreases, the vertical peak acceleration ratio of the m-series joints above the vertical viscous dampers first increases sharply, and after $\alpha \leq 0.5$, the ratio is even greater than 1 in some stories, and basically remains unchanged, which means that at this range, the indoor joints above the vertical viscous dampers of the 3-D isolation structure even has a vibration amplification phenomenon relative to the unisolated structure; the vertical peak acceleration ratio of the l and k-series joints far from the corners remains basically unchanged or slightly increases, and the increasing value is significantly smaller than the m-series joints, indicating that the vertical viscous dampers in the isolation layer has a significantly greater negative impact on the vertical vibration response above it than other parts.

Under the action of two subway vibration waves, for the same damping index α, the vertical peak acceleration ratio of the m-series joints above the viscous dampers is basically the same, while the vertical peak acceleration ratio of the l and k-series joints far from the corners is obviously DTB1 > DTB2.

(2) Z vibration level

The Z vibration level of m, l, and k-series in the upper structure is shown in Figure 3.16. It can be seen that as the vertical damping index α decreases, the Z vibration levels of the three evaluation series joints all increase sharply first, after $\alpha \leq 0.5$, the value remains basically unchanged. At the range of $\alpha \leq 0.5$, the Z vibration level of the m-series joints above the vertical viscous dampers is about 18dB higher than that of the pure 3-D isolation structure under the action of DTB1, and 28dB higher under the action of DTB2; the Z vibration level of the l, k-series joints far from the corners is about 4dB higher than that of the pure 3-D isolation structure under the action of DTB1, and 14dB higher under the action of DTB2, indicating that the vertical viscous dampers in the isolation layer has a significantly greater negative impact on the vertical vibration response above it than other parts in the building. It can also be obtained that the negative impact of vertical viscous dampers is greater under the action of DTB2 compared to DTB1.

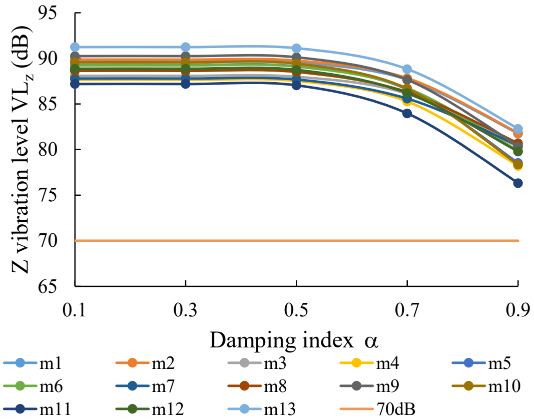

（a）DTB1-m series

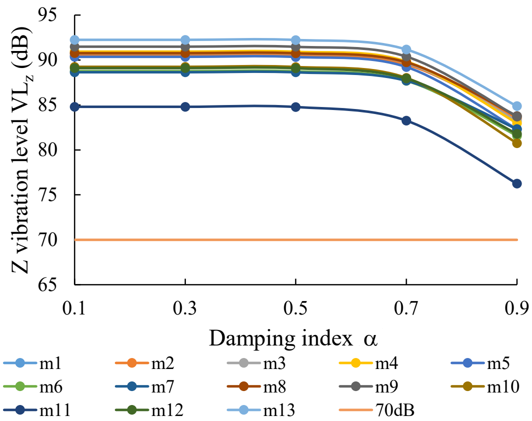

（b）DTB2-m series

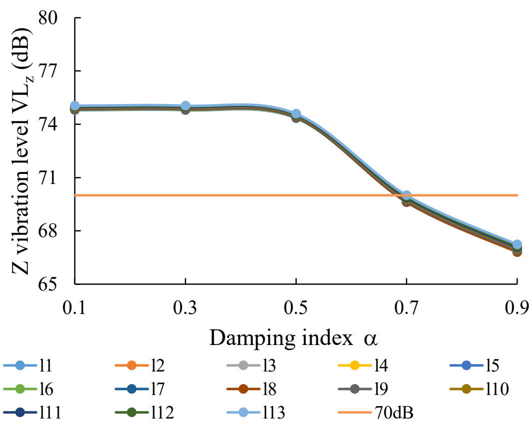

（c）DTB1-l series

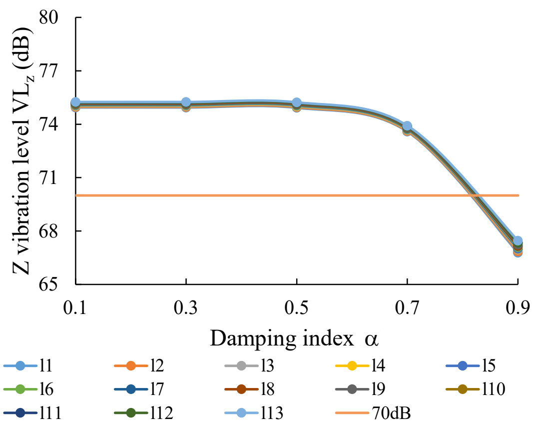

（d）DTB2-l series

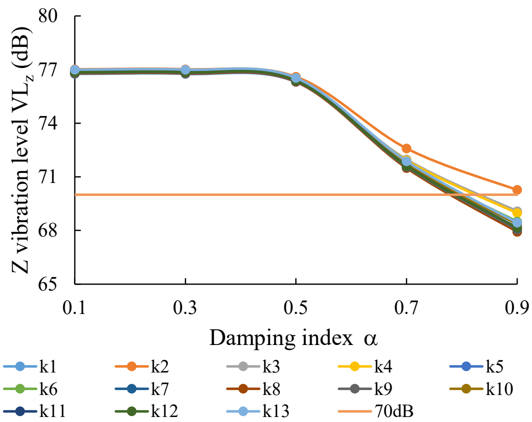

（e）DTB1-k series

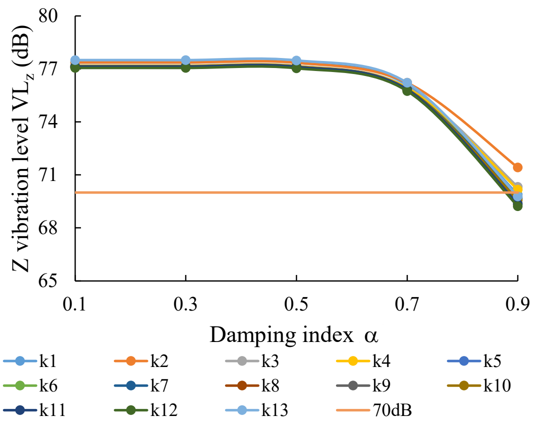

（f）DTB2-k series

Figure 3.16 The Z vibration level VL_z of 3-D vibration and seismic isolation structure

According to the design code "Standard of vibration in urban area environment" GB10070-88, under the action of two subway vibration waves, even if small viscous damping is introduced at the four corners of the isolation layer, such as the damping index α = 0.9, the indoor vibration response of the upper structure will exceed the minimum requirements of the code.

(3) Secondary noise prediction

The equivalent A-weighted sound pressure level of the m, l, and k-series joints in the indoor upper structure is shown in Figure 3.17. It can be seen that as the vertical damping index α decreases, the equivalent A-weighted sound pressure level of the m-series joints above the viscous dampers first increases sharply, after $\alpha \leq 0.5$ it remains basically unchanged and is about 36dB higher than that of the pure 3-D isolation structure both under the action of DTB1 and DTB2. However, the equivalent A-weighted sound pressure level of the l and k-series joints far from the corners basically does not change with the vertical damping index.

According to the design code "Standard for limit and measuring method of building vibration and secondary noise caused by urban rail transit" JGJ/T170-2009, under the action of two subway vibration waves, even if small viscous damping is introduced at the four corners of the isolation layer, such as the damping index α = 0.9, the vibration response of the m-series joints at the four corners of the building will exceed the minimum requirements of the code.

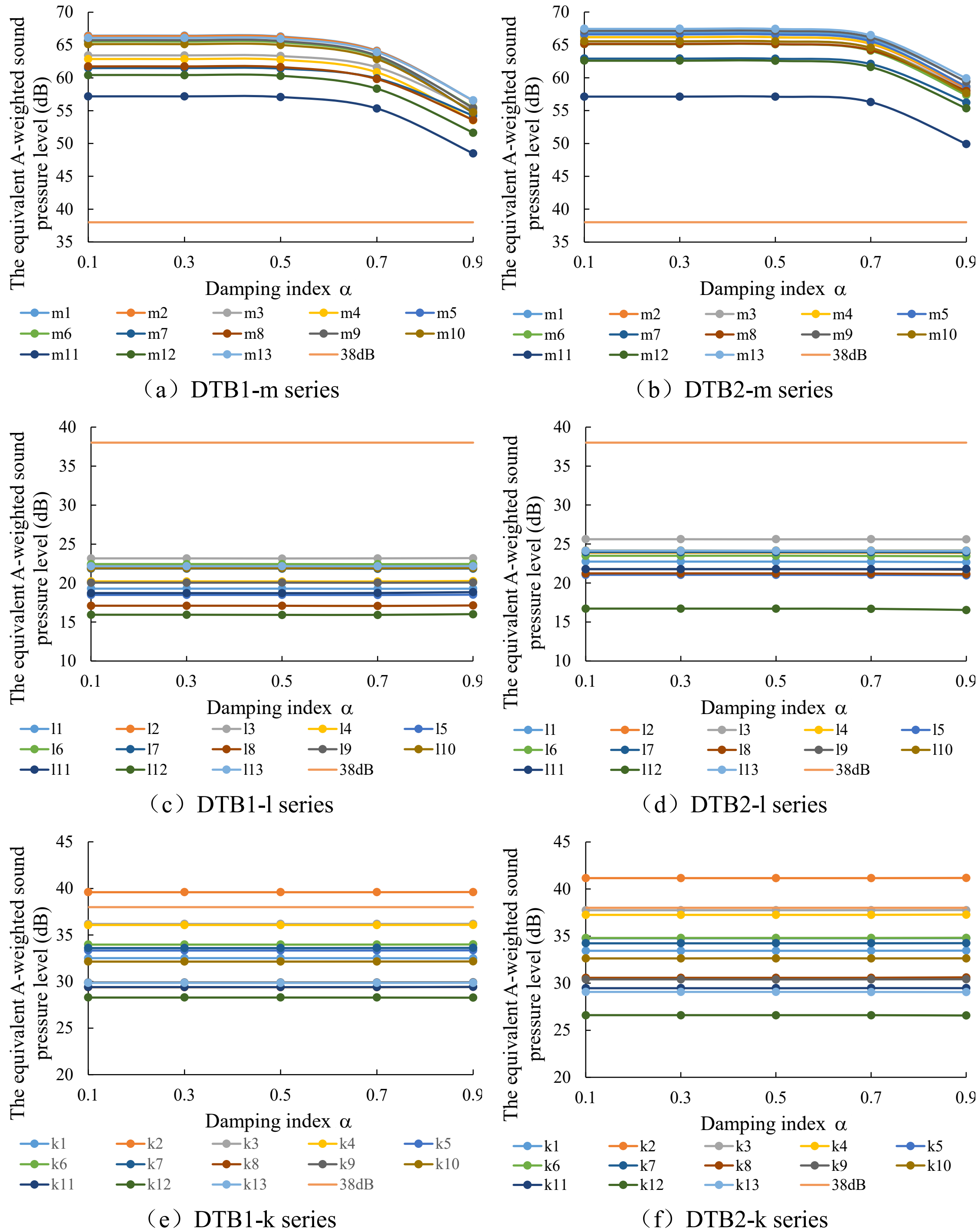

Figure 3.17 The equivalent A-weighted sound pressure level L_{Aeq} of 3-D vibration and seismic isolation structure

3.3.3.3 Explanation of the results

Table 3.5 and Figure 3.18 show the vertical additional dynamic stiffness ratio of the isolation layer with different vertical damping index under the action of two subway vibration waves. In case of the same vertical damping index, when $\alpha > 0.3$ the vertical additional dynamic stiffness ratio of DTB2 is larger than that of DTB1, when $\alpha \leq 0.3$ the vertical additional dynamic stiffness ratio of DTB2 is slightly smaller than that of DTB1.

Table 3.5 The vertical additional dynamic stiffness ratio of isolation layer under different damping indexes

Input		No damper	0.1	0.3	0.5	0.7	0.9
DTB1	Additional dynamic stiffness (kN/mm)	0	8101	8093	1852	256	60
	Additional dynamic stiffness ratio	0	13.03	13.01	2.98	0.41	0.10
DTB2	Additional dynamic stiffness (kN/mm)	0	7484	7484	5881	1604	425
	Additional dynamic stiffness ratio	0	12.03	12.03	9.46	2.58	0.68

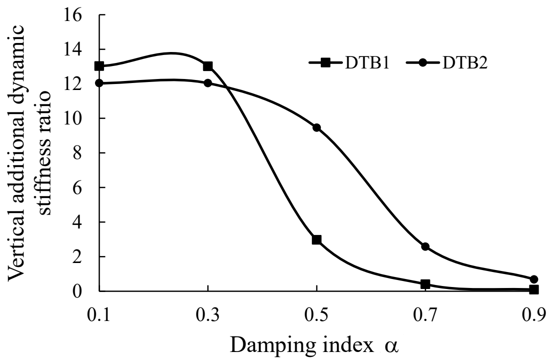

Figure 3.18 The vertical additional dynamic stiffness ratio

When the damping index $\alpha \geq 0.5$, as the damping index decreases, the vertical additional dynamic stiffness ratio keeps increasing, then the vertical total stiffness of the isolation layer keeps increasing. According to the conclusions in Section 3.2, the indoor vertical vibration response of the upper structure keeps increasing. When the damping index $\alpha \leq 0.5$, the vertical additional dynamic stiffness ratio reaches more than 3. At this stage, the increase in the total vertical stiffness of the isolation layer has a stable adverse effect on the indoor vibration response. Therefore, the vertical peak acceleration and Z vibration level basically no longer change with the damping index after $\alpha \leq 0.5$. In addition, because the m-series joints are located above the viscous dampers, the local vertical stiffness of corners at the isolation layer is much greater than other parts, so the vertical vibration response of the m-series joints is greater than that of the l and k-series joints.

3.3.4 Conclusion of the section

(1) After the vertical viscous damping is introduced into the 3-D isolation layer, due to the additional dynamic stiffness of the viscous dampers, the indoor vertical vibration response of joints above the dampers increases significantly, and may even be larger than that of the unisolated structure. However, the adverse impact on the inner part of the building is smaller than the four corners.

(2) As the vertical damping coefficient increases, the vertical vibration response of the upper structure first increases sharply, after $C \geq 2000$, the vertical additional dynamic stiffness ratio of the 3-D isolation layer reaches more than 3, so that the indoor vertical vibration response basically no longer changes with the damping coefficient.

(3) As the vertical damping index decreases, the vertical vibration response of the upper structure first increases sharply, after $\alpha \leq 0.5$, the vertical additional dynamic stiffness ratio of the 3-D isolation layer reaches more than 3, so that the indoor vertical vibration response basically no longer changes with the damping index.

(4) From the perspective of daily vibration isolation of the subway, it is not suitable to introduce vertical viscous dampers into the 3-D isolation layer.

3.4 Conclusion of the chapter

This chapter systematically studies the vertical vibration response of the pure 3-D vibration and seismic isolation structure under the vertical subway vibration excitation. The main conclusions are as follows:

(1) As the vertical stiffness of the isolation layer decreases, the vertical natural frequency of the structure decreases, so the vertical vibration response keeps decreasing, and the rate of decreasing becomes faster and faster.

(2) The appropriate value of the vertical stiffness of the 3-D isolation layer for high-rise buildings should be chosen such that the vertical natural frequency of the structure is below 1.3 Hz.

This chapter systematically studies the vertical vibration response of the 3-D vibration and seismic isolation + vertical viscous dampers structure under the vertical subway vibration excitation. The main conclusions are as follows:

(1) After the vertical viscous damping is introduced into the 3-D isolation layer, due to the additional dynamic stiffness of the viscous dampers, the indoor vertical vibration response of joints above the dampers increases significantly, and may even be larger than that of the unisolated structure. However, the adverse impact on the inner part of the building is smaller than the four corners.

(2) As the vertical damping coefficient increases, the vertical vibration response of the upper structure first increases sharply, after $C \geq 2000$, the vertical additional dynamic stiffness ratio of the 3-D isolation layer reaches more than 3, so that the indoor vertical vibration response basically no longer changes with the damping coefficient.

(3) As the vertical damping index decreases, the vertical vibration response of the upper structure first increases sharply, after $\alpha \leq 0.5$, the vertical additional dynamic stiffness ratio of the 3-D isolation layer reaches more than 3, so that the indoor vertical vibration response basically no longer changes with the damping index.

(4) If the vertical vibration isolation performance of all parts in the upper structure is required, it is recommended that the 3-D isolation layer does not introduce any vertical viscous dampers.

(5) If the vertical vibration isolation requirements near the four corners of the building are discarded, the vertical stiffness of the isolation layer can be further reduced, and then four viscous dampers with parameters of C = 4000~5000 $kN/(m/s)^{\alpha}$ and α = 0.2~0.3 are recommended to add into the corners of the isolation layer. In this situation, the requirements of vertical vibration control in the inner part of the building can not only be satisfied, but the rocking effect of the upper structure can also be effectively suppressed.

Chapter 4 Parameter study of horizontal seismic isolation performance

4.1 Introduction

The 3-D vibration and seismic isolation structure can not only effectively isolate the daily vertical vibration caused by the subway, but also reduce the horizontal seismic response of the upper structure. However, due to the reduction of the vertical stiffness of the isolation layer, the upper structure will have rocking effect under the action of horizontal earthquake, which will cause the inter-story drift angle and lateral displacement of floors increase. By introducing four vertical viscous dampers to the four corners of the isolation layer, the rocking effect of the upper structure can be effectively controlled. At the same time, the dampers can further reduce the horizontal seismic response of the upper structure through hysteretic energy dissipation. On the other hand, if the horizontal viscous dampers are introduced into the isolation layer, not only can the horizontal deformation of the isolation layer be effectively controlled, the horizontal seismic response of the upper structure will also be reduced, but the rocking effect and vertical vibration response almost does not change.

4.2 Seismic isolation performance of the pure 3-D vibration and seismic isolation structure

4.2.1 Analytical model

The analytical model is the same as that in Section 3.2.1. The plane layout of the 3-D vibration and seismic isolation layer is shown in Figure 4.1, and there is no viscous damper in the isolation layer. The seismic fortification intensity is 8 degrees (0.3g), the design earthquake group is Group 3, the site category is Class II, and the site characteristic period is 0.45s. The case design is shown in Table 4.1. In this section, the parameters and layout of the horizontal rubber isolation bearings of each case are the same.

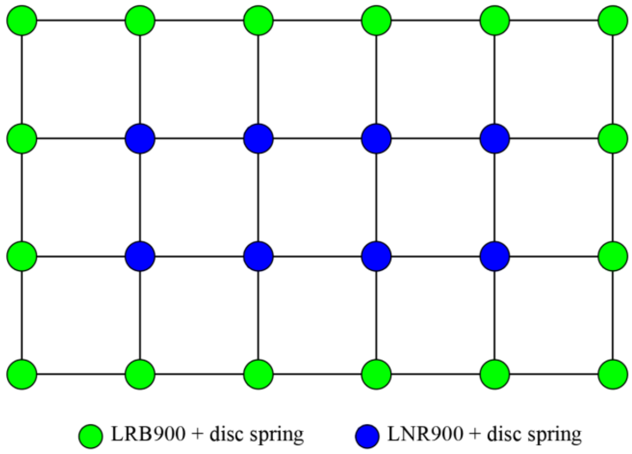

Figure 4.1 The plane layout of 3-D vibration and seismic isolation bearings

Table 4.1 Parameter design of 3-D isolation layer in different cases

Case	Stiffness ratio K_v/K_h	K_v (kN/mm)	1st horizontal natural period (s)	2nd horizontal natural period (s)	Vertical natural frequency (Hz)
1	8	417	5.97	4.85	0.84
2	12	626	5.35	4.54	1.02
3	20	1043	4.81	4.28	1.30
4	40	2085	4.38	4.08	1.78
5	60	3128	4.24	4.02	2.11
6	80	4171	4.16	3.98	2.37
HISO	1964	102416	3.94	3.88	4.96

Attention: K_v means the total vertical stiffness of the 3-D isolation layer; K_h means the total horizontal stiffness of the 3-D isolation layer; "HISO" means the horizontal isolation structure.

When performing the seismic time-history analysis, two natural earthquake waves (El-Centro wave, Lanzhou S0202 seismic wave) and one artificial earthquake wave (generated by YJK structural design software) are chosen. The peak ground acceleration (PGA) of the earthquake waves shall be adjusted in accordance with the relevant requirements of the seismic fortification intensity of 8 degrees (0.3g). The information of three earthquake waves is shown in Table 4.2, and the acceleration diagrams are shown in Figure 4.2.

Table 4.2 Information of the earthquake waves

Earthquake wave		No. of increments	Time interval (s)	Duration (s)
El-Centro	Natural wave	2673	0.02	53.46
S0202	Natural wave	1847	0.02	36.94
RGB	Artificial wave	2501	0.02	50.02

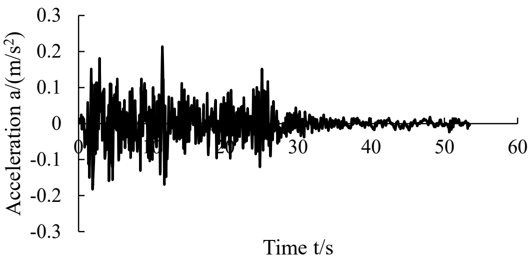

（a）El-centro

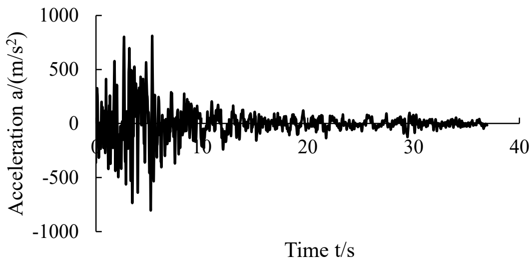

（b）S0202

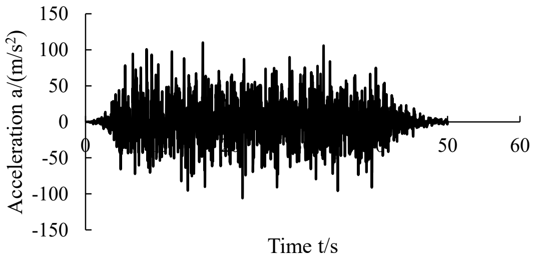

（c）RGB

Figure 4.2 Acceleration diagram of the earthquake waves

4.2.2 Study of vertical stiffness of 3-D isolation layer

In order to obtain the seismic internal force response and floor lateral displacement response of the upper structure, the horizontal seismic action is applied on the 3-D vibration and seismic isolation structure, and then nonlinear dynamic time-history analysis is performed with different vertical stiffness of the isolation layer under fortification earthquakes and rare earthquakes.

4.2.2.1 Comparison of calculation results

Taking the X direction of the structure as an example, the base shear force, base overturning moment, maximum inter-story drift angle, and maximum lateral displacement of top floor of the upper structure are shown in Table 4.3, Table 4.4, Figure 4.3, and Figure 4.4.

It can be seen that under the action of fortification earthquakes and rare earthquakes, as the vertical stiffness of the isolation layer decreases, the base shear force and base overturning moment first decrease and then increase. On the whole, the base internal force response of the 3-D isolation structure is slightly larger than that of the horizontal seismic isolation structure, indicating that the vertical vibration isolation layer has a slight amplification effect on the horizontal seismic action.

The rocking effect of the 3-D isolation structure leads to an increase in the lateral displacement of floors. Under the action of fortification earthquakes and rare earthquakes, as the vertical stiffness of the isolation layer decreases, the rocking effect intensify, so that the maximum inter-story drift angle and maximum lateral displacement of top floor increase, and the increasing rate is getting faster and faster.

Table 4.3 Comparison of the horizontal seismic response of the upper structure under different vertical stiffness of the isolation layer (fortification earthquake)

Item	HISO	K_v/K_h					
		8	12	20	40	60	80
Base shear force (kN)	9163	9701	9584	9149	9227	9384	9460
Ratio (3DISO / HISO)	100%	106%	105%	100%	101%	102%	103%
Base overturning moment ($\times10^5$kN·m)	3.345	3.451	3.440	3.415	3.314	3.210	3.313
Ratio (3DISO / HISO)	100%	103%	103%	102%	99%	96%	99%
Maximum inter-story drift angle (rad)	1/399	1/144	1/196	1/239	1/280	1/306	1/329
Maximum lateral displacement of top floor (mm)	311	596	498	419	370	356	347
Rocking angle ($\times10^{-4}$rad)	0	43.96	28.11	17.41	9.46	6.81	5.27

Attention: “3DISO” means the pure 3-D vibration and seismic isolation structure, “HISO” means horizontal seismic isolation structure with the same layout and parameters of rubber bearings, here after the same.

Table 4.4 Comparison of the horizontal seismic response of the upper structure under different vertical stiffness of the isolation layer (rare earthquake)

Item	HISO	K_v/K_h					
		8	12	20	40	60	80
Base shear force (kN)	18383	19187	18572	18273	18546	18698	18653
Ratio (3DISO / HISO)	100%	104%	101%	99%	101%	102%	101%
Base overturning moment ($\times10^5$kN·m)	6.322	7.016	6.588	6.481	6.613	6.510	6.517
Ratio (3DISO / HISO)	100%	111%	104%	103%	105%	103%	103%
Maximum inter-story drift angle (rad)	1/192	1/71	1/93	1/119	1/135	1/150	1/159
Maximum lateral displacement of top floor (mm)	701	1270	1045	885	824	790	769
Rocking angle ($\times10^{-4}$rad)	0	93.97	57.72	37.30	19.59	13.64	10.35

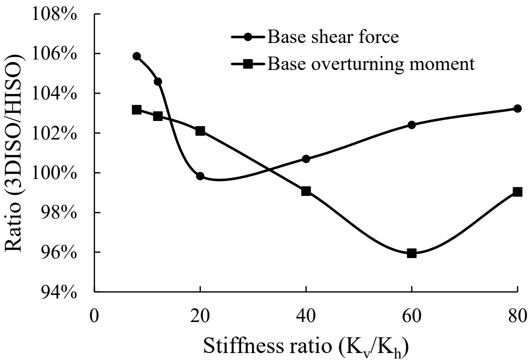

(a) Base internal force

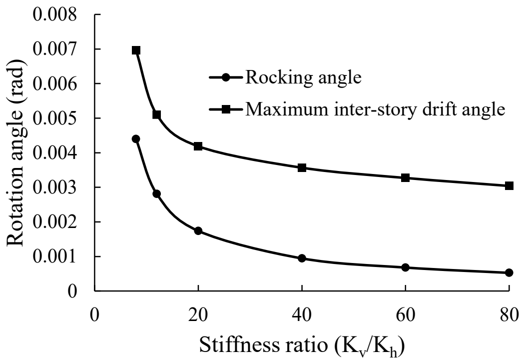

(b) Relevant rotation angle

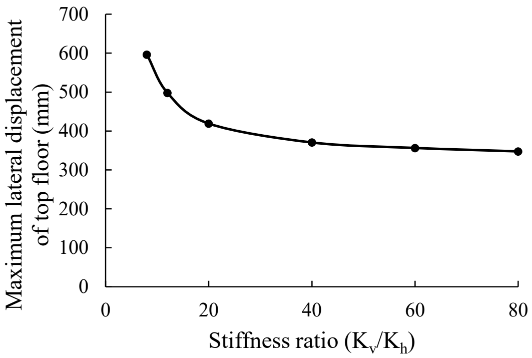

(c) Maximum lateral displacement of top floor

Figure 4.3 Horizontal seismic response of the upper structure (fortification earthquake)

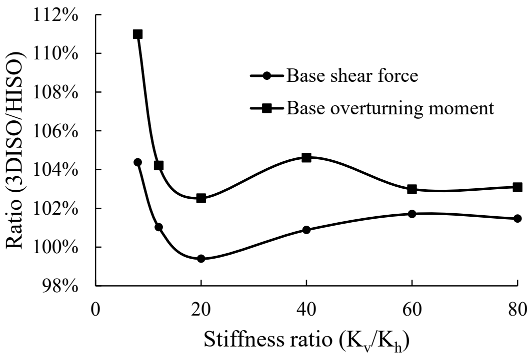

(a) Base internal force

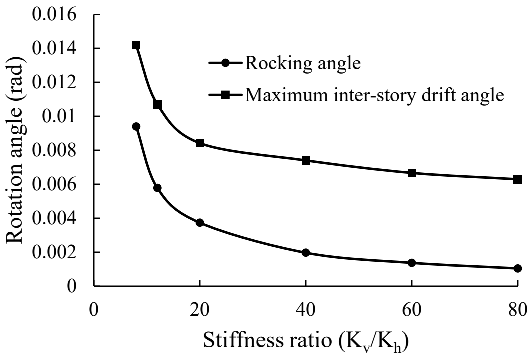

(b) Relevant rotation angle

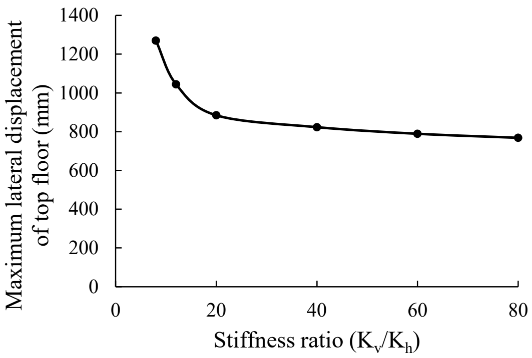

(c) Maximum lateral displacement of top floor

Figure 4.4 Horizontal seismic response of the upper structure (rare earthquake)

4.2.2.2 Explanation of the results

Figure 4.5 shows the horizontal natural period of the structure in X-direction. The horizontal natural period of the 3-D vibration and seismic isolation structure is greater than that of the horizontal seismic isolation structure. As the vertical stiffness of the isolation layer decreases, the horizontal natural period increases, and reaches farther and farther away from the site characteristic period of 0.45s, so that the seismic mitigation performance will be enhanced. Figure 4.6 shows the additional damping ratio of the structure. Under the action of fortification earthquakes and rare earthquakes, the additional damping ratio of the 3-D vibration and seismic isolation structure is smaller than that of the horizontal seismic isolation structure. As the vertical stiffness of the isolation layer decreases, the additional damping ratio decreases, so that the seismic mitigation performance will be weakened, and the weakening effect under the action of fortification earthquakes is greater than that of rare earthquakes. The natural period prolonging effect and the additional damping effect affect the seismic response of the upper structure together. On the whole, the base internal force response of the 3-D isolation structure is slightly larger than that of the horizontal seismic isolation structure, indicating that the vertical vibration isolation layer has a slight amplification effect on the horizontal seismic action.

It can be seen from Section 2.3.3 that as the vertical stiffness of the isolation layer decreases, the rigid rocking angle of the upper structure increases, and the rate of increase becomes faster and faster. Therefore, the maximum inter-story drift angle and maximum lateral displacement of top floor increase, and the rate of increase is getting faster and faster.

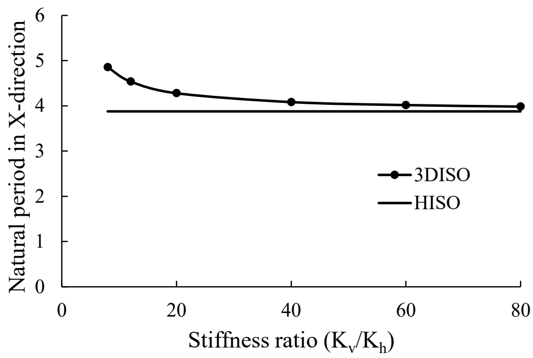

Figure 4.5 The natural period in X-direction

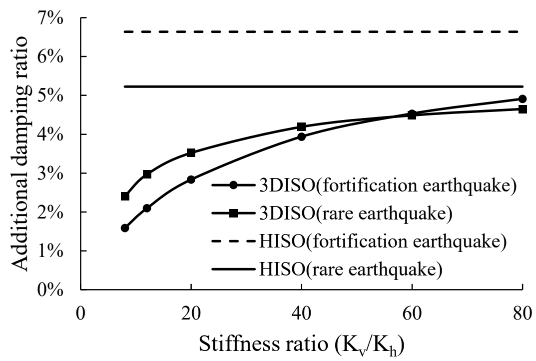

Figure 4.6 The additional damping ratio

4.2.3 Conclusion of the section

From the perspective of horizontal seismic isolation, the vertical stiffness of the isolation layer should not be too small. When the vertical natural frequency of the structure is lower than 1 Hz, severe rocking effect will occur in the upper structure, then the inter-story drift angle and lateral displacement of floors will increase sharply. At the same time, the magnification effect of the horizontal earthquake due to the reduction of the vertical stiffness of the isolation layer is also beginning to be obvious.

Considering the performance of horizontal seismic isolation and vertical subway vibration isolation, the recommended vertical natural frequency of the 3-D vibration and seismic isolation structure is 1.0~1.3Hz.

4.3 Seismic isolation performance of the 3-D vibration and seismic isolation + vertical viscous dampers structure

4.3.1 Analytical model

The analytical model is based on Section 4.2.1, then fixes the vertical stiffness of the isolation layer $K_v = 12K_h$, and adds 4 vertical viscous dampers to the four corners of the isolation layer. The plane layout of the isolation layer is shown in Figure 4.7.

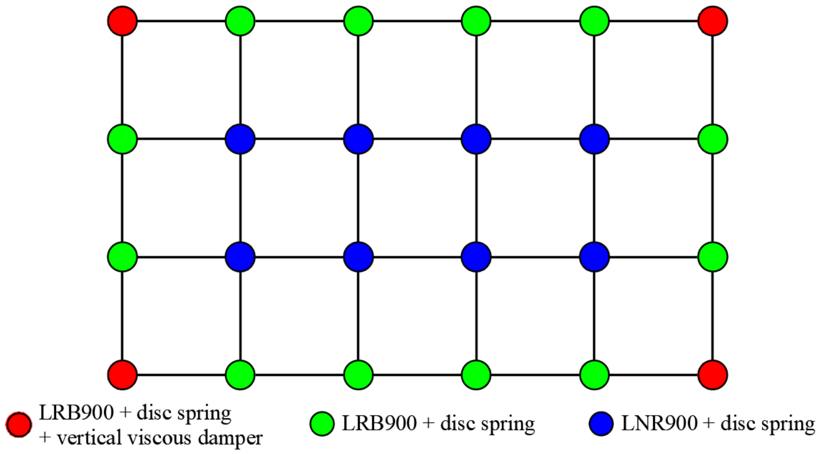

Figure 4.7 The plane layout of 3-D vibration and seismic isolation layer

4.3.2 Study of damping coefficient of vertical dampers

Keeping the parameters and layout of the 3-D vibration and seismic isolation bearings in the isolation layer unchanged, the damping index of the viscous dampers is fixed at $\alpha = 0.5$, and the damping coefficient C is respectively 500, 1000, 2000, 3000, 4000, 5000 $kN/(m/s)^{\alpha}$ for different cases.

In order to obtain the seismic internal force response and floor lateral displacement response of the upper structure, the horizontal seismic action is applied on the 3-D variation and seismic isolation structure, and then nonlinear dynamic time-history analysis is performed with different vertical damping coefficient under fortification earthquakes and rare earthquakes.

4.3.2.1 Comparison of calculation results

Taking the X direction of the structure as an example, the base shear force, base overturning moment, maximum axial stress of rubber bearings, maximum inter-story drift angle, and maximum lateral displacement of top floor of the upper structure are shown in Table 4.5, Table 4.6, Figure 4.8, and Figure 4.9. The damping coefficient *C* = 0 means that there are not any vertical viscous dampers in the isolation layer (that is, the pure 3-D vibration and seismic isolation structure).

It can be seen that under the action of fortification earthquakes and rare earthquakes, as the vertical damping coefficient increases, the base shear force and base overturning moment decrease, and the maximum axial stress of rubber bearings increases. The rubber bearing with largest axial stress in the isolation layer is located at the four corners.

Table 4.5 Comparison of the horizontal seismic response of the upper structure under different vertical damping coefficient (fortification earthquake)

Item	HISO	Vertical damping coefficient *C*					
		500	1000	2000	3000	4000	5000
Base shear force (kN)	9163	9410	9240	8921	8793	8683	8573
Ratio (3DISOVD / HISO)	100%	103%	101%	97%	96%	95%	94%
Base overturning moment ($\times10^5$kN·m)	3.345	3.347	3.271	3.147	3.050	2.962	2.880
Ratio (3DISOVD / HISO)	100%	100%	98%	94%	91%	89%	86%
Maximum axial stress of rubber bearings (MPa)	-0.421	-0.926	-0.923	-0.915	-0.906	-0.898	-0.890
Maximum inter-story drift angle (rad)	1/399	1/192	1/192	1/199	1/208	1/218	1/228
Maximum lateral displacement of top floor (mm)	311	487	477	458	441	424	407
Rocking angle ($\times10^{-3}$rad)	0	2.68	2.54	2.29	2.08	1.88	1.70

Attention: “3DISOVD” means the 3-D vibration and seismic isolation + vertical viscous dampers structure, here after the same.

The rocking effect of the 3-D isolation structure leads to an increase in the lateral displacement of floors. Under the action of fortification earthquakes and rare earthquakes, as the vertical damping coefficient increases, the rocking effect decreases, so that the maximum inter-story drift angle and maximum lateral displacement of top floor decrease, indicating that large vertical damping in the isolation layer is very effective in suppressing the rocking effect of the upper structure.

Table 4.6 Comparison of the horizontal seismic response of the upper structure under different vertical damping coefficient (rare earthquake)

Item	HISO	Vertical damping coefficient *C*					
		500	1000	2000	3000	4000	5000
Base shear force (kN)	18383	18312	18050	17599	17349	17088	16833
Ratio (3DISOVD / HISO)	100%	100%	98%	96%	94%	93%	92%
Base overturning moment ($\times 10^5$kN·m)	6.322	6.498	6.411	6.235	6.059	5.895	5.757
Ratio (3DISOVD / HISO)	100%	103%	101%	99%	96%	93%	91%
Maximum axial stress of rubber bearings (MPa)	-0.020	-0.600	-0.599	-0.590	-0.578	-0.566	-0.553
Maximum inter-story drift angle (rad)	1/192	1/94	1/95	1/97	1/100	1/103	1/107
Maximum lateral displacement of top floor (mm)	701	1032	1019	992	966	939	915
Rocking angle ($\times 10^{-3}$rad)	0	5.62	5.46	5.13	4.79	4.47	4.18

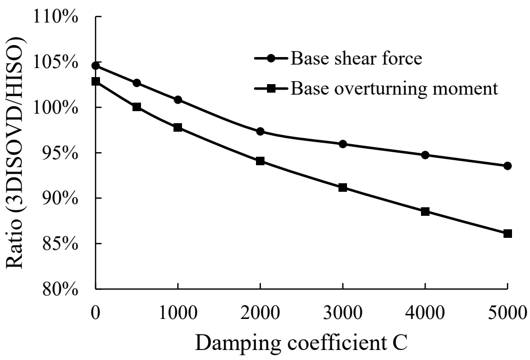

(a) Base internal force

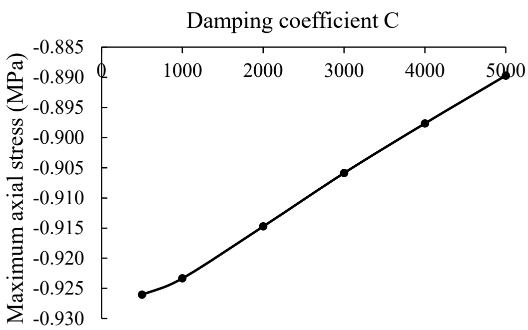

(b) Maximum axial stress of rubber bearings

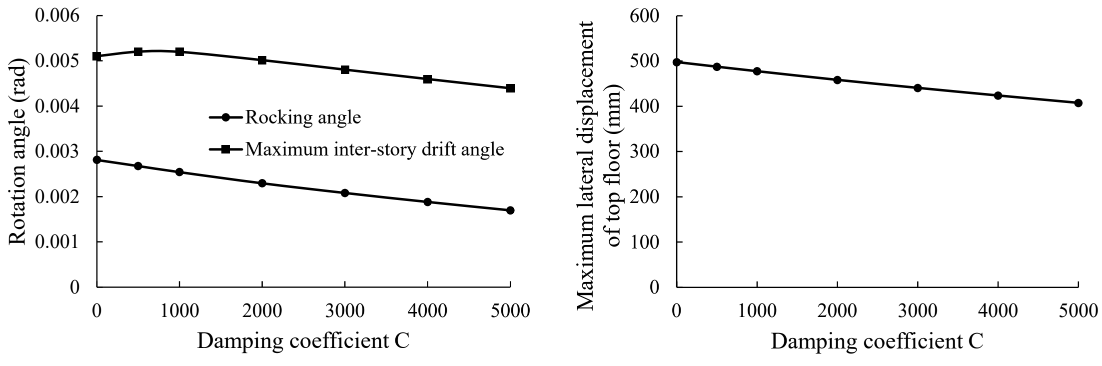

(c) Relevant rotation angle (d) Maximum lateral displacement of top floor

Figure 4.8 Horizontal seismic response of the upper structure (fortification earthquake)

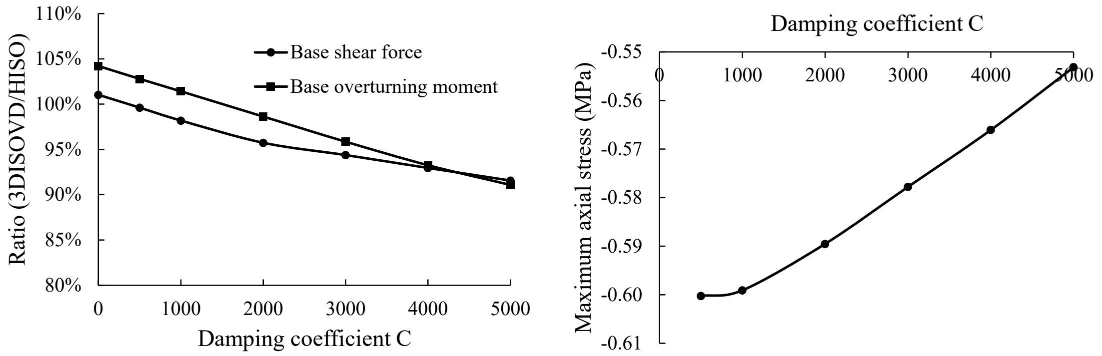

(a) Base internal force (b) Maximum axial stress of rubber bearings

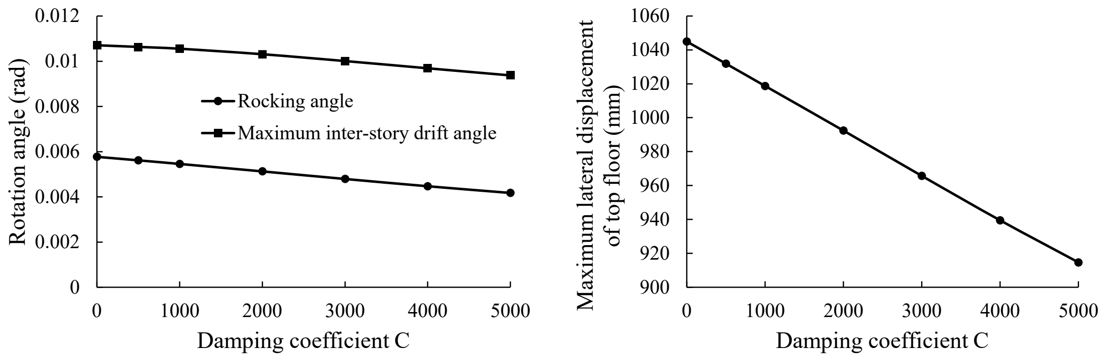

(c) Relevant rotation angle (d) Maximum lateral displacement of top floor

Figure 4.9 Horizontal seismic response of the upper structure (rare earthquake)

4.3.2.2 Explanation of the results

Figure 4.10 shows the additional dynamic stiffness of a single vertical viscous damper in the isolation layer. Under the action of fortification earthquakes and rare earthquakes, as the vertical damping coefficient increases, the additional dynamic stiffness of viscous dampers increases, then the vertical total stiffness of the 3-D isolation bearings located at four corners increases, so that the rocking angle of the upper structure decreases according to section 4.2.2, and the maximum inter-story drift angle and maximum lateral displacement of top floor decrease. As the vertical damping coefficient increases, the local vertical stiffness of the four corners in the isolation layer increases, so the maximum axial stress of rubber bearings at the four corners increases under the action of base overturning moment.

Figure 4.11 shows the additional damping ratio of the structure. Under the action of fortification earthquakes and rare earthquakes, as the vertical damping coefficient increases, the additional damping ratio of the 3-D isolation structure increases, and the energy consumption capacity of the structure is enhanced, so the structural base shear force and base overturning moment are reduced.

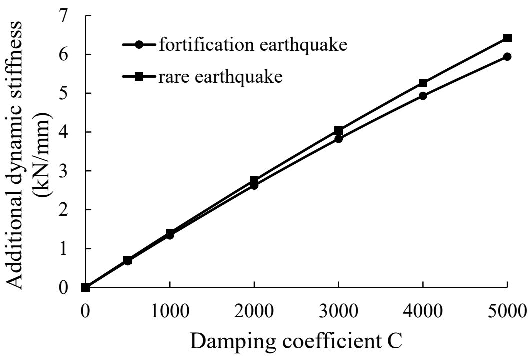

Figure 4.10 The additional dynamic stiffness of a single vertical viscous damper

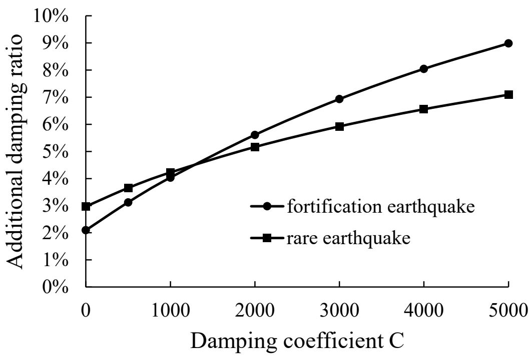

Figure 4.11 The additional damping ratio

In summary, from the perspective of horizontal seismic isolation, the recommended value for the vertical damping coefficient C is a range of 4000~5000 $kN/(m/s)^{\alpha}$, because not only the rocking effect of the upper structure can be effectively controlled, but the base internal force response under the action of horizontal earthquake has also been reduced to a certain extent.

4.3.3 Study of damping index of vertical dampers

Keeping the parameters and layout of the 3-D vibration and seismic isolation bearings in the isolation layer unchanged, the damping coefficient of the viscous dampers is fixed at $C = 5000kN/(m/s)^{\alpha}$, and the damping index α is respectively 0.1、0.3、0.5、0.7、0.9 for different cases.

In order to obtain the seismic internal force response and floor lateral displacement response of the upper structure, the horizontal seismic action is applied on the 3-D variation and seismic isolation structure, and then nonlinear dynamic time-history analysis is performed with different vertical damping index under fortification earthquakes and rare earthquakes.

4.3.3.1 Comparison of calculation results

Taking the X direction of the structure as an example, the base shear force, base overturning moment, maximum axial stress of rubber bearings, maximum inter-story drift angle, and maximum lateral displacement of top floor of the upper structure are shown in Table 4.7, Table 4.8, Figure 4.12, and Figure 4.13.

Table 4.7 Comparison of the horizontal seismic response of the upper structure under different vertical damping index (fortification earthquake)

Item	HISO	Vertical damping index α					No damping
		0.1	0.3	0.5	0.7	0.9	
Base shear force (kN)	9163	9207	8488	8573	8766	9017	9584
Ratio (3DISOVD / HISO)	100%	100%	93%	94%	96%	98%	105%
Base overturning moment ($\times 10^5$kN·m)	3.345	3.024	2.706	2.880	3.045	3.158	3.440
Ratio (3DISOVD / HISO)	100%	90%	81%	86%	91%	94%	103%
Maximum axial stress of rubber bearings (MPa)	-0.421	-0.519	-0.774	-0.890	-0.919	-0.931	-0.987
Maximum inter-story drift angle (rad)	1/399	1/332	1/285	1/228	1/204	1/195	1/196
Maximum lateral displacement of top floor (mm)	311	340	349	407	446	467	498
Rocking angle ($\times 10^{-3}$rad)	0	0.381	1.010	1.697	2.158	2.414	2.811

Table 4.8 Comparison of the horizontal seismic response of the upper structure under different vertical damping index (rare earthquake)

Item	HISO	Vertical damping index α					No damping
		0.1	0.3	0.5	0.7	0.9	
Base shear force (kN)	18383	16111	16007	16833	17377	17679	18572
Ratio (3DISOVD / HISO)	100%	88%	87%	92%	95%	96%	101%
Base overturning moment ($\times 10^5$kN·m)	6.322	6.033	5.515	5.757	6.042	6.238	6.588
Ratio (3DISOVD / HISO)	100%	95%	87%	91%	96%	99%	104%
Maximum axial stress of rubber bearings (MPa)	-0.020	-0.173	-0.419	-0.553	-0.587	-0.605	-0.613
Maximum inter-story drift angle (rad)	1/192	1/136	1/121	1/107	1/99	1/96	1/93
Maximum lateral displacement of top floor (mm)	701	773	832	915	969	1001	1045
Rocking angle ($\times 10^{-3}$rad)	0	2.542	3.279	4.177	4.843	5.226	5.772

It can be seen that under the action of fortification earthquakes and rare earthquakes, as the vertical damping index decreases, the base shear force and base overturning moment first decrease and then increase, and the maximum axial stress of rubber bearings increases. The rubber bearing with largest axial stress in the isolation layer is located at the four corners.

The rocking effect of the 3-D isolation structure leads to an increase in the lateral displacement of floors. Under the action of fortification earthquakes and rare earthquakes, as the vertical damping index decreases, the rocking effect decreases, so that the maximum inter-story drift angle and maximum lateral displacement of top floor decrease, indicating that large vertical damping in the isolation layer is very effective in suppressing the rocking effect of the upper structure.

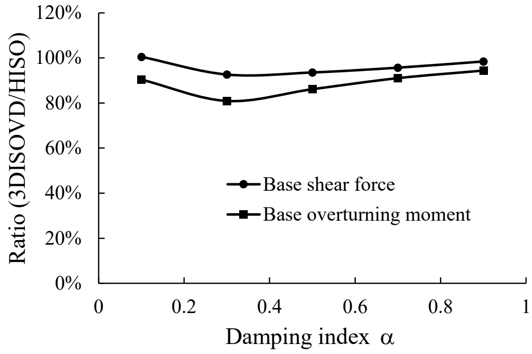

(a) Base internal force

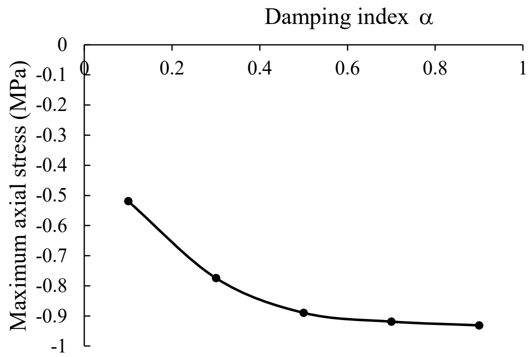

(b) Maximum axial stress of rubber bearings

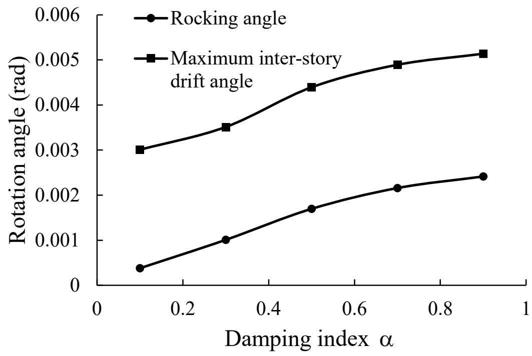

(c) Relevant rotation angle

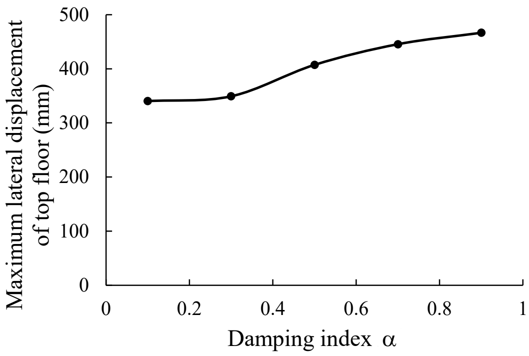

(d) Maximum lateral displacement of top floor

Figure 4.12 Horizontal seismic response of the upper structure (fortification earthquake)

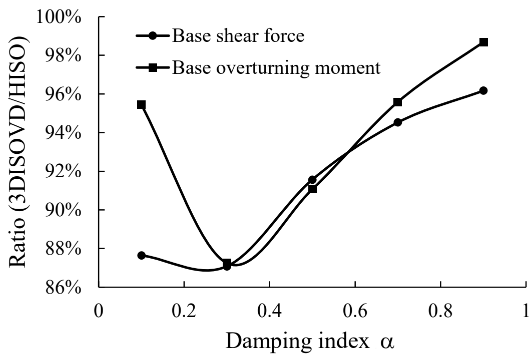

(a) Base internal force

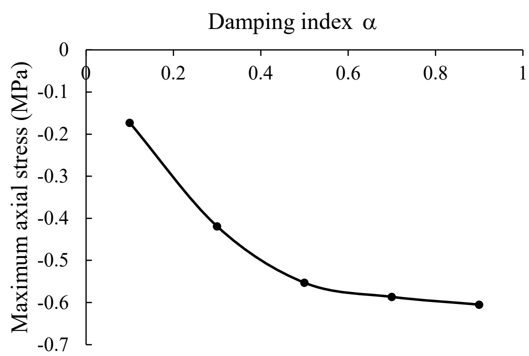

(b) Maximum axial stress of rubber bearings

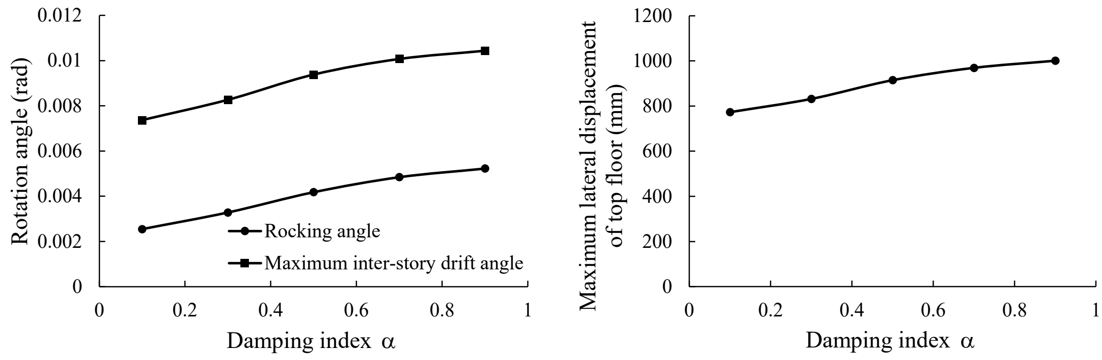

(c) Relevant rotation angle (d) Maximum lateral displacement of top floor

Figure 4.13 Horizontal seismic response of the upper structure (rare earthquake)

4.3.3.2 Explanation of the results

Figure 4.14 shows the additional dynamic stiffness of a single vertical viscous damper in the isolation layer. Under the action of fortification earthquakes and rare earthquakes, as the vertical damping index decreases, the additional dynamic stiffness of viscous dampers increases, then the vertical total stiffness of the 3-D isolation bearings located at four corners increases, so that the rocking angle of the upper structure decreases according to section 4.2.2, and the maximum inter-story drift angle and maximum lateral displacement of top floor decrease. As the vertical damping index decreases, the local vertical stiffness of the four corners in the isolation layer increases, so the maximum axial stress of rubber bearings at the four corners increases under the action of base overturning moment.

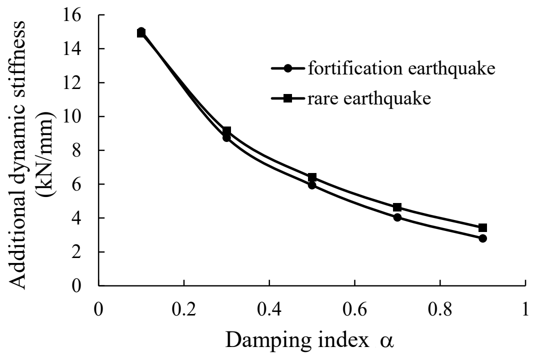

Figure 4.14 The additional dynamic stiffness of a single vertical viscous damper

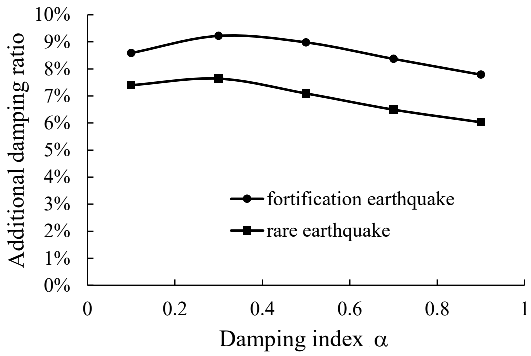

Figure 4.15 The additional damping ratio

Figure 4.15 shows the additional damping ratio of the structure. Under the action of fortification earthquakes and rare earthquakes, as the vertical damping index decreases, the additional damping ratio of the 3-D isolation structure first increases and then decreases, and the energy consumption capacity of the structure is first enhanced and then weakened, so the structural base shear force and base overturning moment first decrease and then increase.

In summary, from the perspective of horizontal seismic isolation, the recommended value for the vertical damping index α is a range of 0.2~0.3, because not only the rocking effect of the upper structure can be effectively controlled, but the base internal force response under the action of horizontal earthquake has also been reduced to a certain extent.

4.3.4 Conclusion of the section

When designing the horizontal seismic isolation performance of the structure, the larger the vertical damping coefficient of dampers, or the smaller the vertical damping index of dampers, the smaller the rocking angle of the upper structure. The vertical viscous dampers arranged at the four corners of the 3-D isolation layer can effectively suppress the rocking effect of the upper structure.

Under the premise of not requiring subway vibration isolation capacity, when the vertical damping coefficient is at a range of 4000~5000 $kN/(m/s)^{\alpha}$ and the vertical damping index is at a range of 0.2~0.3, the base internal force response of the upper structure is smallest under the action of horizontal earthquake, and the rocking effect is also significantly reduced, which indicate that the horizontal seismic isolation performance is optimal.

As for high-rise over-track buildings, considering the vertical subway vibration isolation requirements, only small damping can be introduced into the four corners of the 3-D isolation layer. But at this circumstance the horizontal seismic response of the upper structure is slightly lower than that of the pure 3-D vibration and seismic isolation structure, and the degree of suppression of the rocking effect is also low. At the same time, considering that the additional dynamic stiffness of the vertical viscous dampers under subway vibration excitation is much greater than under horizontal seismic excitation. For example, when C = 500 $kN/(m/s)^{\alpha}$ and $\alpha =$ 0.5, the additional dynamic stiffness of vertical dampers under the action of DTB1 is 580 times that under the action of horizontal seismic waves. The total local vertical stiffness of bearings at four corners under the action of subway vibration waves is approximately equivalent to the vertical stiffness of the rubber bearings. Even with small vertical damping in the 3-D isolation layer, it will make the vertical vibration response of joints above the dampers equal to that of an unisolated structure. Therefore, if the subway vibration isolation performance of all parts in the upper structure is required, the 3-D isolation layer is not recommended to introduce any vertical viscous dampers.

However, in real engineering design, if the vertical stiffness of the isolation layer is too low so that the rocking effect of the upper structure is too significant, the indoor vibration control requirements near the four corners of the building have to be sacrificed. And then the vertical viscous dampers with damping coefficient C = 4000~5000 $kN/(m/s)^{\alpha}$ and α= 0.2~0.3 should be introduced into corners of the 3-D isolation layer. At this circumstance, the requirements of vertical vibration control in the inner part of the building can not only be satisfied, but the rocking effect of the upper structure can also be effectively suppressed, the horizontal seismic mitigation and isolation performance of the structure is optimal.

4.4 Seismic isolation performance of the 3-D vibration and seismic isolation + horizontal viscous dampers structure

4.4.1 Analytical model

The analytical model is based on Section 4.2.1, then fixes the vertical stiffness of the isolation layer K_v = $12K_h$, and adds 8 horizontal viscous dampers to the 3-D isolation layer (4 on the X-direction and 4 on the Y-direction). The plane layout of the isolation layer is shown in Figure 4.16.

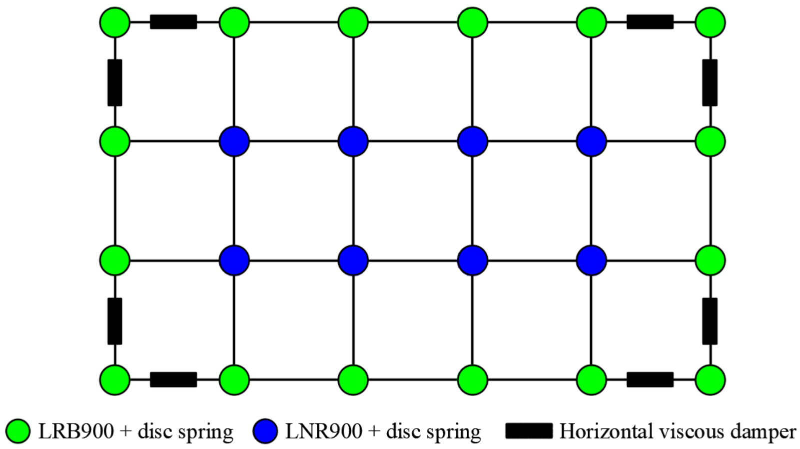

Figure 4.16 The plane layout of 3-D vibration and seismic isolation layer

4.4.2 Study of damping coefficient of horizontal dampers

Keeping the parameters and layout of the 3-D vibration and seismic isolation bearings in the isolation layer unchanged, the damping index of the horizontal viscous dampers is fixed at α = 0.5, and the damping coefficient C is respectively 500, 1000, 2000, 3000, 4000, 5000 $kN/(m/s)^{\alpha}$ for different cases.

In order to obtain the seismic internal force response and floor lateral displacement response of the upper structure, the horizontal seismic action is applied on the 3-D variation and seismic isolation structure, and then nonlinear dynamic time-history analysis is performed with different horizontal damping coefficient under fortification earthquakes and rare earthquakes.

4.4.2.1 Comparison of calculation results

Table 4.9 Comparison of the horizontal seismic response of the upper structure under different horizontal damping coefficient (fortification earthquake)

Item	HISO	Horizontal damping coefficient C					
		500	1000	2000	3000	4000	5000
Base shear force (kN)	9163	8916	8883	9824	10827	11660	12313
Ratio (3DISOHD / HISO)	100%	97%	97%	107%	118%	127%	134%
Base overturning moment ($\times 10^5$kN·m)	3.345	3.086	2.910	3.389	3.768	4.088	4.366
Ratio (3DISOHD / HISO)	100%	92%	87%	101%	113%	122%	131%
Maximum axial stress of rubber bearings (MPa)	-0.421	-0.961	-0.977	-0.924	-0.883	-0.850	-0.820
Maximum horizontal deformation of isolation layer (mm)	217	189	161	130	107	89	76

Attention: "3DISOHD" means the 3-D vibration and seismic isolation + horizontal viscous dampers structure, here after the same

Table 4.10 Comparison of the horizontal seismic response of the upper structure under different horizontal damping coefficient (rare earthquake)

Item	HISO	Horizontal damping coefficient C					
		500	1000	2000	3000	4000	5000
Base shear force (kN)	18383	16338	15439	15196	16428	17592	18643
Ratio (3DISOHD / HISO)	100%	89%	84%	83%	89%	96%	101%
Base overturning moment ($\times 10^5$kN·m)	6.322	5.911	5.385	4.781	5.310	5.770	6.189
Ratio (3DISOHD / HISO)	100%	94%	85%	76%	84%	91%	98%
Maximum axial stress of rubber bearings (MPa)	-0.020	-0.670	-0.723	-0.779	-0.719	-0.668	-0.623
Maximum horizontal deformation of isolation layer (mm)	520	419	370	302	254	217	188

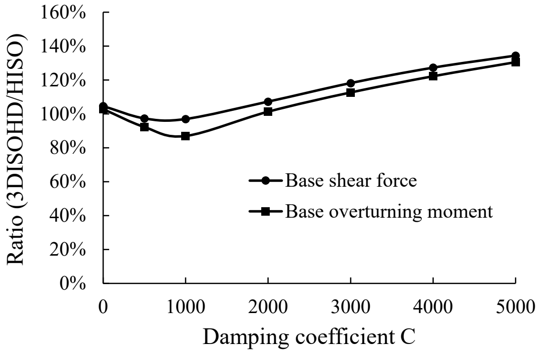

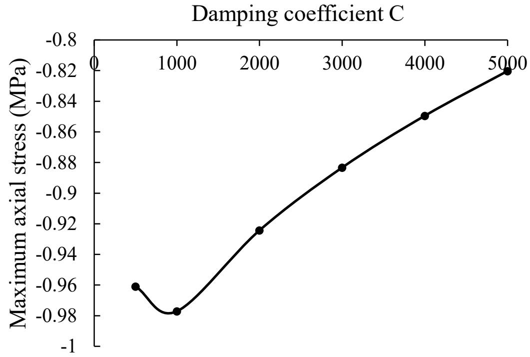

(a) Base internal force (b) Maximum axial stress of rubber bearings

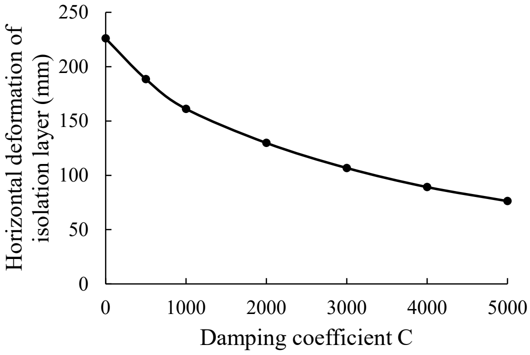

(c) Maximum horizontal deformation of isolation layer

Figure 4.17 Horizontal seismic response of the upper structure (fortification earthquake)

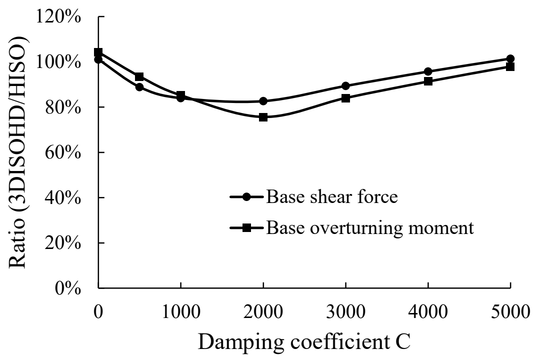

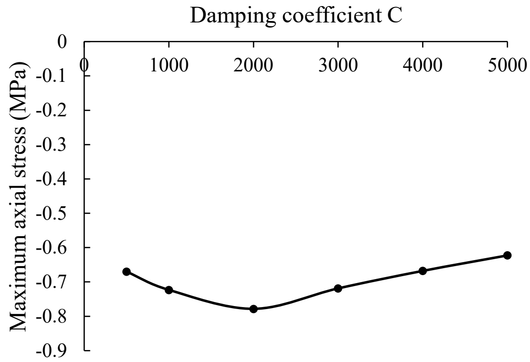

(a) Base internal force (b) Maximum axial stress of rubber bearings

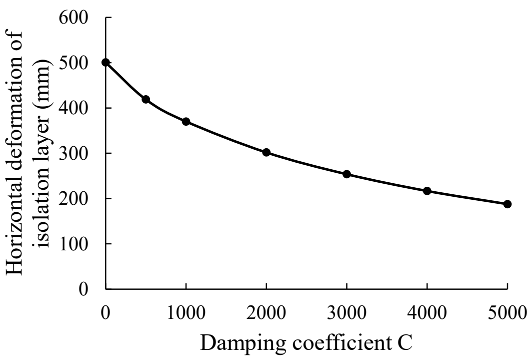

(c) Maximum horizontal deformation of isolation layer

Figure 4.18 Horizontal seismic response of the upper structure (rare earthquake)

Taking the X direction of the structure as an example, the base shear force, base overturning moment, maximum axial stress of rubber bearings, and maximum horizontal deformation of isolation layer are shown in Table 4.9, Table 4.10, Figure 4.17, and Figure 4.18. The damping coefficient C = 0 means that there are not any horizontal viscous dampers in the isolation layer (that is, the pure 3-D vibration and seismic isolation structure).

It can be seen that under the action of fortification earthquakes and rare earthquakes, as the horizontal damping coefficient of dampers increases, the base shear force, base overturning moment, and maximum axial stress of rubber bearings first decrease and then increase, and the extreme point is near C = 1000 under the action of fortification earthquake, near C = 2000 under the action of rare earthquake. As the horizontal damping coefficient of dampers increases, the maximum horizontal deformation of isolation layer keeps decreasing.

4.4.2.2 Explanation of the results

Figure 4.19 shows the horizontal additional dynamic stiffness ratio of the 3-D isolation layer, which is defined as Equation 4.1:

$$\eta = \frac{K_{damper}}{K_H} \tag{4.1}$$

Where, K_{damper} is the total additional dynamic stiffness of all horizontal dampers, K_H is the total horizontal stiffness of the 3-D isolation layer.

It can be seen that under the action of fortification earthquakes and rare earthquakes, as the horizontal damping coefficient of dampers increases, the horizontal additional dynamic stiffness ratio increases, so the maximum horizontal deformation of isolation layer decreases.

Figure 4.20 shows the additional damping ratio of the structure. It can be seen that under the action of fortification earthquakes and rare earthquakes, as the horizontal damping coefficient of dampers increases, first of all, the additional damping effect is greater than the additional dynamic stiffness effect, so the base internal force response and the maximum axial stress of rubber bearings decrease. Subsequently, the additional dynamic stiffness effect is greater than the additional damping effect, so the base internal force response and the maximum axial stress of rubber bearings increase. The horizontal additional dynamic stiffness effect of fortification earthquakes is greater than that of rare earthquakes, and the additional damping effect of fortification earthquakes is less than that of rare earthquakes, so the extreme points of the base internal force curve and maximum axial stress curve of rubber bearings are smaller than those of rare earthquakes.

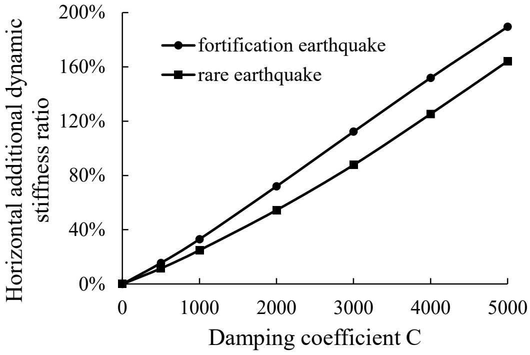

Figure 4.19 Horizontal additional dynamic stiffness ratio of the isolation layer

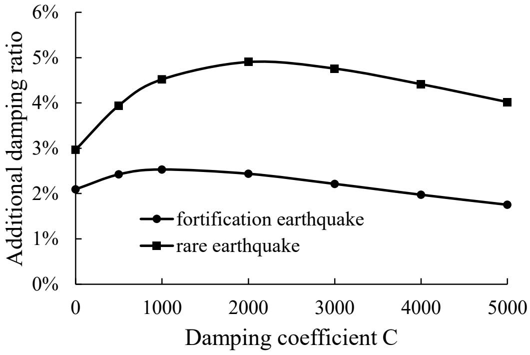

Figure 4.20 Additional damping ratio of the structure

In summary, from the perspective of horizontal seismic isolation, the recommended value for the horizontal damping coefficient C is a range of $1000\text{~}2000kN/(m/s)^{\alpha}$.

4.4.3 Study of damping index of horizontal dampers

Keeping the parameters and layout of the 3-D vibration and seismic isolation bearings in the isolation layer unchanged, the damping coefficient of the horizontal viscous dampers is fixed at $C = 2000kN/(m/s)^{\alpha}$, and the damping index α is respectively 0.1、0.3、0.5、0.7、0.9 for different cases.

In order to obtain the seismic internal force response and floor lateral displacement response of the upper structure, the horizontal seismic action is applied on the 3-D variation and seismic isolation structure, and then nonlinear dynamic time-history analysis is performed with different horizontal damping index under fortification earthquakes and rare earthquakes.

4.4.3.1 Comparison of calculation results

Taking the X direction of the structure as an example, the base shear force, base overturning moment, maximum axial stress of rubber bearings, maximum horizontal deformation of isolation layer are shown in Table 4.11, 4.12, and Figure 4.21, 4.22.

It can be seen that under the action of fortification earthquakes, as the horizontal damping index of dampers decreases, the base shear force, base overturning moment, and maximum axial stress of rubber bearings increase, and the maximum horizontal deformation of isolation layer decreases. Under the action of rare earthquakes, as the horizontal damping index of dampers decreases, the base shear force, base overturning moment, and maximum axial stress of rubber bearings first decrease and then increase, and the maximum horizontal deformation of isolation layer decreases.

Table 4.11 Comparison of the horizontal seismic response of the upper structure under different horizontal damping index (fortification earthquake)

Item	HISO	Horizontal damping index α					No damping
		0.1	0.3	0.5	0.7	0.9	
Base shear force (kN)	9163	12034	10315	9824	9612	9465	9584
Ratio (3DISOHD / HISO)	100%	131%	113%	107%	105%	103%	105%
Base overturning moment ($\times10^5$kN·m)	3.345	4.776	3.841	3.389	3.135	2.969	3.440
Ratio (3DISOHD / HISO)	100%	143%	115%	101%	94%	89%	103%
Maximum axial stress of rubber bearings (MPa)	-0.421	-0.777	-0.876	-0.924	-0.952	-0.971	-0.987
Maximum horizontal deformation of isolation layer (mm)	217	76	100	130	151	167	226

Table 4.12 Comparison of the horizontal seismic response of the upper structure under different horizontal damping index (rare earthquake)

Item	HISO	Horizontal damping index α					No damping
		0.1	0.3	0.5	0.7	0.9	
Base shear force (kN)	18383	17668	14982	15196	15409	15526	18572
Ratio (3DISOHD / HISO)	100%	96%	81%	83%	84%	84%	101%
Base overturning moment ($\times10^5$kN·m)	6.322	5.495	4.991	4.781	4.926	5.083	6.588
Ratio (3DISOHD / HISO)	100%	87%	79%	76%	78%	80%	104%
Maximum axial stress of rubber bearings (MPa)	-0.020	-0.699	-0.754	-0.779	-0.770	-0.753	-4.041
Maximum horizontal deformation of isolation layer (mm)	520	201	258	302	335	362	501

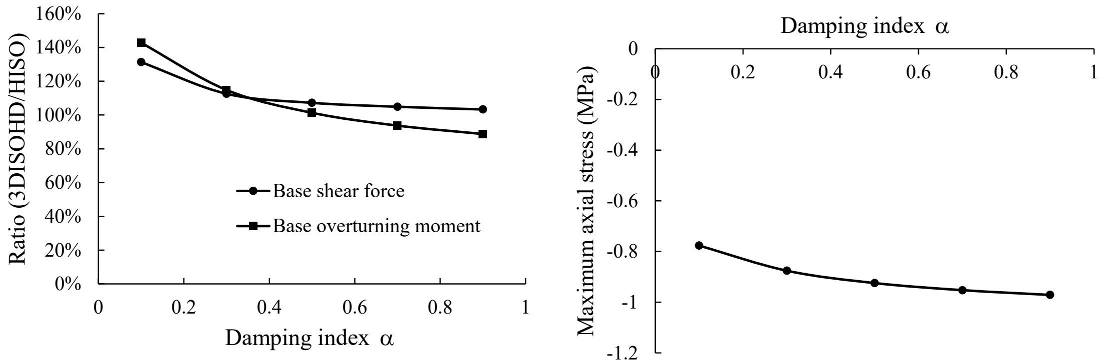

(a) Base internal force (b) Maximum axial stress of rubber bearings

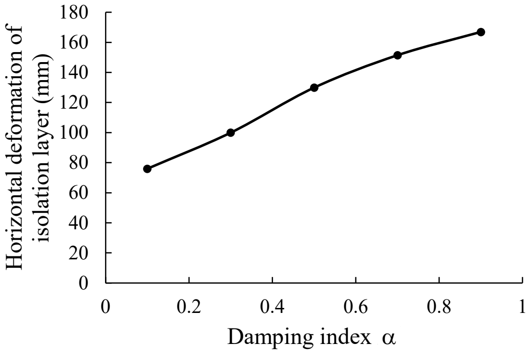

(c) Maximum horizontal deformation of isolation layer

Figure 4.21 Horizontal seismic response of the upper structure (fortification earthquake)

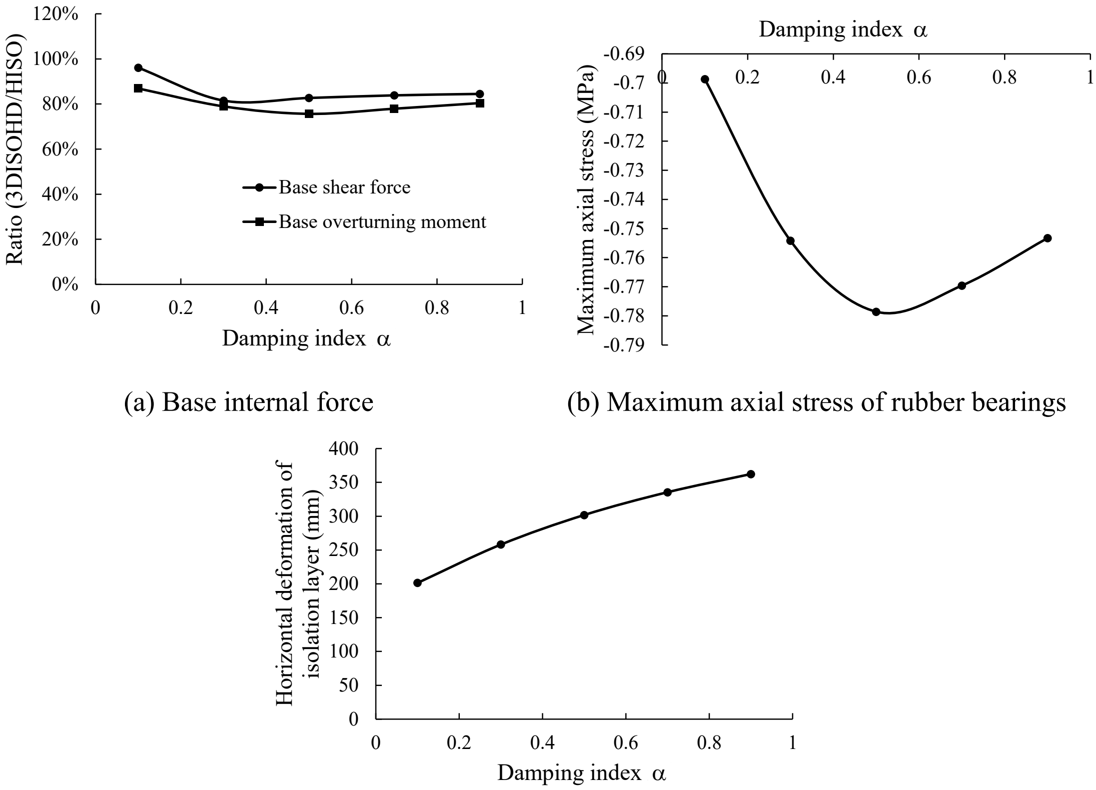

(a) Base internal force

(b) Maximum axial stress of rubber bearings

(c) Maximum horizontal deformation of isolation layer

Figure 4.22 Horizontal seismic response of the upper structure (rare earthquake)

4.4.3.2 Explanation of the results

Figure 4.23 shows the horizontal additional dynamic stiffness ratio of the isolation layer. It can be seen that under the action of fortification earthquakes and rare earthquakes, as the horizontal damping index of dampers decreases, the horizontal additional dynamic stiffness ratio increases, so the horizontal deformation of the seismic isolation layer decreases.

Figure 4.24 shows the additional damping ratio of the structure. It can be seen that under the action of fortification earthquakes, as the horizontal damping index of dampers decreases, the additional dynamic stiffness effect is always greater than the additional damping effect, so the base internal force response and the maximum axial stress of rubber bearings increase. While under the action of rare earthquakes, as the horizontal damping index of dampers decreases, first of all, the additional damping effect is greater than the additional dynamic stiffness effect, so the base internal force response and the maximum axial stress of rubber bearings decrease. Subsequently, the additional dynamic stiffness effect is greater than the additional damping effect, so the base internal force response and the maximum axial stress of rubber bearings increase.

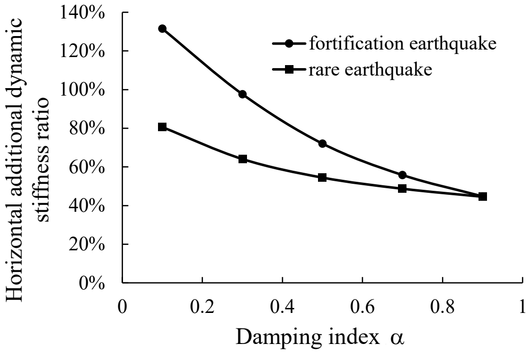

Figure 4.23 Horizontal additional dynamic stiffness ratio of the isolation layer

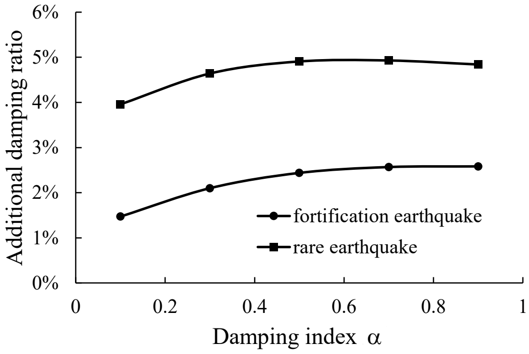

Figure 4.24 Additional damping ratio of the structure

In summary, from the perspective of horizontal seismic isolation, the recommended value for the horizontal damping index α is a range of 0.3~0.5.

4.4.4 Conclusion of the section

The introduction of horizontal viscous dampers into the 3-D vibration and seismic isolation layer has almost no impact on the subway vibration isolation and the rocking effect of the upper structure, but it can significantly further improve the horizontal seismic mitigation capacity of the structure, especially under the action of rare earthquakes.

When the horizontal damping coefficient is at a range of 1000~2000 $kN/(m/s)^{\alpha}$ and the horizontal damping index is at a range of 0.3~0.5, the base internal force response of the upper structure is smallest under the action of horizontal earthquakes, which indicate that the horizontal seismic mitigation and isolation performance is optimal.

4.5 Conclusion of the chapter

This chapter systematically studies the horizontal seismic response of three kind of 3-D vibration and seismic isolation structure under the action of horizontal earthquakes. The main conclusions are as follows:

(1) The pure 3-D vibration and seismic isolation structure: The base internal force response is slightly larger than that of the horizontal seismic isolation structure, indicating that the vertical vibration isolation layer has a slight amplification effect on the horizontal seismic action. At the same time, the vertical stiffness of the isolation layer should not be too small. When the vertical natural frequency of the structure is lower than 1 Hz, severe rocking effect will occur, then the inter-story drift angle and lateral displacement of floors will increase sharply.

(2) The 3-D vibration and seismic isolation + vertical viscous dampers structure: The vertical viscous dampers arranged at the four corners of the 3-D isolation layer can effectively suppress the rocking effect of the upper structure, and reduce the base internal force response of the upper structure to a certain extent under the action of horizontal earthquakes. Considering the subway vertical vibration isolation requirements and horizontal seismic isolation performance, it’s not recommended to introduce vertical viscous dampers in the 3-D isolation layer. However, in real engineering design, if the vertical stiffness of the isolation layer is too low so that the rocking effect of the upper structure is too significant, the indoor vibration control requirements near the four corners of the building have to be sacrificed. And then the vertical viscous dampers with damping coefficient C = 4000~5000 $kN/(m/s)^{\alpha}$ and α= 0.2~0.3 should be introduced into corners of the 3-D isolation layer. At this circumstance, the requirements of vertical vibration control in the inner part of the building can not only be satisfied, but the rocking effect of the upper structure can also be effectively suppressed, the horizontal seismic mitigation and isolation performance of the structure is optimal.

(3) The 3-D vibration and seismic isolation + horizontal viscous dampers structure: The introduction of horizontal viscous dampers into the 3-D isolation layer has almost no impact on the subway vibration isolation and the rocking effect of the upper structure, but it can significantly further improve the horizontal seismic mitigation capacity of the structure, especially under the action of rare earthquakes. The recommended engineering design parameters of horizontal dampers in the 3-D

isolation layer are 1000~2000 $kN/(m/s)^{\alpha}$ for horizontal damping coefficient and 0.3~0.5 for horizontal damping index.

Table 4.13 compares the horizontal seismic mitigation efficiency of the upper structure with viscous dampers arranged in different directions in the 3-D isolation layer. It can be seen that if the subway vibration control requirements are not considered, the seismic mitigation efficiency of the structure with vertical viscous dampers in the isolation layer is better than that with horizontal viscous dampers in the isolation layer. What's more, the rocking effect of the upper structure can also be effectively controlled if vertical viscous dampers are arranged at the isolation layer.

For high-rise over-track buildings, considering that even if very small damping is introduced into the isolation layer, it is very unfavorable for the vibration isolation of the upper structure. Therefore, it is recommended to use pure 3-D vibration and seismic isolation structure or 3-D vibration and seismic isolation + horizontal viscous dampers structure for high-rise over-track buildings.

Table 4.13 Comparison of horizontal seismic mitigation efficiency of the upper structure with viscous dampers arranged in horizontal and vertical direction in the 3-D isolation layer

Item	3DISOVD	3DISOHD
Recommended damping parameters	C = 4000~500, α = 0.2~0.3	C = 1000~2000, α = 0.3~0.5
Horizontal seismic response	Fortification earthquake: reduce 5%~10%	Fortification earthquake: increase 5%~15%
	Rare earthquake: reduce 10%~15%	Rare earthquake: reduce 15%~20%
Rocking effect	Controlled effectively	No impact
Deformation of 3-D isolation layer	Reduce vertical deformation	Reduce horizontal deformation

Attention: The ratio of change in the "horizontal seismic response" row is relative to that of the horizontal isolation structure with the same arrangement and parameters of rubber bearings

Chapter 5 Engineering case study

5.1 Overview

5.1.1 Project overview

Jinqiao Metro Over-track Project is located in Jinqiao area of Pudong, Shanghai of China. The construction site is about 1775 meters long and 435 meters wide, with a planned land area of about 59 hectares. Shanghai Rail Transit Company plans the site as a shared space for the three subway lines of Line 9, Line 12, and Line 14. The design region of this project is shown in the box on the right side of Figure 5.1. The newly built buildings belong to the joint library of subway Line 9, which is divided into 4 areas according to the upper property development. In this thesis, a single building in area E2 is selected for 3-D vibration and seismic isolation design.

The structural finite element model is shown in Figure 5.2. The building is composed of an aboveground part and a basement. The aboveground part is used for residential. The underground first floor is a parking lot, and the underground second floor is used for subway operation, parking and repairment. There are 12 floors above ground, the first floor is 4.4m high, the 2-12 floors are 2.9m high, the total building height is 33.4m. The underground first floor is 5.5m high, and the underground second floor is 9.4m high. The architectural plan of the above-ground standard floor is shown in Figure 5.3. The structural system has 6 spans with a length of 30m in the X direction and 2 spans with a length of 11m in the Y direction. The upper structure has a total of 7×3 = 21 reinforced concrete columns, of which only 9 extend to the ground, and the other columns fall on the main beams of the steel-concrete giant frame in the basement.

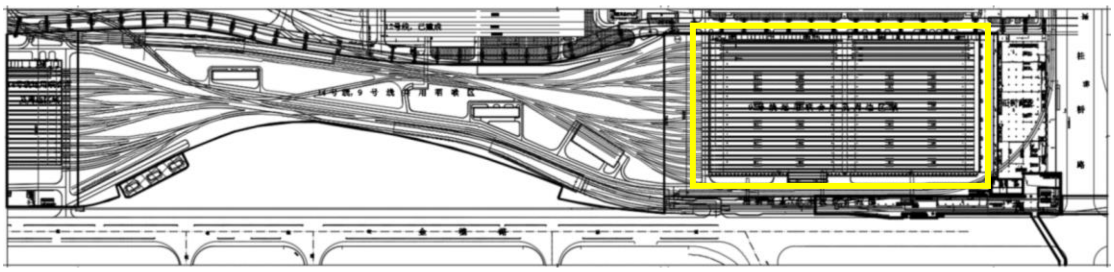

Figure 5.1 Overall site plan

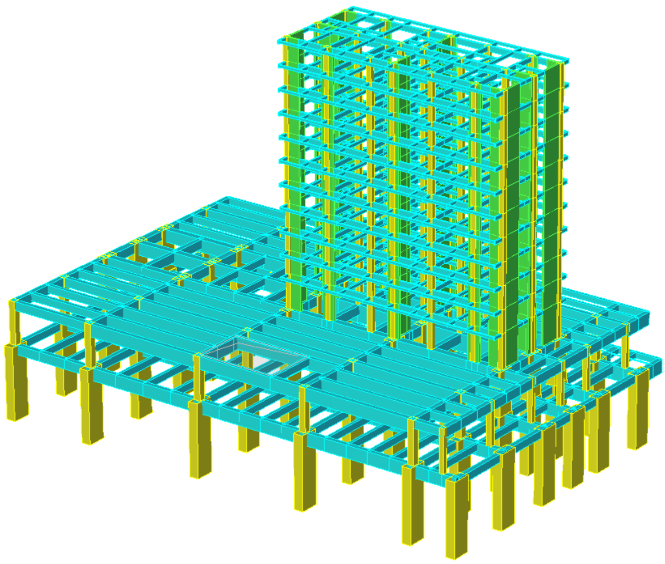

Figure 5.2 The finite element model of the building

Figure 5.3 The architectural plan of the above-ground standard floor

5.1.2 Seismic action

The parameters of horizontal seismic action and structural model are illustrated in Table 5.1 and Table 5.2 respectively.

Table 5.1 Parameters of horizontal seismic action

Fortification intensity	Design earthquake group	Site category	Site characteristic period (s)
7 degree (0.10g)	Group 1	IV	0.9

Two artificial seismic waves and five natural seismic waves (with a site characteristic period of 0.9s) provided in the Shanghai Seismic Design Code are selected as the input excitation for non-linear time history analysis. The information of seismic waves is shown in Table 5.3.

Table 5.2 Parameters of structural model for non-linear dynamic analysis

Level	Frequent earthquake	Fortification earthquake	Rare earthquake
Peak ground acceleration (gal)	35	100	220
Maximum horizontal seismic effect coefficient	0.08	0.23	0.50
Site characteristic period (s)	0.9	0.9	0.9
Damping ratio	0.05	0.05	0.05

Table 5.3 The information of seismic waves

Earthquake wave	Wave data			
	Type	No. of increments	Time interval (s)	Duration (s)
AWX0.9-1	Artificial (RGB1)	3250	0.02	65.00
AWY0.9-2	Artificial (RGB2)	1502	0.02	30.04
NRY0.9-3	Natural (TRB1)	2695	0.02	53.90
NRY0.9-4	Natural (TRB2)	2950	0.02	59.00
NRX0.9-5	Natural (TRB3)	2434	0.02	48.68
NRY0.9-6	Natural (TRB4)	3525	0.02	70.50
NRX0.9-7	Natural (TRB5)	3163	0.02	63.26

Figure 5.4 shows the comparison between the seismic wave response spectra and the design response spectrum. Table 5.4 shows the comparison of seismic effect coefficient at the main period of the structure on the seismic wave average response spectrum and the design response spectrum. It can be seen that the difference between the unisolated structure and 3-D isolation structure is less than 20%, which meets the code limitation.

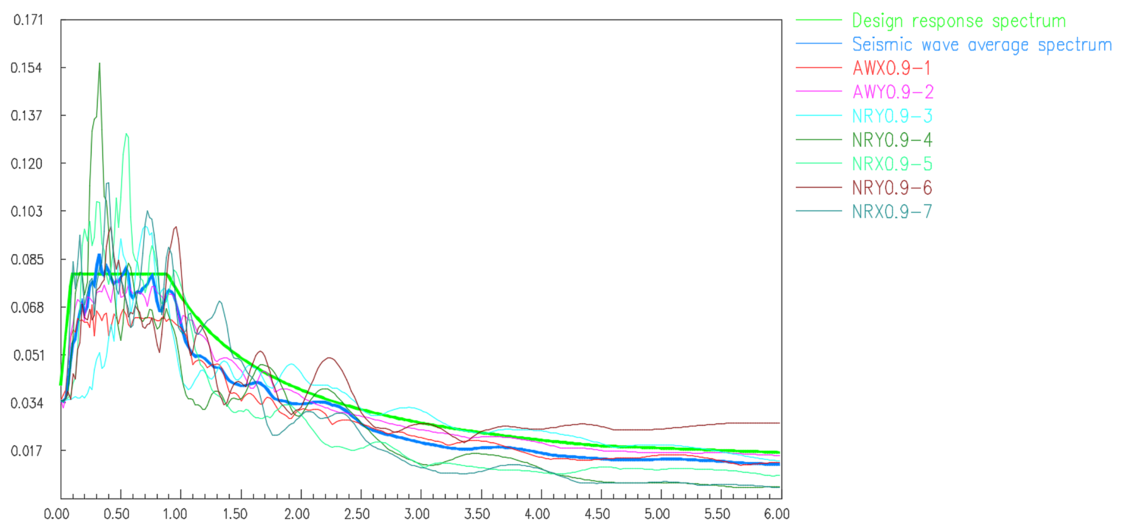

Figure 5.4 Comparison of the seismic wave response spectra and the design response spectrum

Table 5.4 Comparison of seismic effect coefficient at the main period of the structure

Mode	Unisolated structure		3-D isolation structure	
	Period (s)	Error (%)	Period (s)	Error (%)
1	0.86	-12.63	2.03	-11.77
2	0.84	-15.56	1.79	-17.22
3	0.61	-9.99	1.67	-10.49

According to the seismic wave selection rules of “Code for seismic design of buildings” in China, the base shear force calculated by each seismic wave in elastic time-history analysis is not less than 65% of the value calculated by response spectrum method and not more than 135%. At the same time, the average base shear force calculated by the chosen 7 seismic waves should not be less than 80% of the value calculated by response spectrum method. Table 5.5 shows the base shear forces of unisolated structure under the action of frequent earthquakes. It can be seen that the chosen 7 seismic waves meet the requirements of the code and can be used as input seismic excitation for non-linear time history analysis.

Table 5.5 Base shear forces of unisolated structure under the action of frequent earthquakes

Seismic case	X direction		Y direction	
	Base shear force (kN)	Ratio	Base shear force (kN)	Ratio
Response Spectrum method	5084	100%	5006	100%
AWX0.9-1	4247	84%	4232	85%
AWY0.9-2	4848	95%	4774	95%
NRY0.9-3	4835	95%	4639	93%
NRY0.9-4	4371	86%	4696	94%
NRX0.9-5	4306	85%	4530	90%
NRY0.9-6	4235	83%	4222	84%
NRX0.9-7	4597	90%	4218	84%
Average of 7 seismic cases	4491	88%	4473	89%

5.1.3 Subway vibration excitation

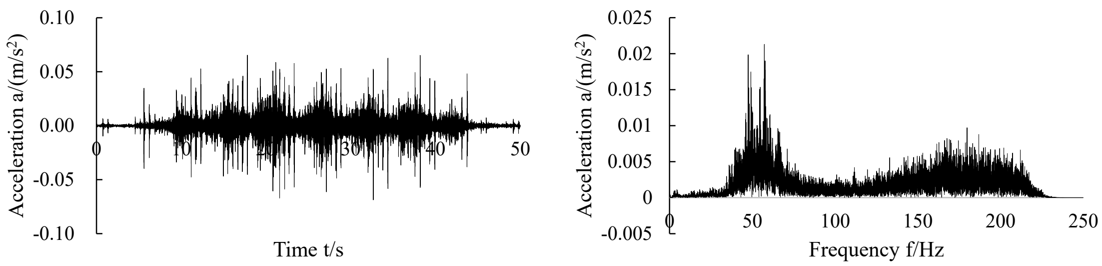

(a) Acceleration diagram (b) Spectrum diagram

Figure 5.5 Wuzhong Road Metro Station subway vibration wave

Because the project lacks the measured subway vibration acceleration wave around the building, the subway vibration wave of Wuzhong Road Metro Station of Line 15 in Shanghai (see section 3.2.1) is chosen for the time history analysis. The acceleration diagram and spectrum diagram of the subway vibration wave are shown in Figure 5.5.

5.2 Design of the 3-D vibration and seismic isolation structure

The original structural scheme of this building is a frame shear wall system. The first and second order natural periods of the structure are 0.86s and 0.84s respectively, which are quite close to the site characteristic period 0.9s, so the horizontal seismic response of the structure is significant. At the same time, since no vertical vibration isolation measures have been taken, the vibration response in the aboveground building is significantly higher than the code limitation.

Due to the dual requirements of vertical vibration isolation and horizontal seismic isolation, a 3-D isolation structural system is applied to the building. By reducing both the horizontal and vertical stiffness of the isolation layer, the horizontal seismic response and vertical vibration response of the upper structure can both be reduced significantly.

The design procedure of the 3-D vibration and seismic isolation structure for the over-track buildings is shown in Figure 5.6. Since the base internal force response of the 3-D isolation structure and horizontal isolation structure under the action of horizontal earthquakes is very close (see section 4.2), the traditional horizontal isolation design method can be used to arrange the horizontal rubber bearings in the 3-D isolation layer. Then the vertical natural frequency of the structure is estimated according to the single-degree-of-freedom vibration system. The estimation of this simplified method is very accurate, and as the vertical stiffness of the isolation layer decreases, the error between the estimated result and the finite element calculation result is getting smaller. By repeatedly adjusting the vertical stiffness of the isolation layer, the vibration response of the upper structure can meet exactly the code limitation requirements, so as to reduce the rocking effect as much as possible. Then, the vertical stiffness of a single disc spring is determined according to the representative gravity load applied on it, so that the vertical deformation of each spring is as close as possible in daily operation. Finally, the horizontal seismic analysis and rocking effect check are carried out.

The 3-D vibration and seismic isolation structure scheme is based on the original frame shear wall scheme, removing all the shear walls in the upper structure, and keeping the cross-section dimensions of columns, primary and secondary beams unchanged. This building adopts the inter-story isolation scheme, the 3-D isolation layer is set between the upper structure and the basement, as shown in Figure 5.7.

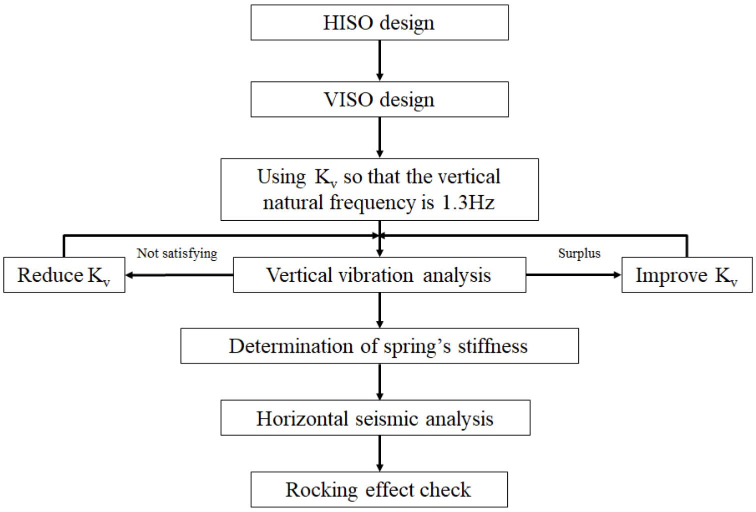

Figure 5.6 Design procedures for the 3-D vibration and seismic isolation structure

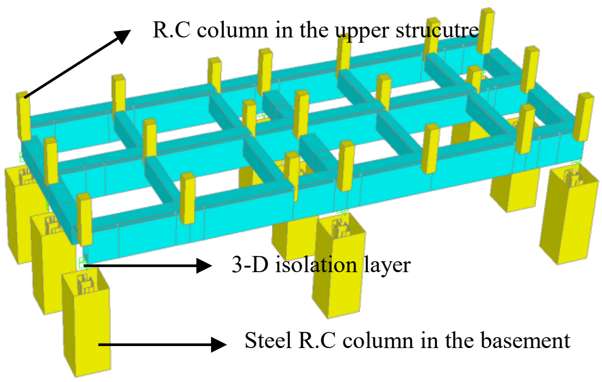

Figure 5.7 Layout of the 3-D isolation layer

5.2.1 Horizontal seismic isolation design

According to the long-term surface pressure of the horizontal rubber bearings under the action of 1.0 times the vertical dead load and 0.5 times the vertical live load, the corresponding rubber bearings are selected. And the lead rubber bearings are arranged at edges of the isolation layer, the natural rubber bearings are arranged inside the isolation layer. The layout of the rubber bearings is shown in Figure 5.8, and the performance parameters of the rubber bearings are shown in Table 5.6. Figure 5.9 shows the long-term surface pressure of the rubber bearings under the action of the representative vertical load. It can be seen that the maximum long-term surface pressure of all rubber bearings is 14.2 MPa, which is less than 15 MPa and meets the daily use requirements of rubber bearings.

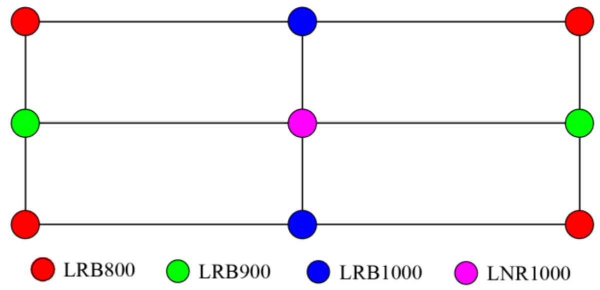

Figure 5.8 Layout of the rubber bearings in 3-D isolation layer

Table 5.6 Performance parameters of the rubber bearings in 3-D isolation layer

Type	Vertical stiffness (kN/mm)	100% Equivalent horizontal stiffness (kN/mm)	Stiffness before yielding (kN/mm)	Yielding force (kN)	Stiffness ratio after yielding
LRB800	3973	2.290	16.459	160	0.077
LRB900	4438	2.565	18.441	203	0.077
LRB1000	4903	3.114	20.507	303	0.077
LNR1000	4335	1.536	-	-	-

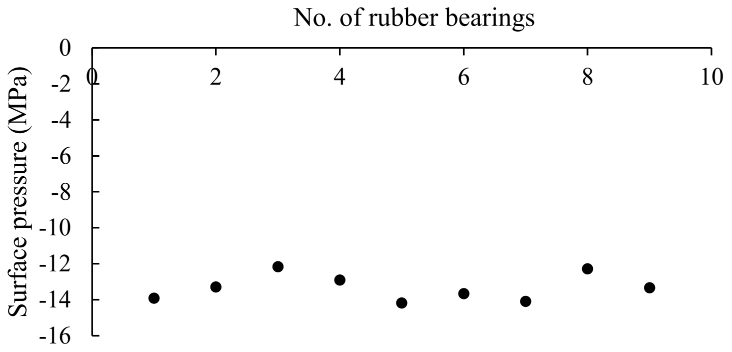

Figure 5.9 The long-term surface pressure distribution of the rubber bearings

5.2.2 Vertical vibration isolation design

The vertical vibration isolation devices adopt disc springs and is installed in series under each horizontal rubber seismic isolation bearing. The total horizontal stiffness of the 3-D isolation layer $K_h = 22.05\,\text{kN/mm}$ and the total vertical stiffness of the 3-D isolation layer $K_v = 25K_h = 551.35\text{kN/mm}$. In this situation, the vertical natural frequency of the structure is 1.35Hz. The vertical stiffness of a single disc spring is determined according to the representative vertical load (1.0

times the vertical dead load and 0.25 times the vertical live load) applied on it to ensure that the vertical compression of each spring is as close as possible. The layout and performance parameters of the disc springs are shown in Figure 5.10 and Table 5.7 respectively. The error between vertical compression of all disc springs is controlled within 10%.

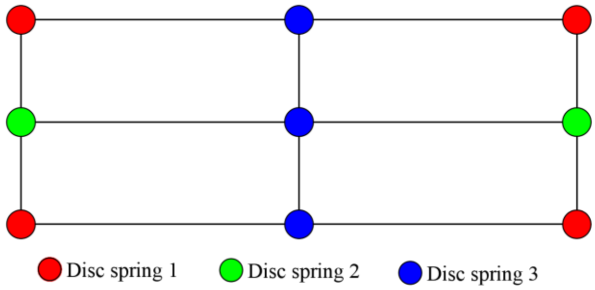

Figure 5.10 The layout of the disc springs in 3-D isolation layer

Table 5.7 The performance parameters of the disc springs in 3-D isolation layer

Type	Vertical stiffness (kN/mm)	Number	Compression deformation (mm)	Total vertical stiffness of 3-D isolation layer (kN/mm)
Disc spring 1	49.39	4	114.1, 118.4, 123.2, 117.8	551.35
Disc spring 2	79.99	3	133.1, 128.4, 132.3	
Disc spring 3	56.89	2	116.1, 120.2	

5.3 Comparison of two schemes

5.3.1 Basic characteristics

Table 5.8 shows the lateral resistant system of the upper structure. The 3-D vibration and seismic isolation scheme removes all the shear walls of the original frame-shear wall scheme, and only retains the vertical frame columns. Table 5.9 shows the total weight of the upper structure. The 3-D isolation scheme can reduce the horizontal seismic response of the upper structure, so the lateral resistant members reduce, and the total structural weight is reduced by about 9%. Table 5.10 shows the first three natural period of the structure. The 3-D isolation scheme reduces the horizontal stiffness of both the upper structure and the isolation layer, thereby prolonging the structural natural period and effectively reducing the horizontal seismic response.

Table 5.8 The lateral resistant system of the upper structure

Scheme	Original rigid structure	3-D isolation structure
Structural system	Frame-shear wall	Frame
Anti-lateral force members	R.C shear walls and columns	R.C columns
Dimensions of columns	600×600 C50	600×600 C50
Dimensions of shear walls	200mm C40	-

Table 5.9 The total weight of the upper structure

Scheme	Original rigid structure	3-D isolation structure
Dead load (kN)	70976	64827
Live load (kN)	10094	10113
Vertical representative gravity load (kN)	76023	69884

Table 5.10 The first three structural natural periods (Unit: s)

Vibration mode	Original rigid structure	3-D isolation structure
1	0.86	4.60
2	0.84	3.84
3	0.61	3.01

5.3.2 Vertical vibration isolation performance

Input the subway vibration wave into the unisolated structure and the 3-D vibration and seismic isolation structure respectively, and compare the vertical vibration response in the upper structure.

A total of 12×2 = 24 joints in the upper structure are selected as the indoor vibration evaluation points, as shown in Figure 5.11. Among them, the m-series evaluation points are located at the corners of the building, and the k-series evaluation points are located at the exact middle of the building. Each series of evaluation points includes joints from the 1st to 12th floors of the building.

The vertical Z vibration level VL_z, maximum vibration level of frequency bands VL_{max}, and equivalent A-weighted sound pressure level L_{Aeq} of the evaluation points in the upper structure are shown in Table 5.11~Table 5.13, Figure 5.12~Figure 5.14. According to the design code "Standard of vibration in urban area environment" GB10070-88, the upper structure belongs to residential area, and its daytime environmental vibration limit is 70dB (see Table 2.4). And according to the design code "Standard for limit and measuring method of building vibration and secondary noise caused by urban rail transit" JGJ/T170-2009, the limit of maximum vibration level of frequency bands VL_{max} is 65dB for residential areas in the daytime, while the limit of environmental secondary radiation noise is 38dB (see Table 2.5). It can be seen that the 3-D vibration and seismic isolation structure greatly reduces the indoor vibration response of the upper structure, and controls the vibration indicators within the code limit, while the indoor vibration response of the unisolated structure far exceeds the code limit.

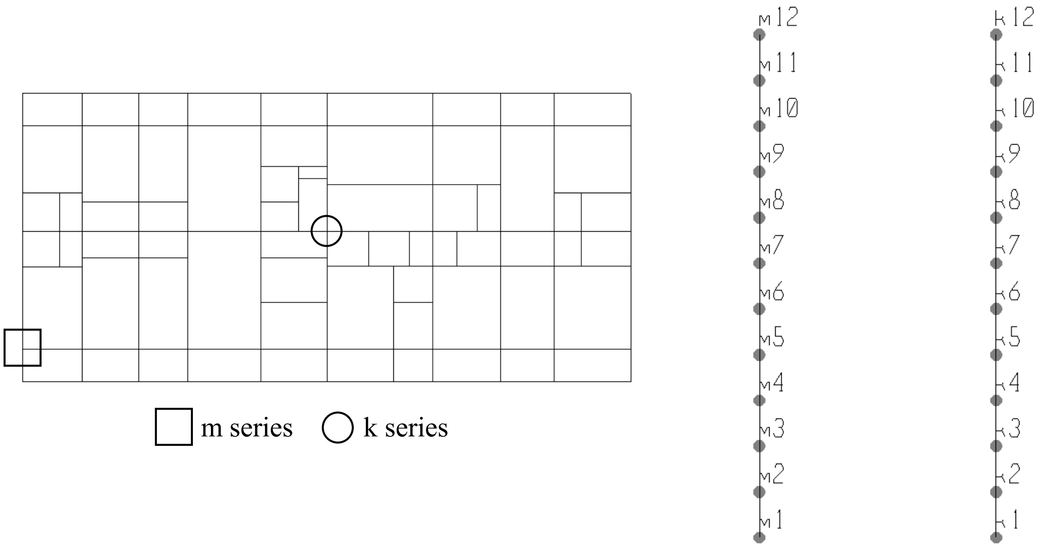

(a) Location in the plan (b) Location in the elevation

Figure 5.11 The positon of indoor vibration evaluation points

Table 5.11 Comparison of Z vibration level VL_z

3-D isolation structure				Original rigid structure				Limit (dB)
m-series	VL_z (dB)	k-series	VL_z (dB)	m-series	VL_z (dB)	k-series	VL_z (dB)	
m1	67.99	k1	67.33	m1	93.71	k1	93.31	70
m2	68.00	k2	67.46	m2	95.76	k2	89.77	
m3	68.01	k3	67.59	m3	96.13	k3	89.68	
m4	67.98	k4	67.71	m4	95.98	k4	90.92	
m5	67.90	k5	67.82	m5	95.05	k5	91.50	
m6	67.80	k6	67.94	m6	93.06	k6	90.90	
m7	67.75	k7	68.04	m7	89.57	k7	89.07	
m8	67.80	k8	68.13	m8	87.08	k8	86.75	
m9	67.97	k9	68.21	m9	90.10	k9	86.97	
m10	68.19	k10	68.28	m10	93.47	k10	89.67	
m11	68.37	k11	68.33	m11	95.44	k11	91.93	
m12	68.45	k12	68.36	m12	96.05	k12	93.16	

Table 5.12 Comparison of maximum vibration level of frequency bands VL_{max}

3-D isolation structure				Original rigid structure				Limit (dB)
m-series	VL_{max} (dB)	k-series	VL_{max} (dB)	m-series	VL_{max} (dB)	k-series	VL_{max} (dB)	
m1	63.23	k1	59.38	m1	94.26	k1	95.35	65

m2	63.36	k2	59.70	m2	98.01	k2	89.35	
m3	63.49	k3	60.00	m3	98.71	k3	89.80	
m4	63.61	k4	60.26	m4	98.65	k4	91.50	
m5	63.71	k5	60.48	m5	97.64	k5	92.80	
m6	63.81	k6	60.67	m6	95.43	k6	92.30	
m7	63.88	k7	60.84	m7	90.78	k7	89.84	
m8	63.95	k8	60.97	m8	85.14	k8	84.35	
m9	63.99	k9	61.09	m9	90.93	k9	85.91	
m10	64.03	k10	61.18	m10	95.46	k10	89.69	
m11	64.05	k11	61.24	m11	97.76	k11	91.88	
m12	64.07	k12	61.28	m12	98.42	k12	93.04	

Table 5.13 Comparison of equivalent A-weighted sound pressure level L_{Aeq}

3-D isolation structure				Original rigid structure				Limit (dB)
m-series	L_{Aeq} (dB)	k-series	L_{Aeq} (dB)	m-series	L_{Aeq} (dB)	k-series	L_{Aeq} (dB)	
m1	36.57	k1	31.49	m1	72.85	k1	72.65	38
m2	37.35	k2	29.95	m2	74.24	k2	68.41	
m3	38.11	k3	28.33	m3	74.58	k3	67.47	
m4	38.24	k4	26.57	m4	74.62	k4	68.72	
m5	37.47	k5	24.62	m5	73.89	k5	69.45	
m6	35.61	k6	22.68	m6	72.01	k6	69.03	
m7	32.70	k7	21.12	m7	68.30	k7	67.07	
m8	31.18	k8	20.09	m8	63.60	k8	62.72	
m9	33.82	k9	19.97	m9	66.62	k9	61.41	
m10	36.65	k10	20.98	m10	70.88	k10	65.45	
m11	37.32	k11	22.21	m11	73.21	k11	68.55	
m12	37.92	k12	22.62	m12	73.95	k12	70.37	

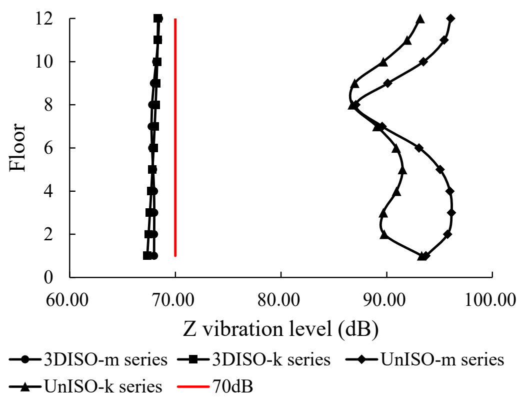

Figure 5.12 Comparison of Z vibration level VL_z

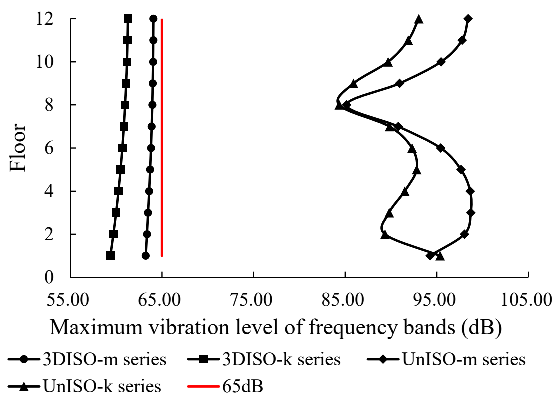

Figure 5.13 Comparison of maximum vibration level of frequency bands VL_{max}

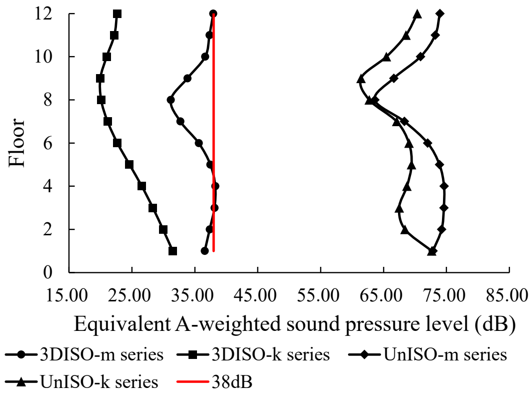

Figure 5.14 Comparison of equivalent A-weighted sound pressure level L_{Aeq}

5.3.3 Horizontal seismic isolation performance

5.3.3.1 Base internal force

Under the action of fortification earthquakes, the base shear force and base overturning moment of the upper structure of original rigid structure and 3-D vibration and seismic isolation structure are shown in Table 5.14. It can be seen that the 3-D isolation structure significantly reduces the horizontal seismic internal force response of the upper structure by more than 60%. The goal of horizontal seismic isolation design is achieved. The upper structure can be designed according to the fortification intensity reduction by one degree.

Table 5.14 The comparison of base internal force response

Item		X-direction	Y-direction
Base shear force (kN)	Original rigid structure	12841	12986
	3-D isolation structure	2384	1977
	Reducing ratio	81%	85%
Base overturning moment ($\times10^5$kN·m)	Original rigid structure	3.109	2.953
	3-D isolation structure	0.785	0.518
	Reducing ratio	75%	82%

5.3.3.2 Inter-story drift angle

Under the action of frequent earthquakes, the inter-story drift angles of the original rigid structure, the horizontal seismic isolation structure (with the parameters and layout of rubber bearings the same), and the 3-D vibration and seismic isolation structure are shown in Figure 5.15. It can be seen that the original rigid frame-shear wall structure and the horizontal seismic isolation frame structure both meet the code limit requirements. The 3-D vibration and seismic isolation frame structure can meet the requirement of 1/550 limitation in the X direction, but cannot meet the limit requirements in the Y direction. According to Section 2.3.3 of this thesis, when the building height is fixed, the greater the aspect ratio, the more significant the rigid rocking effect of the 3-D isolation structure. The aspect ratio of this building is 1.1 in X-direction, and 3.0 in Y-direction. Therefore, the rocking effect in the Y direction is significantly greater than that in the X direction. According to the traditional seismic design code, the maximum inter-story drift angle of the 3-D isolation structure is often difficult to meet the limit requirements.

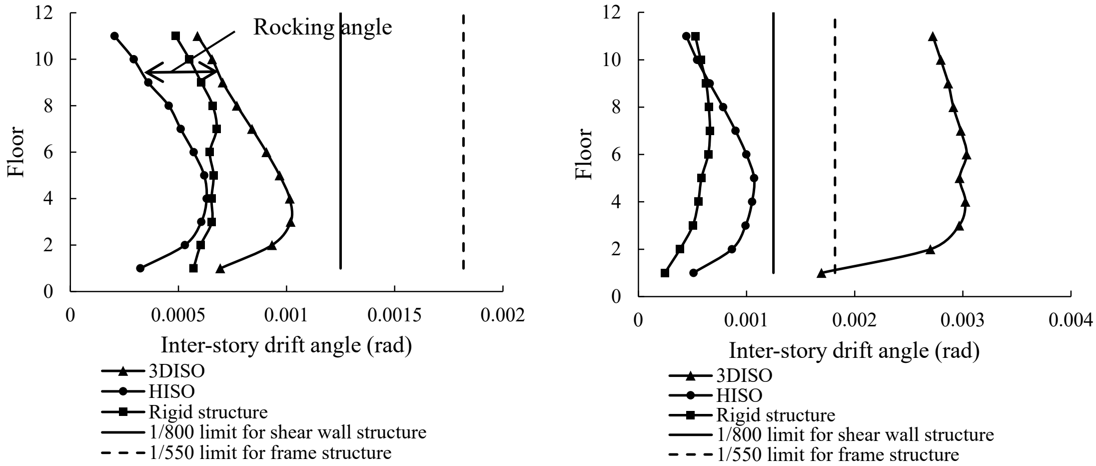

(a) Inter-story drift angle in X direction (b) Inter-story drift angle in Y direction

Figure 5.15 Inter-story drift angle of the upper structure under the action of frequent earthquakes

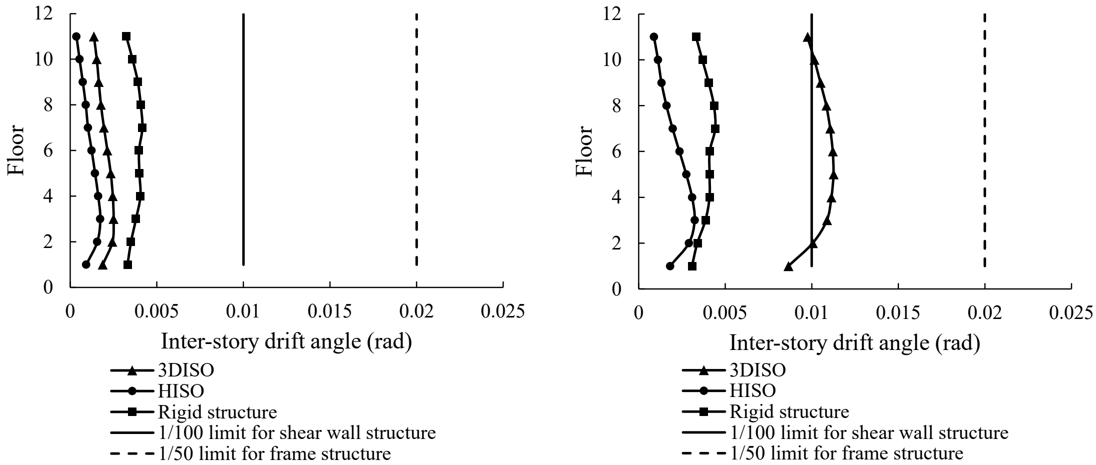

(a) Inter-story drift angle in X direction (b) Inter-story drift angle in Y direction

Figure 5.16 Inter-story drift angle of the upper structure under the action of rare earthquakes

Based on the above comments, it is necessary to deduct the rigid rocking angle component from the inter-story drift angle of the 3-D isolation structure in real engineering design (see Equation 2.7), and only compare the unfavorable inter-story drift angle of the structure with the code limit requirements. A simple method is to compare whether the inter-story drift angle of the horizontal seismic isolation structure (with the parameters and layout of rubber bearings the same) meets the code requirements (as shown in Figure 5.15a).

Under the action of rare earthquakes, the inter-story drift angles of the original rigid structure, the horizontal seismic isolation structure, and the 3-D vibration and seismic isolation structure are shown in Figure 5.16. It can be seen that both the original rigid frame-shear wall structure and the horizontal seismic isolation frame structure meet the code limit requirements. And even if the 3-D isolation frame structure has significant rocking effects, the maximum inter-story drift angles in the X and Y directions both meet the requirements of 1/50 code limitation.

5.4 Verification of the 3-D isolation structure

5.4.1 Short-term surface pressure verification of rubber bearings

(1) Short-term maximum surface pressure

The short-term extreme surface pressure of the rubber isolation bearings under the action of rare earthquakes is an important indicator in the design of the 3-D isolation layer. The short-term extreme surface pressure considers the combination of the representative vertical gravity load and the three-dimensional rare earthquake actions.

Figure 5.17 shows the short-term maximum surface pressure of each rubber bearing. The maximum value of all bearings is 18MPa in compression, which meets the code limit of 25MPa.

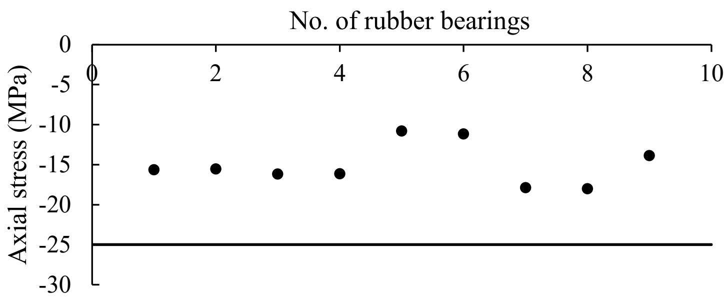

Figure 5.17 Short-term maximum surface pressure distribution of rubber bearings

(2) Short-term minimum surface pressure

Figure 5.18 shows the short-term minimum surface pressure of each rubber bearing. The minimum value of all bearings is 7.6MPa in compression, which meets the code limit of 1MPa in tension.

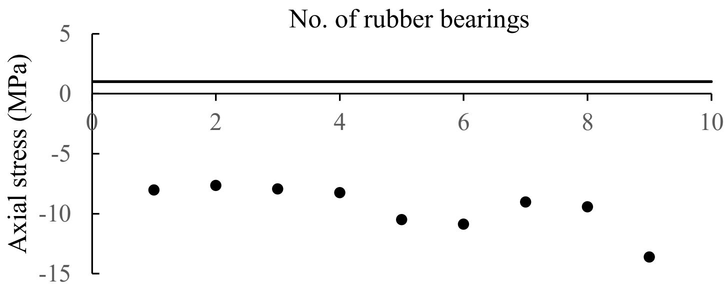

Figure 5.18 Short-term minimum surface pressure distribution of rubber bearings

5.4.2 Deformation of the isolation layer

Table 5.15 shows the maximum horizontal deformation of the rubber bearings under the action of rare earthquakes. It can be seen that the maximum horizontal deformation is 299mm, which is far less than 0.55 times the effective diameter of the rubber bearing and 3 times the total thickness of rubber layers. The maximum horizontal deformation meets the code requirements perfectly.

Table 5.15 Maximum horizontal deformation of the rubber bearings

No. of rubber bearing	Maximum deformation in X direction (mm)	Maximum deformation in Y direction (mm)
1	297	274
2	299	274
3	299	284
4	297	284
5	298	274
6	298	284
7	298	279
8	297	278
9	298	279
Maximum of above (mm)	299	284

5.4.3 Verification of overturning

The overturning verification of the upper structure under the action of rare earthquakes is shown in Table 5.16.

It can be seen that under the action of rare earthquakes, the resisting overturning moment of the upper structure is 8.9 times the base overturning moment in the X direction, and 2.9 times in the Y direction. The safety factor is greater than 1.2, which meets the requirement of design codes.

Table 5.16 Overturning verification of the upper structure

Floor	Weight (kN)	Centroid coordinates		Contribution of resisting overturning moment (kN·m)	
		X-direction	Y-direction	X-direction	Y-direction
11	5101	15.3	7.2	72883	15890
10	5102	15.3	7.2	72917	16037
9	5102	15.3	7.2	72940	16187
8	5102	15.3	7.2	72964	16343
7	5099	15.3	7.2	72948	16493
6	5099	15.3	7.2	72975	16657
5	5099	15.3	7.2	73006	16823
4	5099	15.3	7.2	73041	16989
3	5099	15.3	7.2	73077	17154
2	5099	15.4	7.2	73114	17314
1	5236	15.6	7.3	73836	17606
Isolation layer	13649	15.6	7.3	192549	46238
Sum		Resisting overturning moment (kN·m)		996249	229731
		Base overturning moment (kN·m)		112462	79553
Safety factor				8.9	2.9

5.5 Conclusion of the chapter

Based on the research results of Chapters 2 to 4, this chapter applies the 3-D vibration and seismic isolation technology to a real building so as to achieve the dual effects of reducing the horizontal seismic response and the vertical vibration response of the upper structure.

When achieving the adequate performance for indoor subway vibration isolation of upper structure, the vertical stiffness of the 3-D isolation layer is greatly reduced, then the maximum inter-story drift angle of the 3-D isolation structure often exceeds the code limitation due to severe rocking effect under the action of horizontal frequent earthquakes. At this circumstance, the inter-story drift angle should be verified according to the corresponding horizontal seismic isolation structure (with the parameters and layout of rubber bearings the same). At the same time, the rocking effect causes a significant increase in the lateral displacement of the upper structure, then the overturning verification should be paid attention to.

Chapter 6 Conclusions and outlooks

6.1 Main conclusions

Chapter 1 starts from the great significance of the property development of over-track buildings, lays the foundation for the engineering application value of the over-track 3-D vibration and seismic isolation structures. In response to the urgent need for vertical vibration and horizontal seismic isolation of the over-track buildings, several vertical vibration isolation methods and horizontal seismic isolation methods are summarized, highlighting the irreplacable advantages of the 3-D vibration and seismic isolation technology. The composition of 3-D vibration and seismic isolation structure is clarified, and the model of the tandem 3-D vibration and seismic isolation bearing used in the calculation and analysis of this thesis is pointed out. Then research status of the 3-D isolation bearings, engineering applications of the 3-D isolation structures, and the rocking effect is summarized. Finally, the main research contents and innovation points of this thesis are clarified.

Chapter 2 illustrates the vibration mitigation mechanism of the 3-D isolation structure from the transmission ratio curve of a vertical SDOF vibration isolation system, and explains the seismic mitigation mechanism from the natural period prolonging effect and additional damping effect in the design response spectra. Then the constitutive model and finite element software simulation method of the commonly used 3-D isolation and damping devices are introduced. At the same time, a method for defining the rocking angle is proposed, the formula for calculating the rocking angle of a two-dimensional simplified model is derived, and the influence of the vertical stiffness of the isolation layer and the structural aspect ratio on the rocking angle is studied through numerical simulation. Finally, the vibration evaluation standards under the excitation of subway vibration are summarized, then the definitions and code limits of the vertical peak acceleration, the Z vibration level, and the equivalent A-weighted sound pressure level are summarized.

Chapter 3 first studies the vertical vibration isolation performance of the pure 3-D vibration and seismic isolation structure, and draws the following conclusions:

(1) As the vertical stiffness of the isolation layer decreases, the vertical natural

frequency decreases, the vertical peak acceleration ratio of the 3-D isolation structure to the unisolated structure decreases, and the decreasing speed is basically constant; the reduction value of Z vibration level and equivalent A-weighted sound pressure level increase, and the increasing speed is getting faster and faster.

(2) The appropriate value of the vertical stiffness of the 3-D isolation layer for high-rise buildings should be chosen such that the vertical natural frequency of the structure is below 1.3 Hz.

Then this chapter studies the vertical vibration isolation performance of the 3-D vibration and seismic isolation + vertical viscous dampers structure, and draws the following conclusions:

(1) After the vertical viscous damping is introduced into the 3-D isolation layer, due to the additional dynamic stiffness of the viscous dampers, the indoor vertical vibration response of joints above the dampers increases significantly, and may even be larger than that of the unisolated structure. However, the adverse impact on the inner part of the building is smaller than the four corners.

(2) As the vertical damping coefficient increases, the vertical vibration response first increases sharply, after $C \geq 2000$, the vertical additional dynamic stiffness ratio of the 3-D isolation layer reaches more than 3, so that the vertical vibration response basically no longer changes with the vertical damping coefficient.

(3) As the vertical damping index decreases, the vertical vibration response first increases sharply, after $\alpha \leq 0.5$, the vertical additional dynamic stiffness ratio of the 3-D isolation layer reaches more than 3, so that the vertical vibration response basically no longer changes with the vertical damping index.

(4) If the vertical vibration isolation performance of all parts in the upper structure is required, it is recommended that the 3-D isolation layer does not introduce any vertical viscous dampers. If the vertical vibration isolation requirements near the four corners of the building are discarded, the vertical stiffness of the isolation layer can be further reduced, and then four viscous dampers with parameters of C = 4000~5000 $kN/(m/s)^{\alpha}$ and α = 0.2~0.3 are recommended to add into the corners of the isolation layer. In this situation, the requirements of vertical vibration control in the inner part of the building can not only be satisfied, but the rocking effect of the upper structure can also be effectively suppressed.

Chapter 4 first studies the horizontal seismic isolation performance of the pure 3-D vibration and seismic isolation structure, and draws the following conclusions:

(1) As the vertical stiffness of the isolation layer decreases, the natural period prolonging effect and additional damping effect are mutually restricted, on the whole there is a slight amplification effect on the horizontal seismic response, and the rocking effect of the upper structure increases, the inter-story drift angle and lateral displacement of top floor increase.

(2) Considering the performance of horizontal seismic isolation and vertical subway vibration isolation, the recommended vertical natural frequency of the 3-D vibration and seismic isolation structure is 1.0~1.3Hz.

Then this chapter studies the horizontal seismic isolation performance of the 3-D vibration and seismic isolation + vertical viscous dampers structure, and draws the following conclusions:

(1) The larger the vertical damping coefficient, or the smaller the damping index, the greater the additional dynamic stiffness of the damper and the smaller the rocking angle of the upper structure. The high vertical damping can effectively suppress the rocking effect.

(2) Under the premise of not requiring subway vibration isolation capacity, when the vertical damping coefficient is at a range of 4000~5000 $kN/(m/s)^{\alpha}$ and the vertical damping index is at a range of 0.2~0.3, the base internal force response of the upper structure is smallest under the action of horizontal earthquake, and the rocking effect is also significantly reduced, which indicate that the horizontal seismic isolation performance is optimal.

(3) As for high-rise over-track buildings, even with small vertical damping in the 3-D isolation layer, it will make the vertical vibration response of joints above the dampers equal to that of an unisolated structure, and the degree of suppression of the rocking effect is also low. Therefore, if the subway vibration isolation performance of all parts in the upper structure is required, the 3-D isolation layer is not recommended to introduce any vertical viscous dampers.

(4) In real engineering design, if the vertical stiffness of the isolation layer is too low so that the rocking effect of the upper structure is too significant, the indoor vibration control requirements near the four corners of the building have to be sacrificed. And then the vertical viscous dampers with damping coefficient C = 4000~5000 $kN/(m/s)^{\alpha}$ and α= 0.2~0.3 should be introduced into corners of the 3-D isolation layer. At this circumstance, the requirements of vertical vibration control in the inner part of the building can not only be satisfied, but the rocking

effect of the upper structure can also be effectively suppressed, the horizontal seismic mitigation and isolation performance of the structure is optimal.

This chapter then studies the horizontal seismic isolation performance of the 3-D vibration and seismic isolation + horizontal viscous dampers structure, and draws the following conclusions:

(1) The introduction of horizontal viscous dampers into the 3-D isolation layer has almost no impact on the subway vibration isolation and the rocking effect of the upper structure, but it can significantly further improve the horizontal seismic mitigation capacity of the structure, especially under the action of rare earthquakes, and the horizontal deformation of the isolation layer is also effectively controlled.

(2) The recommended engineering design parameters of horizontal dampers in the 3-D isolation layer are 1000~2000 $kN/(m/s)^{\alpha}$ for horizontal damping coefficient and 0.3~0.5 for horizontal damping index. Under this circumstance, the seismic base internal force response is the smallest, indicating that the seismic mitigation performance is the best.

Chapter 5 mainly introduces the application of 3-D isolation technology in the Shanghai Jinqiao over-track building project. The comparison between the 3-D isolation structure and traditional rigid structure shows that the 3-D isolation structure not only reduces the vertical vibration response, but also reduces the lateral force-resistant members and reduces the horizontal seismic response.

6.2 Recommendations and outlooks

(1) The 3-D vibration and seismic isolation + horizontal and vertical viscous dampers structure system is suggested to be further studied and discussed in the follow-up research.

(2) In this thesis, only the most representative combination of viscous dampers and 3-D isolation devices was studied. Subsequent combinations of different types and forms of dampers and 3-D isolation devices can be further analyzed.

(3) This thesis only conducts research on the 3-D isolation frame structure. It is recommended that different types of structural system can be discussed in the future.

(4) It is recommended that more subway vibration waves can be measured and input into the 3-D isolation structure to obtain a more comprehensive result.

References

[1] 孙晓静. 地铁列车振动对环境影响的预测研究及隔振措施分析[D]. 北京:北京交通大学，2008

[2] Duarte. Perception threshold of people exposed to sinusoidal vibration [J]. Vibration Measurement at Baker Street, 2003(1):3791-3798

[3] 徐建. 建筑工程振动手册[M]. 北京:中国建筑工业出版社，2001

[4] 吕丽芳. 高速铁路引起的环境振动研究[D]. 上海:同济大学，2005

[5] 魏龙. 地铁列车运行诱发的振动对环境的影响研究[D]. 兰州:兰州交通大学，2016

[6] 夏禾，曹艳梅. 轨道交通引起的环境振动问题[J]. 铁道科学与工程学报，2004(1):102-104

[7] 田春芝. 地铁振动对周围建筑物影响的研究概况[J]. 铁路节能环保与安全卫生，2000(1):67-70

[8] 张洁，林建辉，高品贤. 高速铁路振动及噪声测试技术[M]. 成都:西南交通大学出版社，2010

[9] 刘卫丰，刘维宁，聂志理，等. 地铁列车运行引起的振动对精密仪器影响的预测研究[J]. 振动与冲击，2013，32(08):18-23

[10] 马蒙，韩嵩，刘维宁，等. 地铁与路面交通振动对精密仪器的影响测试[J]. 北京交通大学学报，2012，36(04):50-54

[11] 钟科举. 地铁上盖高层建筑层间隔震方案对比研究[D]. 广州:广州大学，2015

[12] 贾孝东，张玉敏，兰壮志. 地铁周边建筑物设置碟形弹簧竖向减振效果[J]. 华北理工大学学报（自然科学版），2016，38(04):106-112

[13] 钱七虎. 迎接我国城市地下空间开发高潮[J]. 岩土工程学报，1998，20(4):112-113

[14] 翁大根，张超，吕西林等. 附加黏滞阻尼器减震结构实用设计方法研究[J]. 振动与冲击，2012，31(21):80-88

[15] 刘鹏. 高层隔震建筑结构研究与应用[D]. 上海:同济大学，2017

[16] 中日联合考察团，周福霖，崔鸿超，等. 东日本大地震灾害考察报告[J]. 建筑结构，2012(4):1-20

[17] 钱培风. 日本南兵库地震工程震害的真正教训是什么[J]. 四川建筑科学研究，1995(3):28-32, 43

[18] 岡村茂樹，深沢剛司，杣木孝裕，等. 3 次元免震装置の研究開発その 2 : 3 次元免震装置仕様. 日本建築学会大会学術講演梗概集，2018，21556，1111-1112

[19] Shuichi Yabana, Akihiro Matsuda. Mechanical properties of laminated rubber bearings for three-dimensional seismic isolation[C]. 12th World Conference on Earthquake Engineering, Auckland, New Zealand, 2000(2452)

[20] Kanazawa K, Hirta K, Matsuda A. Shaking table test of three-dimensional base isolation system using laminated thick rubber bearings [J]. 1999

[21] Uriu M, Yamamoto M, Shinzawa K, et al. Three-dimensional seismic isolation floor system using air spring and its installation into a nuclear facility[J]. 1993

[22] Suhara J, et al. Research on 3-D base isolation system applied to new power reactor 3-D seismic isolation device with rolling seal type air spring: part 1[C]. Transaction of the 17th SMiRT, Prague, Czech Republic, August, Division K, Thesis #K09-4, 2003

[23] Kageyama M, et al. Development of three-dimensional base isolation system with cable reinforcing air spring[C]. Transaction of the 17th SMiRT, Prague, Czech Republic, August, Division K, Thesis #K09-5, 2003

[24] Kashiwazaki A, et al. Study on 3-dimensional base isolation system applying to new type power plant reactor (hydraulic 3-dimensional base isolation system: no.1) [C]. Transaction of the 17th SMiRT, Prague, Czech Republic, August, Division K, Thesis #K09-2, 2003

[25] 熊世树，唐建设，梁波，等. 装有 3DB 的三维隔震建筑的平扭-竖向地震反应分析[J]. 工程抗震与加固改造，2004(05):17-22

[26] 魏陆顺，周福霖，任珉，等. 三维隔震新技术保障地铁平台上部安全[J]. 建设科技，2007(09): 38-39

[27] 王维，李爱群，周德恒，等. 新型三维多功能隔振支座设计及其隔振分析[J]. 东南大学学报(自然科学版), 2014, 44(04): 787-792

[28] 郭阳照，潘毅，吴体，等. LRB-DSB 三维隔震系统的隔震效果分析[J]. 西南交通大学学报, 2018, 53(06): 1195-1204

[29] Somaki T, Fukasawa T, Okamura S, et al. Research and development of three-dimensional isolation system for sodium-cooled fast reactor: part 5 — isolation performance applied to reactor building[C]. Proceedings of the Volume 9: Seismic Engineering, Virtual Online, 2020, V009T09A019, ASME

[30] 杣木孝裕，諸菱亮太，野坂泰介，等. 3 次元免震装置の研究開発その 23: 原子炉建屋地震応答解析の概要[J]. 日本建築学会大会学術講演梗概集，2020，21563，1125-1126

[31] 野坂泰介，杣木孝裕，諸菱亮太，等. 3 次元免震装置の研究開発その 24: 3 次元免震装置の地震応答解析モデル[J]. 日本建築学会大会学術講演梗概集，2020，21564，1127-1128

[32] 諸菱亮太，杣木孝裕，野坂泰介，等. 3 次元免震装置の研究開発その 25: 地震応答解析結果[J]. 日本建築学会大会学術講演梗概集，2020，21565，1129-1130

[33] Takafumi F, Shinobu H, Shoji T, et al. A three-dimensional isolation floor for earthquake and ambient micro-vibration using multi-stage rubber bearings (2nd report, development of a new device for vertical isolation)[C]. Proceedings of Japan Society of Mechanical Engineer, 56(521), No 89-0577B

[34] 武居泰，藤井光治郎，伊積康彦，等. 線路上空利用建築物への免震: 防振構造システムの適用[J]. 日本建築学会技術報告集, 2007, 13(25): 49-54

[35] Makris N, Constantinou M C. Spring-viscous damper systems for combined seismic and vibration isolation[J]. Earthquake Engineering & Structural Dynamics, 1992, 21(8): 649-664

[36] 吴宏磊. 带水平向黏滞阻尼器的弹簧支座隔振结构抗震性能研究[J]. 建筑结构, 2020. 50(03): 66-71, 136

[37] 魏陆顺,周福霖,任珉,等. 三维隔震(振)支座的工程应用与现场测试[J]. 地震工程与工程振动, 2007(03): 121-125

[38] 赵鹏. 钢弹簧隔振减震装置性能试验与结构振动控制设计分析研究[D]. 青岛：青岛理工大学，2020

[39] Tomita N, Fujita S. Study on the rocking vibration induced in three-dimensional seismic isolation system[C]. Pressure Vessels and Piping Conference, American Society of Mechanical Engineers, 2017, 57984: V005T11A017

[40] Zhou Zhiguang, Wong J, Mahin S. Potentiality of using vertical and three-dimensional isolation systems in nuclear structures[J]. Nuclear Engineering and Technology, 2016, 48(5): 1237-1251

[41] Mori S, Suhara I, Saruta M, et al. Simulation analysis of free vibration test in a building “Chisuikan” using three-dimensional seismic base isolation system[C]. 15th world conference on earthquake engineering, Lisbon, Portugal. 2012

[42] GB10070-88 城市区域环境振动标准[S]. 北京: 国家环境保护部，1988

[43] JGJ/T170-2009 城市轨道交通引起建筑物振动与二次辐射噪声限值及其振动方法标准[S]. 北京: 中国建筑工业出版社，2009